



HAL
open science

Experimental and numerical study of metal foam composites in innovative application of thermal energy storage

Feng Zhu

► **To cite this version:**

Feng Zhu. Experimental and numerical study of metal foam composites in innovative application of thermal energy storage. Materials. Université de Technologie de Troyes, 2017. English. NNT : 2017TROY0009 . tel-02419964

HAL Id: tel-02419964

<https://theses.hal.science/tel-02419964>

Submitted on 19 Dec 2019

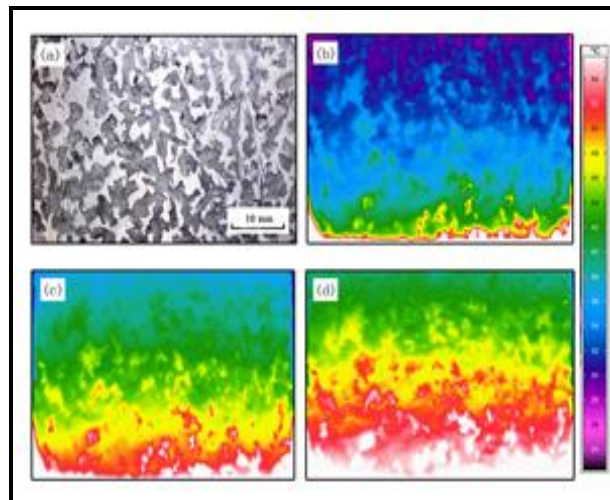
HAL is a multi-disciplinary open access archive for the deposit and dissemination of scientific research documents, whether they are published or not. The documents may come from teaching and research institutions in France or abroad, or from public or private research centers.

L'archive ouverte pluridisciplinaire **HAL**, est destinée au dépôt et à la diffusion de documents scientifiques de niveau recherche, publiés ou non, émanant des établissements d'enseignement et de recherche français ou étrangers, des laboratoires publics ou privés.

Thèse
de doctorat
de l'UTT

Feng ZHU

Experimental and Numerical Study of Metal Foam Composites in Innovative Application of Thermal Energy Storage



Spécialité :
Matériaux, Mécanique, Optique et Nanotechnologie

2017TROY0009

Année 2017

THESE

pour l'obtention du grade de

DOCTEUR de l'UNIVERSITE DE TECHNOLOGIE DE TROYES

Spécialité : MATERIAUX, MECANIQUE, OPTIQUE ET NANOTECHNOLOGIE

présentée et soutenue par

Feng ZHU

le 16 mars 2017

Experimental and Numerical Study of Metal Foam Composites in Innovative Application of Thermal Energy Storage

JURY

M. C. CODDET	PROFESSEUR DES UNIVERSITES	Président
M. B. ABBÈS	PROFESSEUR DES UNIVERSITES	Rapporteur
M. J. GARDAN	ENSEIGNANT CHERCHEUR EPF	Examineur
M. X.-L. GONG	PROFESSEUR DES UNIVERSITES	Directeur de thèse
M. S. HE	PROFESSOR	Examineur
M. P. LECLAIRE	PROFESSEUR DES UNIVERSITES	Rapporteur

Acknowledgements

Three years and a half research experiences in France are challenging, unforgettable and meaningful, and it will be a valuable lesson for my life. During the study, all the work could not be completed without the assistance of the surrounding people in the University of Technology of Troyes (UTT). I would like to express my deepest gratitude to them as well as the China Scholarship Council (CSC) for the financial support.

First of all, I am especially grateful to my supervisor, Professor GONG Xiao-Lu, for his valuable guidance, constructive suggestions and constant encouragement. He not only provides a good research foundation for this thesis but also gives me much precious advice in the experiment design and result analysis. His positive attitude for work always prompts me to move forward in both scientific research and daily life.

Thanks to the president of the committee, Prof. C. CODDET, for his assistance in the organization of the defense. Thanks to Prof. B. ABBES and Prof. P. LECLAIRE for their reviews on my thesis. I would like to thank to the members of jury, Prof. S.Y. HE and Dr. J. GRADAN, for their attendance in my defense.

I am hugely appreciative to F. WEIL and B. LESAGE for their assistances in the preparation of the samples in Halle industrielle. And thanks to Dr. J. GRADAN of EPF who provides us with the mold prepared by 3D impression. Thanks to the project Effi-SiEMCE for the technical and material support.

I am also grateful to my friends HAN.HC, WEN.ZM, ZHANG XH, ZHANG C, ZHANG Y and other friends at UTT, who help and accompany me along these years. Finally, I would like to thank my parents and my wife for their love and wait in expectation.

ZHU Feng

Abstract

The objective of this Ph.D. thesis is to study the thermal behavior of the aluminum foam and phase change material (PCM) composite by both experimental and numerical methods in order to know the phenomena of storage of thermal energy in these materials. The manufacturing process of open-cell aluminum foam is firstly analyzed numerically to reduce the manufacturing defects in the samples. The heat transfer characteristics of PCM embedded in aluminum foams with different porosities are then investigated by analyzing the melting processes and the temperature variations in the composites. Two numerical models for low and high porosity aluminum foam are established to evaluate the energy storage performance of the composites. The results show that the aluminum foam can greatly improve the heat transfer performance in PCM due to its high thermal conductivity. The energy storage performance depends strongly on the porosity of the aluminum foam/PCM composite. An optimized porosity highlights this performance and improves the thermal behavior. The last part of this thesis proposes an improved structure of aluminum foam with respect to the uniform structure: Association of the metal fin and the foam with graded porosity. This new structure possesses a better energy storage performance especially in the case of the isothermal heat source.

Keywords: Metal foams; Heat storage; Metallic composites; Thermal analysis; Simulation methods

Résumé

L'objectif de cette thèse de doctorat est d'étudier expérimentalement et numériquement le comportement thermique des mousses d'aluminium et des matériaux à changement de phase (MCP), présentés sous la forme d'un composite, afin de connaître le phénomène de stockage d'énergie thermique dans ces matériaux. Le procédé de fabrication de la mousse d'aluminium à cellules ouvertes est d'abord analysé numériquement dans le but de réduire les défauts formés durant la fabrication. Les caractéristiques de transfert de chaleur du MCP dans les mousses d'aluminium comportant différentes porosités sont ensuite étudiées en analysant les processus de fusion et la variation de températures dans ces composites. Deux modèles numériques pour la mousse d'aluminium à faible et à haute porosité sont établis afin d'évaluer la performance de stockage d'énergie des composites. Les résultats montrent que la mousse d'aluminium peut améliorer considérablement la performance de transfert de chaleur du MCP en raison de sa conductivité thermique élevée. La performance de stockage d'énergie dépend fortement de la porosité des mousses d'aluminium. Une porosité optimisée met en évidence cette performance et l'amélioration du comportement thermique. La dernière partie de la thèse porte sur une structure améliorée de la mousse par rapport à la structure uniforme: Association de l'ailette métallique et du gradient de porosité de la mousse. Cette nouvelle structure donne ainsi une performance de stockage d'énergie encore meilleure surtout dans le cas d'une source de chaleur isotherme.

Mots clés : Mousses métalliques; Chaleur -- Stockage; Composites à matrice métallique; Analyse thermique; Simulation, Méthodes de

Table of contents

Abstract.....	I
Résumé	II
Table of contents.....	III
Glossaries.....	VII
General introduction	1
Chapter 1. Bibliography: Metal foam/phase change material composite.	5
1.1 Introduction.....	7
1.2 Preparation methods and related structure characteristics of metal foam.....	8
1.2.1 Infiltration casting method	8
1.2.2 Powder metallurgy method.....	9
1.2.3 Investment casting method	11
1.2.4 Electro-deposition method.....	12
1.3 Thermal properties of metal foam	13
1.3.1 Thermal conduction.....	13
1.3.2 Thermal convection.....	15
1.3.3 Thermal radiation	16
1.4 Application of metal foam in thermal energy storage.....	17
1.4.1 Phase change material	18
1.4.2 Enhancement methods of heat transfer.....	20
1.4.3 Research progress of metal foam/PCM composite.....	24
1.5 Modelling of heat transfer in metal foam/PCM composite	26
1.5.1 Micro model of metal foam.....	27
1.5.2 Macro model of metal foam	29
1.5.3 Model of phase transition process	31
1.6 Conclusion	33
Chapter 2. Numerical analysis of the defects in aluminum foam.	35

2.1 Introduction.....	37
2.2 Manufacturing process of the aluminum foam	38
2.2.1 Materials and equipment	38
2.2.2 Process of infiltration casting method	39
2.2.3 Common defects in aluminum foam	40
2.3 Modeling method of manufacturing process	41
2.3.1 Theory of infiltration process	42
2.3.2 Description of the model	45
2.3.3 Governing equations.....	46
2.3.4 Boundary condition and validation of the model	48
2.4 Numerical analysis of the causes of defects	50
2.4.1 Cause of the defect	50
2.4.2 Effect of the manufacturing parameters on the defect.....	53
2.4.3 Prevention of the defect.....	57
2.5 Conclusion	61

Chapter 3. Experimental and numerical investigation of thermal performance of LPAF/PCM composite..... 63

3.1 Introduction.....	65
3.2 Heat transfer characteristic of paraffin	66
3.2.1 Thermal property of paraffin	66
3.2.2 Melting process of paraffin.....	68
3.3 Heat transfer characteristic of LPAF.....	70
3.3.1 Micro model of LPAF.....	71
3.3.2 Simulation of effective thermal conductivity	71
3.4 Thermal performance of LPAF/paraffin composite.....	74
3.4.1 Preparation of LPAF/ paraffin composite.....	74
3.4.2 Test apparatus	75
3.4.3 Uncertainty analysis	76
3.4.4 Heat transfer characteristic of LPAF/paraffin composite	77
3.4.5 Effect of the porosity on the heat transfer in composite.....	81
3.5 Numerical analysis of heat transfer in the LPAF/ paraffin composite	87
3.5.1 Modeling method.....	88
3.5.2 Determination of the structural parameters	89
3.5.3 Numerical procedure and boundary conditions.....	90
3.5.4 Comparison of the equilibrium model and non-equilibrium model	91
3.5.5 Flow characteristics for different heat source locations	93
3.6 Conclusion	94

Chapter 4. Numerical analysis of thermal performance of HPAM/PCM composite.	97
4.1 Introduction.....	99
4.2 Model of HPAM/PCM composite	100
4.2.1 Modeling method.....	100
4.2.2 Boundary conditions and validation.....	103
4.3 Determination of the optimized porosity of aluminum foam	106
4.3.1 Melting process of the composite with different porosities.....	106
4.3.2 Evaluation of the thermal efficiency of the composite.....	108
4.4 Enhancement methods of the effective thermal efficiency of composite	111
4.4.1 Description of methods and conditions	111
4.4.2 Melting characteristics of the enhancement methods.....	114
4.4.3 Comparison among three enhancement methods	118
4.4.4 Proposition of optimization methods.....	122
4.4.5 Comprehensive evaluation of enhancement methods.....	123
4.5 Conclusion	124
Chapter 5. Thermal behavior of aluminum foam/PCM composite with modified structure.....	127
5.1 Introduction.....	129
5.2 Heat transfer characteristic of the composite under constant temperature	130
5.2.1 Physical model.....	130
5.2.2 Effect of the porosity	132
5.2.3 Effect of the pore size.....	135
5.3 Proposition and investigation of the composite with modified structure.....	137
5.3.1 Description of the aluminum foam with modified structure	137
5.3.2 Validation of model of the aluminum foam with graded porosity.....	139
5.3.3 Melting characteristic of PCM in FFGP structure	141
5.4 Optimization of the structural parameters of FFGP structure.....	142
5.4.1 Effect of the thickness of metal fin.....	143
5.4.2 Effect of the porosity gradient	145
5.4.3 Effect of the pore per inch (PPI).....	146
5.5 Preliminary study of the aluminum foam prepared by 3D printing.....	148
5.5.1 Feasible methods	148
5.5.2 Manufacturing process of the aluminum foam with 3D printing method .	149
5.5.3 Thermal behavior of the aluminum foam prepared by 3D printing.....	151
5.6 Conclusion	153

Conclusions and perspectives	155
Conclusions	156
Perspectives	158
Résumé en français	159
1. Introduction	161
2. Analyse numérique des défauts de fabrication	163
2.1 Principe d'élaboration	163
2.2 Modélisation sur procédé de fabrication	163
2.3 Analyse numérique des causes des défauts	165
2.4 Prévention pour éviter les défauts	168
3. Etude de la performance thermique du composite MAFP/MCP	169
3.1 Procédé de fusion de la paraffine	169
3.2 Procédé de fusion du composite mousse d'aluminium/paraffine	170
3.3 Effet de la porosité sur le transfert de chaleur dans le composite.....	172
3.4 Modélisation de transfert de chaleur composite MAFP/MCP.....	173
4. Analyse numérique des performances thermiques du composite MAHP/MCP ...	176
4.1 Modèle physique	176
4.2 Détermination de la porosité optimisée.....	177
4.3 Méthodes d'amélioration de l'efficacité thermique efficace du composite	179
5. Comportement thermique de composite à structure modifiée en température constante.....	181
5.1 Modèle physique	181
5.2 Optimisation des paramètres de la structure modifiée.....	183
5.3 Etude préliminaire de la mousse d'aluminium élaborée par impression 3D...	185
6. Conclusion	186
References	190

T_u	upper melting temperature, K	se	effective value of solid
t	time, s	tc	thermocouple
		total	total melting
		w	wall

General introduction

Open-cell aluminum foam has the potential application in many domains due to its metal matrix and interconnected porous structure. As a kind of structure material, the mechanical behavior of open-cell aluminum foam has been studied more than ten years in our laboratory. In fact, open-cell aluminum foam is also a promising functional material which could be applied in thermal energy storage field. This thesis mainly focuses on the study of the thermal performance of the aluminum foam and its enhancement effect on the energy storage system.

Phase change material (PCM) is the critical material for thermal energy storage, which could store and release a mass of latent heat during the phase transition (solid/liquid). However, due to the small thermal conductivity, the pure PCM always suffers from the low efficiency of energy storage. In order to solve this problem, the scientists proposed the metal foam/PCM composite prepared by inserting metal foam into PCM. The addition of metal foam could enhance significantly the effective thermal conductivity, thus melting or solidification rate of PCM is improved. In the past decade, the most researchers studied the heat transfer characteristic in the composite by both experimental and numerical methods. But, to the author's knowledge, the investigation of the effect of metal foam on the energy storage performance is relatively rare.

The present work aims at the study of the thermal behavior of aluminum foams and aluminum foam/PCM composite to evaluate and improve the energy storage performance of the composite. The manufacturing process of the open-cell aluminum foam is first analyzed numerically in order to reduce the defects in the aluminum foam. The experimental investigation is then carried out to understand heat transfer characteristics of composites with different porosities. Two numerical models for low porosity aluminum foam (LPAF, $50 < \varepsilon < 85\%$) and high porosity

(HPAF, $\epsilon > 85\%$) are established to calculate the energy storage performance of these composites. Some methods are also proposed and compared to further improve the energy storage performance.

The chapter 1 presents a bibliographic study of aluminum foam and PCM. The preparation methods and thermal properties of aluminum foam are introduced as well as the characteristic of PCM. The literature review summarizes thermal performance enhancement methods for PCM and the research progress of the metal foam/PCM composite. Finally, modeling methods of the metal foam/PCM composite are also introduced.

In chapter 2, a 3D model is established to analyze the defects formed in the process of infiltration casting method. The numerical results could visualize the movement of the bubble in the molten liquid and solidification sequence of the sample. Besides, the effects of some manufacturing parameters on the defects are investigated, including temperature, pressure, and particle size. At last, we propose several remedy methods to reduce the defects.

In chapter 3, the experiment is performed to study the heat transfer characteristics of paraffin embedded in low porosity aluminum foam (LPAF). The temperature variations and the evolution of solid/liquid interface could reveal the heat transfer mode in the composite. The 3D macro models of LPAF/PCM composite are also established by using equilibrium model and non-equilibrium model.

The chapter 4 introduces the establishment of a 2D model of high porosity aluminum foam (HPAM)/PCM composite based on non-equilibrium equation. The energy storage efficiencies of composites with the porosity ranging from 65% to 95% are calculated to obtain optimized porosity. After determining optimized porosity, three enhancement methods are proposed and compared to further

enhance the energy storage efficiency of the composite. At last, combining the advantages of these methods, a new method is obtained which owns the largest melting rate.

The chapter 5 concerns the numerical analysis of the thermal behavior of the aluminum foam/PCM composite with constant temperature heat source. The effects of the porosity and pore size of aluminum foam on the energy storage performance are revealed. To further improve the thermal performance, we propose a modified structure named finned metal foam with graded porosity (FFGP), and optimize the structural parameters in FFGP. At last, the aluminum foam with Kelvin structure is prepared by combination of 3D printing and casting method, and the preliminary study of its thermal performance is carried out.

In chapter 6, the main conclusions of this thesis are summarized and some perspectives are provided for future studies.

Chapter 1.
**Bibliography: Metal foam/phase
change material composite**

Chapter 1. Bibliography: Metal foam/phase change material composite

1.1 Introduction.....	7
1.2 Preparation methods and related structure characteristics of metal foam.....	8
1.2.1 Infiltration casting method	8
1.2.2 Powder metallurgy method.....	9
1.2.3 Investment casting method	11
1.2.4 Electro-deposition method.....	12
1.3 Thermal properties of metal foam	13
1.3.1 Thermal conduction.....	13
1.3.2 Thermal convection.....	15
1.3.3 Thermal radiation	16
1.4 Application of metal foam in thermal energy storage.....	17
1.4.1 Phase change material	18
1.4.2 Enhancement methods of heat transfer.....	20
1.4.3 Research progress of metal foam/PCM composite.....	24
1.5 Modelling of heat transfer in metal foam/PCM composite	26
1.5.1 Micro model of metal foam.....	27
1.5.2 Macro model of metal foam	29
1.5.3 Model of phase transition process	31
1.6 Conclusion	33

1.1 Introduction

The metal foam is a porous structure consisting of metal matrix and void pores. This kind of material is firstly reported in a French patent proposed by Meller in 1926 [1], and the first commercial production is realized in 1990s. Due to the cellular structure, the metal foam is a promising material which possesses low density and high internal surface area. Until now, many research works are performed to investigate its mechanical, thermal and acoustic performances [2-4]. It is found that the metal foam has potential applications in many domains: aerospace, heat recovery, solar energy, transportation, etc.

At present, there are several kinds of metal foams as commercial products. According to the pore structure, the metal foams could be divided into two types[5]: closed-cell metal foam and open-cell metal foam, as presented in Fig. 1.1. It is observed that the pores in closed-cell metal foam are sealed and isolated from each other, while the open-cell metal foam has the interconnected structure. In this study, we mainly focus on the open-cell metal foam, thus the metal foam mentioned in the thesis always means the open-cell metal foam.

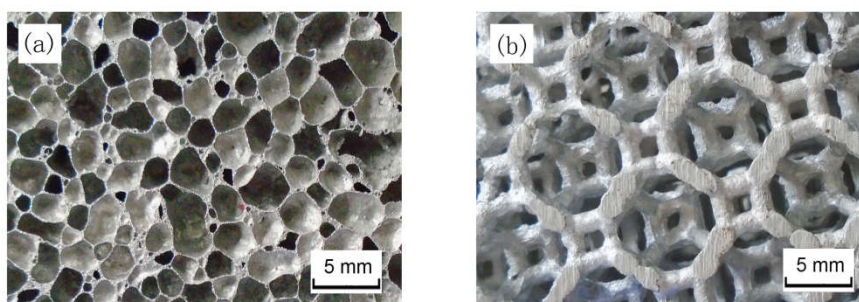


Fig. 1.1. Illustration of metal foam structures (a) closed-cell metal foam (b) open-cell metal foam

In this section, a review of the investigation of open-cell metal foam is performed. Firstly, the manufacturing method and the related structure characteristic of metal foam are introduced. The second part describes the thermal

properties of the metal foam. The third parts focus on the application of material, and the research works of the metal foam in the thermal energy storage are summarized. Finally, the modeling methods of the metal foam/PCM composite are presented, including micro model and macro model.

1.2 Preparation methods and related structure characteristics of metal foam

With the development of manufacturing technology, several the preparation methods of open-cell metal foam are proposed and modified in recent decades[6]. In order to obtain the interconnected pores, two kinds of technologies are applied generally in industry area: using the removable particles as preform and using the polymer foam as template[7]. According to the different manufacturing methods, the structures and properties of open-cell metal foam are also distinct, such as porosity, pore per inch (PPI), and permeability. In this section, several common manufacturing technologies of metal foam are described.

1.2.1 Infiltration casting method

Infiltration casting method is a traditional preparation method for open-cell metal foam, which could prepare the sponge of Al, Mg, and Zn. There are many advantages of this method, such as simple process, low cost, and good size and porosity control [8]. The salt particle is always applied as the preform to make the open cell structure. The schematic diagram of infiltration casting method is presented in Fig. 1.2. The main processes consist of injection, infiltration, and solidification. Firstly, the mold filled with the salts should be preheated to keep the viscosity of the molten metal during the infiltration process. Because the molten metal and salt are no wetting, the surface tension could prevent the liquid from filling up all the space between the salt partials. Hence, after the molten metal is

injected into the mold, the pressure should be conducted immediately to make the molten metal fills into the spaces between the preform. The pressure could be either negative or positive. After solidification, the sample will be put into the water to remove the preform. As a result, the interconnected structure in metal foam could be obtained.

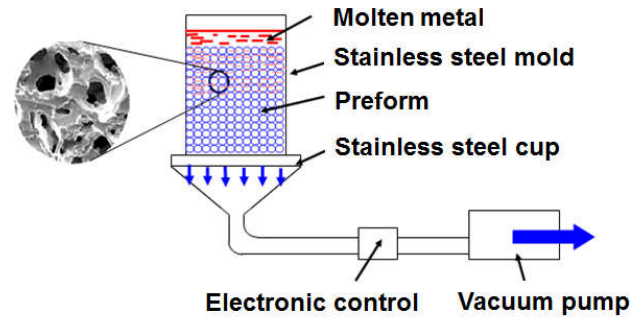


Fig. 1.2. Schematic diagram of infiltration casting method

The structure characteristics of metal foam prepared by infiltration casting method are illustrated in Fig. 1.3. It can be seen that the pore structure is based on the form of the particle. The pores, large metal ligaments, and the channels make up the open-cell metal foam. This kind of metal foam usually has the low porosity and good mechanical property, which could be applied in the metal foam/ polymer composite material and energy absorption domain [9].

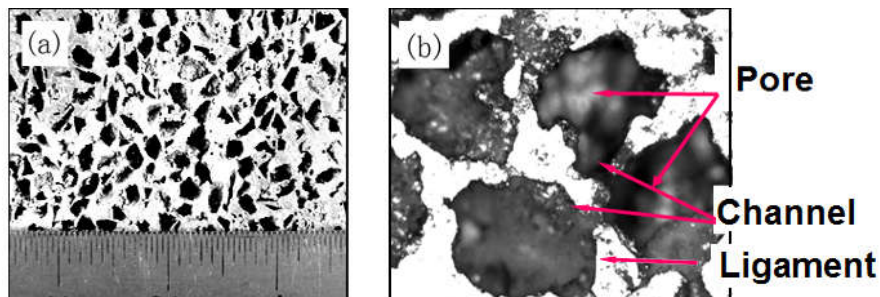


Fig. 1.3. Structure characteristics of metal foam prepared by infiltration casting method (a) macrostructure (b) microstructure

1.2.2 Powder metallurgy method

As the popular technology of the preparation of the composite material, the

powder metallurgy method could also be utilized to fabricate the open-cell metal foam. The detailed process of this method is presented in Fig. 1.4. Initially, the metal powder is mixed with the space holders in a rolling container. This mixture should be compacted to increase the density of the sample, and then the space holder is removed by either dissolution or heating methods. The sintering is final stage, which is usually performed near the melting temperature of the metal. The powder metallurgy method could produce the metal foam sample with varied shapes. Besides, because the removing process is prior to the sintering, the preform as the space holder does not need the high melting temperature. Therefore, the selection range of the preform material is widened. The porosity of the metal foam prepared by this method could be also controlled well. According to Ref. [10], the porous material with porosity as high as 98% could be realized by this method.

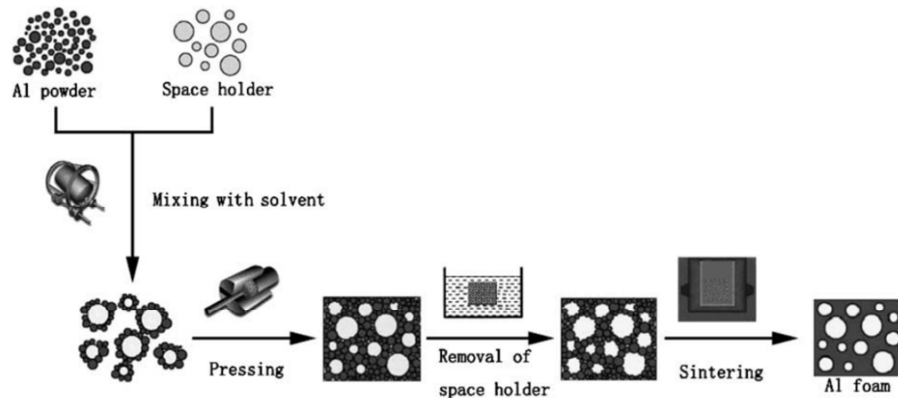


Fig. 1.4. Schematic diagram of powder metallurgy method [11]

Fig. 1.5 shows the structure of the metal foam prepared by powder metallurgy method. Due to the utilization of spherical space holder, the pore shape is directly related to the preform. The space between the spherical particles could not be filled with the metal power in the process of mixing and compacting, thus the open-cell structure could be obtained. Although the framework is constructed by individual metal particles, the microstructure of metal foam is relatively

homogenous, as presented in Fig. 1.5(b).

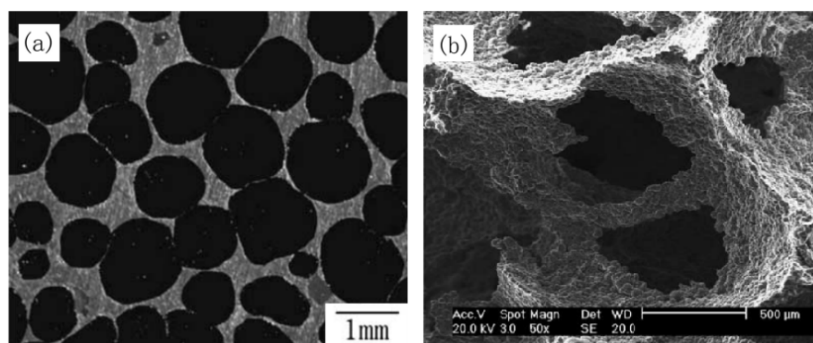


Fig. 1.5. Structure characteristics of metal foam prepared by powder metallurgy method (a) photograph (b) SEM image [11]

1.2.3 Investment casting method

The investment casting method adopts the polymer foam as the template to prepare the open-cell metal foam. The polymer foam always has the uniform cell size and reticulation structure. Through casting method, the molten metal will replace the structure of the polymer foam to obtain the metal foam. The manufacturing process is illustrated in Fig. 1.6, and it is described as following: (1) Filling the plaster into the polymer foam; (2) Eliminating the polymer by heating; (3) Injecting the molten metal into the mold; (4) Solidification of the metal foam; (5) Removing the plaster remained in metal foam.

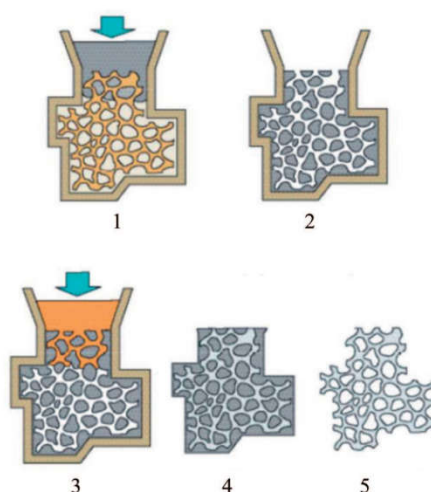


Fig. 1.6. Schematic diagram of investment casting method [12]

The metal foam prepared by investment casting method with polymer foam as template always has the 3D reticulated structure, as shown in Fig. 1.7. The porosity and permeability of this kind of metal foam are relatively higher than other products, thus it is considered that it has the potential application as the heat exchanger [13]. However, the mechanical performance is worse [14] because of the less volume of the metal and the thin of the ligament. So this metal foam is not suitable to be employed as the structural material.

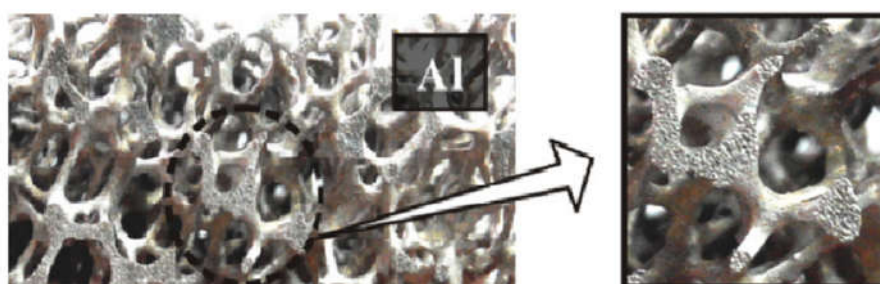


Fig. 1.7. Structure characteristics of metal foam prepared by investment casting method [15]

1.2.4 Electro-deposition method

In order to replace the polymer foam by metal, the electro-deposition method is developed in recent two decades, and the schematic diagram is depicted in Fig. 1.8. This method should be performed in the electrolyte with metal ions. With the help of the electric current, the metal ions could be deposited on polymer foam with the conductive coating. Finally, the polymer in the metal foam is removed by heating the sample. The electro-deposition method could produce nickel and copper foams with good pores connectivity and uniform structure. However, the structure of the metal foam produced by this method is hollow, as shown in Fig. 1.9. Thus, this kind of metal foam has a lower density than the product made by casting, which will worsen their mechanical and thermal performance [15].

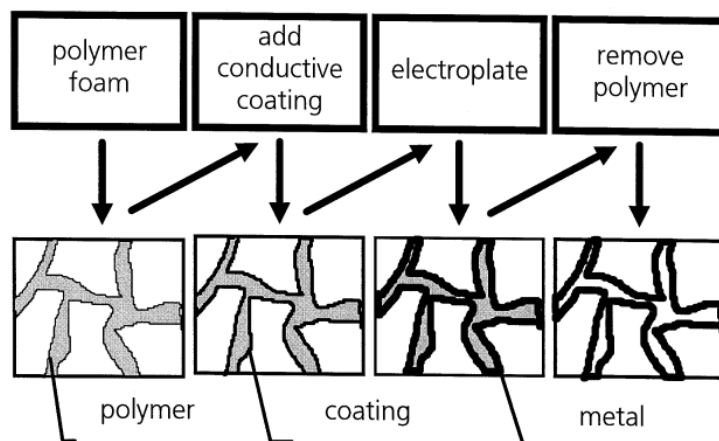


Fig. 1.8. Schematic diagram of electro-deposition method[16]

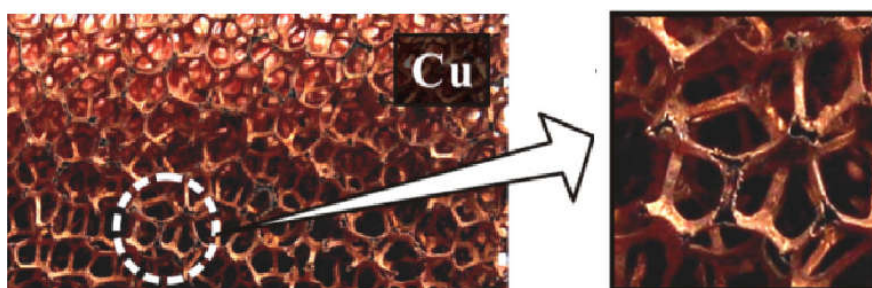


Fig. 1.9. Structure characteristics of metal foam prepared by electro-deposition method [15]

1.3 Thermal properties of metal foam

As the research continues, mechanical properties, thermal properties and acoustical properties of metal foam have been studied. In the thermodynamic field, the researchers consider that the open-cell metal foam is a promising material for heat exchanger [17, 18], because the high interior surface area and porous structure could contribute to the heat transfer process. Comparing with the traditional metal fin, the metal foam owns the similar surface area density and higher mechanical strength [19]. In this section, the thermal properties of metal foam are introduced, including thermal conduction, convection, and radiation.

1.3.1 Thermal conduction

The thermal conductivity is a vital parameter which could affect the

conductive heat transfer in the material. Since the metal foam could be treated as the composite material composed of metal and air, the effective thermal conductivity (k_{eff}) is considered as a meaningful parameter for the porous material [20]. Similar to solid material, the determination of k_{eff} of metal foam could adopt the steady-state method based on Fourier Law. Song and He [21] examined the k_{eff} of the metal foam with porosity 57%-67%, and the value of k_{eff} of high porosity metal foam is obtained by Calmidi and Mahajan [22]. Additionally, the analytical method is also developed to determine the value of k_{eff} . Due to the great difference in the thermal properties between metal and air, the mixture law, as shown in Eq.(1-1), is not suitable for the metal foam.

$$k_{eff} = \varepsilon k_f + (1 - \varepsilon)k_s \quad (1-1)$$

Where, k_f is the thermal conductivity of fluid; k_s is the thermal conductivity of solid; ε is the volume fraction of fluid. In order to consider the effect of structure and property of metal foam, some effective thermal conductivity models have been proposed by researchers [22-25], as listed in Table 1.1. It is found that the value of k_{eff} is mainly affected by the porosity and pore size of metal foam.

Table 1.1 Correlations of effective thermal conductivity of metal foam

Correlation	No.	Ref.
$k_{eff} = k_{\Pi}^F k_{\perp}^{(1-F)} ; F = C \left(0.3031 + 0.0623 \ln \left(\phi \frac{k_s}{k_f} \right) \right)$	(1-2)	[22]
$\frac{k_{eff}}{k_s} = \frac{1}{\sqrt{2}} \left\{ \frac{4\lambda}{2e^2 + \pi\lambda(1-e)} + \frac{3e-2\lambda}{e^2} + \frac{(\sqrt{2}-2e)^2}{2\pi\lambda^2(1-2e\sqrt{2})} \right\}^{-1}$	(1-3)	[23]
$k_{eff} = 0.35(\varepsilon k_f + (1 - \varepsilon)k_s) + \frac{0.65}{\left(\frac{\varepsilon}{k_f} + \frac{1 - \varepsilon}{k_s} \right)}$	(1-4)	[24]

1.3.2 Thermal convection

Due to the interconnected structure, the forced convection or natural convection existed in the metal foam could contribute significantly to the heat transport. In the past decades, many investigations of the convection in porous media have been carried out [26-28]. The metal foam could be treated as the porous media, thus some theories and expressions obtained in porous media are also applicable to the metal foam. Among these studies, Darcy law is one of the most important theories, which reveals the relationship between the flow velocity and the pressure gradient in porous media. The expression is as follow:

$$u = \frac{K}{\mu} \left(-\frac{dP}{dx} \right) \quad (1-5)$$

Where, u is the velocity; μ is the viscosity; P is the pressure; K is the permeability. The value of permeability is a critical parameter in the analysis of the flow in metal foam. The equation proposed by Ergun [29] is a general method to determine K , which is validated by the experiment results obtained in the packed bed. The correlation is expressed as:

$$K = \frac{d_p^2 \varepsilon^3}{150(1 - \varepsilon)} \quad (1-6)$$

Where, d_p is the average diameter of particle and ε is the porosity of packed bed. It is found that this correlation could be applied in the low porosity metal foam. Because the structure of high porosity metal foam is different with the packed bed, this equation is not suitable for metal foam with porosity above 85%. So far, some research works [30, 31] are conducted to obtain the permeability of high porosity metal foam. Despois and Mortensen [30] proposed a microstructure-based model for the permeability, and the expression is as follow:

$$K = \frac{\Delta r^2}{\pi} \left[\frac{\Delta - \Delta_0}{3(1 - \Delta_0)} \right]^{3/2} \quad (1-7)$$

Where, Δ is the solid density; Δ_0 is the initial packing density. This expression is available for the metal foam with porosity 60%-90%, thus it is applied in many literature reports for simulation of the heat transport in metal foam [32, 33].

Furthermore, the heat transport between metal foam and the fluid media is also very significant in the investigation of the thermal convection in metal foam. The heat transfer process is based on Newton' law of cooling, thus the heat transfer coefficient is of great importance. The determination methods of heat transfer coefficient are always obtained in the condition of forced convection by experimental or numerical methods. But, it is considered that this equation could also be used in the analysis of natural convection [34]. In Ref. [34-36], several common expressions of heat transfer coefficient are described. It is found that the heat transfer coefficient could be determined by either flow velocity (Re number) or temperature difference between solid and fluid (Ra number), and each equation has its own application scope. Therefore, it is noted that we should choice the appropriate equation according to the operation condition.

1.3.3 Thermal radiation

The thermal radiation in metal foam should be considered when it operates at high temperature condition. However, the related investigation for the metal foam is rare, and the models of radiation used in metal foam are almost obtained from the experimental or numerical results in packed bed. Besides, for the porous material, the radiation heat transfer is just about 10% of the heat conduction when it works at the temperature ranging from 300°C to 530°C [37]. Thus, at the low temperature(<100°C), the effect of thermal radiation could be neglected in the

analysis of heat transfer in metal foam.

1.4 Application of metal foam in thermal energy storage

To deal with the mismatch between the energy supply and consumption, the technology of thermal energy storage (TES) is always an attractive topic. The thermal energy is a low-grade form of energy, and it could be stored in different forms, such as sensible heat, latent heat, and reaction heat [38]. Thus, there are many technologies of TES applied in engineering applications. Among these methods, latent heat storage by using phase change material (PCM) is a promising way, because it has high energy storage density and could store and release the latent heat at a narrow temperature range[39]. Due to these advantages, the latent heat storage technology is applied in solar energy[40], heat recovery[41], energy conservation building[42], protection of electronic element[43], etc.

In the past decades, thermal performance of TES system with PCM has been studied to optimize the thermal efficiency or extend the application range. Fig. 1.10 shows the areas of research in TES system. It is found that the research of TES system involves two major parts: preparing the suitable PCM and enhancing the heat exchange in PCM. Our work mainly focuses on the second part, and the detail investigations will be discussed in the following.

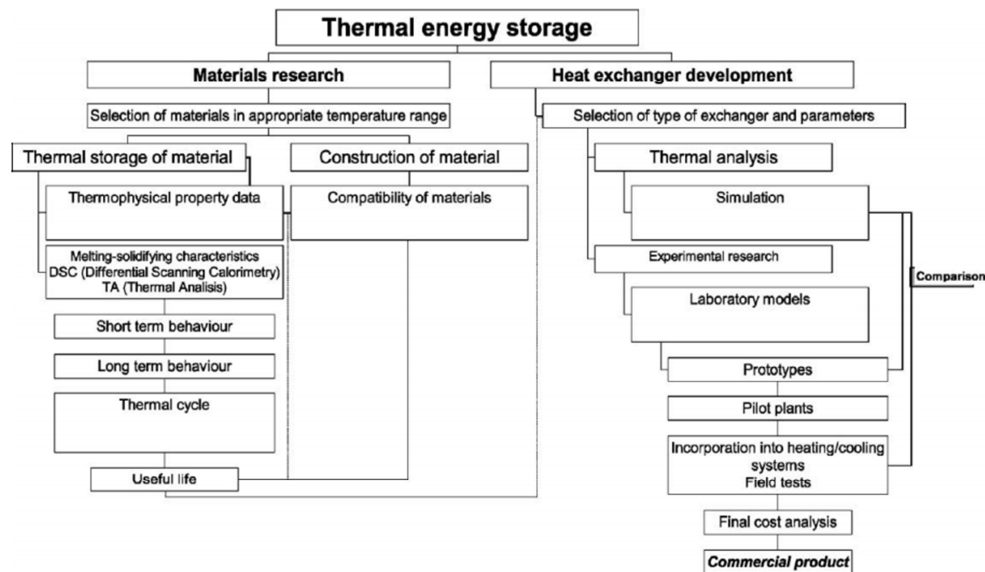


Fig. 1.10. Areas of research in thermal storage system [44]

1.4.1 Phase change material

The energy stored in the phase change material (PCM) concludes sensible heat and latent heat [45], and the basic principle of phase change energy storage is presented in Fig. 1.11. As the temperature increasing, the energy stored in the material is sensible heat at beginning. When the temperature reaches the melting point, the phase transition from solid to liquid occurs in the material. In this process, the increasing rate of temperature decrease and the energy is mainly stored as the form of latent heat. After PCM is totally melted, the sensible heat is accumulated continuously in liquid with the rising of the temperature. The PCM always has a large value of melting latent heat. For instance, the energy absorbed in the process of melting a given mass of ice is 80 times than increasing the temperature of the same mass of water (ice) by 1°C [46]. Therefore, PCM could store large amounts of energy during the phase change process with small temperature variation, which is worth to be further studied.

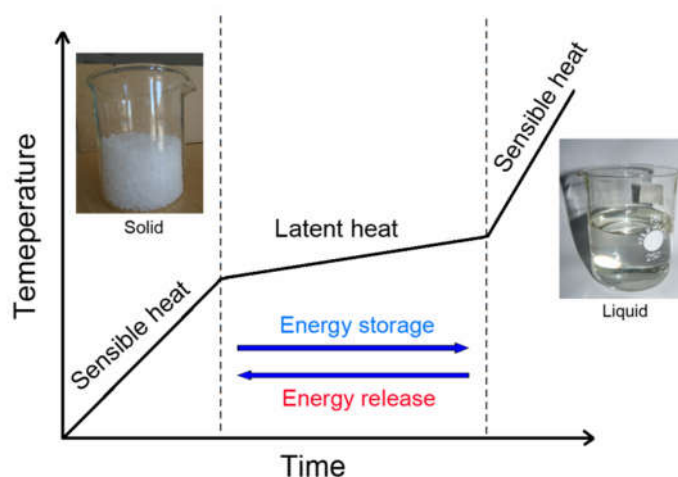


Fig. 1.11. Basic principle of energy storage and release of PCM

For many materials, the absorption and release of latent heat is accompanied with the phase transition process, but some important properties of the material are necessary if it is applied as PCM. They are described as following [47]: (1) the latent heat of PCM should be as large as possible, and the phase change temperature is fitted to the application condition; (2) the variation of the volume during the phase change should be small; (3) the chemical properties are stability, safety, nonflammable; (4) the phase separation should be avoided. Based on these characteristics, some kinds of PCM are developed and utilized in the industry and research domain, which could be classified into two types: organic material and inorganic material. Due to the different elements, these two types of PCM possess different properties. Table 1.2 lists the advantages and disadvantages of organic/inorganic materials. It is seen that both types of PCM are not perfect, thus we should select the suitable material according to the operation condition.

Table 1.2 Characteristics of the organic/inorganic PCM

Type	Representation materials	Advantages	Disadvantages
Organic PCM	Paraffin	No corrosive;	Low latent heat;
	Polyethylene glycol	Low undercooling;	Low thermal
	Fatty acid	Chemical and thermal stability	conductivity; Inflammability
Inorganic PCM	$\text{Na}_2\text{SO}_4 \cdot 10\text{H}_2\text{O}$	Large latent heat	Undercooling;
	$\text{Na}_2\text{HPO}_4 \cdot 12\text{H}_2\text{O}$		Corrosion;
	$\text{Na}(\text{CH}_3\text{COO}) \cdot 3 \text{H}_2\text{O}$		Phase separation;

Because PCM serves in the condition of heating–cooling cycle, the efficiency of heat transfer in PCM plays a vital role in TES system. However, the thermal conductivity of PCM is always low ($< 2 \text{ W m}^{-1} \text{ K}^{-1}$), which slows down the phase transition process and limits the practical application. So, this is a serious problem of PCM which should be solved.

1.4.2 Enhancement methods of heat transfer

As discussed above, most PCMs usually suffer from the low thermal conductivity. In order to improve the thermal performance of PCM, several methods have been developed, including (1) encapsulating PCM in microcapsule; (2) adding the particles with high thermal conductivity; (3) inserting metal matrix. Comparing with pure PCM, these methods could accelerate the heat transfer process in PCM, and the detail information is described below.

(1) Encapsulating PCM in microcapsule

The microencapsulation is deemed to be a method that could increase the heat exchange between heat source and PCM [48]. This technology divides PCM into many small sealed units by encapsulating PCM in microcapsule. Coacervation method and spray dry method are two common technologies to realize this process

[49]. The structure and profile of the microcapsule are presented in Fig. 1.12. Due to be covered by shell material, the PCM particles have many advantages like large heat transfer area per unit volume, high safety performance, ability to adapt various construction forms, etc. Thus, the microencapsulation of PCM is widely adopted in the energy saving building to adjust the temperature and reduce the CO₂ emission [50, 51].

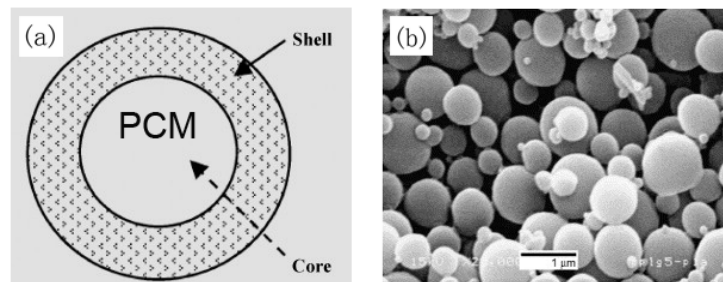


Fig. 1.12. Description of microcapsule (a) structural diagram[52] (b) SEM image[49]

For the research works of microencapsulation, the scientists mainly concern the preparation method and stability examination. The thermal performance of encapsulated PCM is always investigated in the form of slurry by numerical method [53-55]. However, Regin et al. [56] considered that the microencapsulation suppressed the natural convection and thus reduced the heat transfer rate. In fact, this opinion is worth to be studied, because none of the extensive comparisons is conducted for the performance between encapsulated PCM and pure PCM.

(2) Adding the particles with high thermal conductivity

It is found that the dispersion of the particles with high thermal conductivity in PCM could enhance significantly the thermal performance of TES system. With the development of the material science, the kinds of the additives are also various. There are some common particles in the literature: graphite, nano-particle, carbon fiber, etc[57-59]. The graphite possesses high thermal conductivity, porous

structure, and high absorbability. Thus, the thermal conductivity of PCM/graphite composite is improved greatly, as shown in Fig. 1.13. But, the preparation process of the composite needs more time and energy consumption if the pore size of graphite is very small [60]. With the advances of nanotechnology, the nano-particles become the interesting additives in PCM, such as nano-copper, nano-silver, and nano-aluminum. Wu et al.[61] compared the effect of three different nano-particles on the heat transfer rate, and the results indicated that the performance of Cu nano-particle dispersed in PCM is the best. However, the shortcoming of the nano-particles is the corrosion and compatible problem. Recently, it is found that the utilization of the carbon fibre could solve these problems exactly. The carbon fibre has the low density and the ability of compatible with most PCMs, thus the method draws the attention of many researchers [62-64].

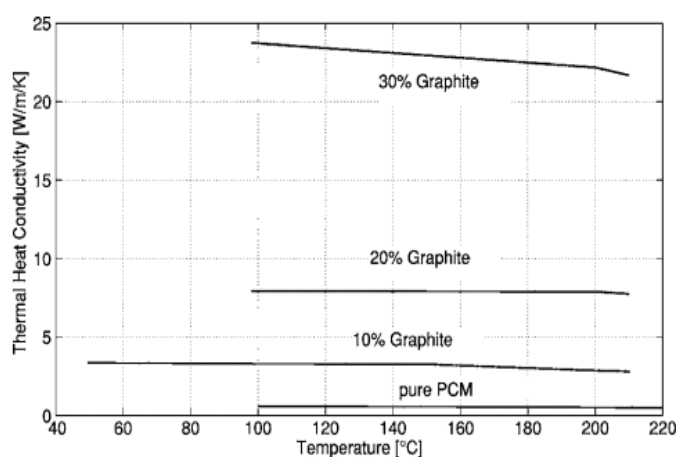


Fig. 1.13. Effective thermal conductivity of PCM/graphite composite dependent on temperature for various compositions [65]

Although the addition of particles could accelerate the heat transfer in PCM, the dispersion problem is still a limiting factor. The agglomerate and sedimentation in PCM will deteriorate greatly the thermal performance of TES system [66], thus the prevention method should be noted and adopted. Moreover,

as the increase of the additive fraction, the cost of the composite material increases and the energy storage capacity of the system reduces. Hence, the volume of the particle should be controlled and evaluated in the practical application to optimize the efficiency of TES system.

(3) Inserting metal matrix

Inserting metal matrix into PCM is another approach to increase the heat transfer rate of TES system. Due to the high thermal conductivity and the extended surface of the metal matrix, the energy could be transferred quickly from the heat source to the interior PCM. Fig. 1.14 illustrates three different configurations of metal matrix: metal fin, metal pin fin and metal mesh. Among these structures, metal fin is the most general configuration and it is investigated by many researchers [67-70]. The results in Ref. [70] demonstrated that the addition of metal fin could enhance the thermal conduction in PCM while the thermal convection will be hampered as increasing the number of fin. The detailed study has been performed by Lacroix and Benmadda [69], and it turned out that the optimum number of fin depended on the temperature of heat source. The addition of the metal matrix may increase the density of TES unit and reduce the total energy storage capacity, thus the determination of metal fraction should take into account of these factors.

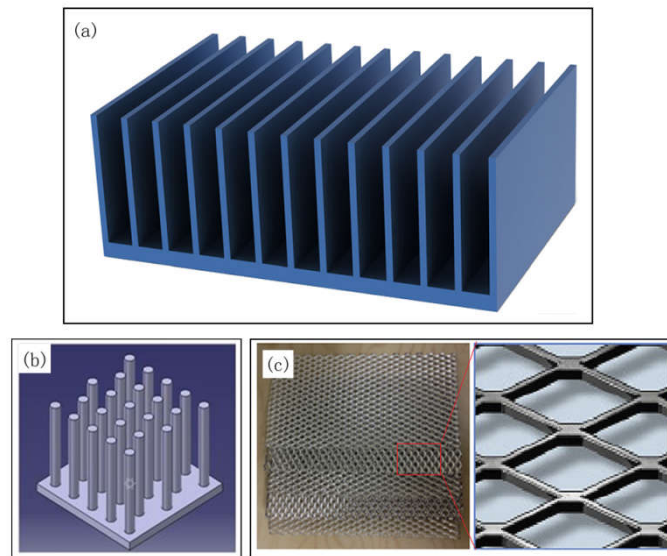


Fig. 1.14. Several common structure types of metal matrix (a) metal fin [71] (b) metal pin fin [72](c) metal mesh [73]

1.4.3 Research progress of metal foam/PCM composite

In the investigations of the enhancement methods, embedding PCM in metal foam to make metal foam/PCM composite is considered as an efficient method to improve the heat transport from heat source to PCM. Because the metal foam possesses the high thermal conductivity, the 3D porous structure, large interior surface area and good mechanical property, some drawbacks existed in others methods could be avoided by using metal foam, such as agglomerate, sedimentation and difficulty of preparation. Thus, this method draws the attention of many research workers. In the study of the heat transfer in metal foam/PCM composite, it is found that the heat flux is transferred to the entire region along the ligaments of metal foam and each PCM unit in the pore of metal foam could be heated by the metal foam matrix. So, the heat conduction of the composite is improved significantly by metal foam. Moreover, the natural convection of the melting PCM also exists in the composite due to the porous structure of metal

foam, which could enhance the heat transfer and make the temperature in the liquid region more uniform[48, 74]. In this case, the addition of metal foam could enhance the heat transfer rate of PCM [75].

For the investigation for the metal foam/PCM composite, the heat transfer process in the composite is complex which could be affected by many factors. Moreover, the ultimate purpose of this method is to improve the efficiency of energy storage. Therefore, the research works about composite mainly focus on two topics: heat transfer study and structure optimization.

(1) Heat transfer study

The heat transport of the metal foam/ PCM composite could be affected by porosity, pore size, metal matrix, input power, etc. Thus, many researchers concerned the effect of the metal foam parameters on the thermal conduction and convection in the composite. Lafdi et al. [76] examined the effect of the pore size and porosity on the phase change process by experiment. They found that the metal foam with lower porosity or smaller pore size enhances heat conduction and the higher porosity foam could be beneficial for the natural convection. Sundarram and Li [77] established a 3D model of metal foam, and they concluded that the smaller pore could help dissipate the heat more rapidly from the heat source. Zhao et.al [78] compared the both melting and solidification process of metal foam/PCM composite and pure PCM, the results revealed that the addition of metal foam could increase the overall heat transfer rate by 3-10 times. Liu et.al [79] analyzed the heat transfer enhancement of metal foam in a shell-and-cube type of TES system by numerical method, and they found that the heat transfer could be enhanced by seven times with the addition of metal foam. In conclusion, these results indicate that the melting rate of PCM is enhanced by the addition of metal foam. Although these works could conclude that the thermal behavior of PCM

embedded in metal foam is much better than that of the pure PCM, the metal foam requires deep-going research to obtain the optimized structure.

(2) Structure optimization

Recently, some researchers start to concern the effect of the macro structure of metal foam on the heat transfer in composite [80], and they propose a new kind of structure: the gradient metal foam, which could further enhance the property of TES system. The gradient metal foam is composed of metal foams with different porosities or pore sizes. The manufacturing method is different with the uniform ones, including investment casting with compressed preform, sintering method, and adhesion method [81-83]. Until now, the thermal performance of gradient metal foam attracts the interest of many scientists. Yang et.al [84] proposed the metal foam with linearly changed porosity, and the numerical results demonstrated that this structure could enhance the phase change process in PCM. Tao et.al [85] used Lattice Boltzmann method to investigate the effect of the nonuniform porosity on the heat transfer performance. Yang et.al [15] studied the metallic foam with graded morphologies by experimental method, and it is found that this structure could improve the solidification of the water saturated in it. The new structure could take full advantage of metal foam by coordinating the effect of thermal conduction and convection of PCM, which is worth to be investigated further.

1.5 Modelling of heat transfer in metal foam/PCM composite

The heat transfer process of PCM in metal foam is complex, which includes thermal conduction in metal foam, the heat exchange between metal foam and PCM, thermal convection in PCM, etc. For the phase transition of the composite,

the experimental approach could only record the temperature variation and the interface evaluation. Some phenomena occurring in the interior of the composite are difficult to be observed, and the temperature variation of the whole sample could not be obtained. These results are significant for the calculation of the energy storage performance. In order to solve the problem, the numerical method is applied by many researchers. With the simulation method, not only the transient results in the composite during the phase change process could be analyzed, but also it could reduce the development period of the product. As the skeleton material, the metal foam plays a vital role in the composite. Thus, the modelling method of metal foam is important for the simulation of the composite, which includes micro model and macro model.

1.5.1 Micro model of metal foam

The micro model of metal foam represents an individual metal foam unit, which consists of pores, metal ligaments and the nodes. The metal foam is considered as the combination of many micro models with periodic arrangement. Because the configuration of the micro model is based on the real metal foam, the scientists often use this geometry structure to predict and study the properties of metal foam, such as compression performance[86], thermal behavior[87] and permeability[88]. With the help of the micro model, the heat transfer process in the metal foam could be visualized numerically.

In order to obtain the structure of interconnect cellular, some 3D geometries are combined and modified. There are some micro models proposed in the literature, as presented in Fig. 1.15. Lu et.al [89] used the simple cubic unit cells as the model of metal foam, and this model could be applied to calculate the overall heat transfer coefficient and pressure drop. After that, the tetrakaidecahedron consisting of quadrangle and hexagon is developed by Boomsma and Poulikakos

[25], as shown in Fig. 1.15 (b). The authors found that this geometric shape could be used to estimate the effective thermal conductivity of the metal foam and the results agree well with the experiment data. This structure, which is defined as Kelvin model, is widely used in the investigation of metal foam because it is considered similar to the real metal foam [90, 91]. In addition, some other structures of metal foam could be obtained by subtracting the unit cell cube from the sphere located at body center [92] or face center [77], as shown in Fig. 1.15 (c) and (d). These kinds of foam structures are also applied in the analysis of thermal performance of metal foam, and the results obtained could be used to guide the practical application.

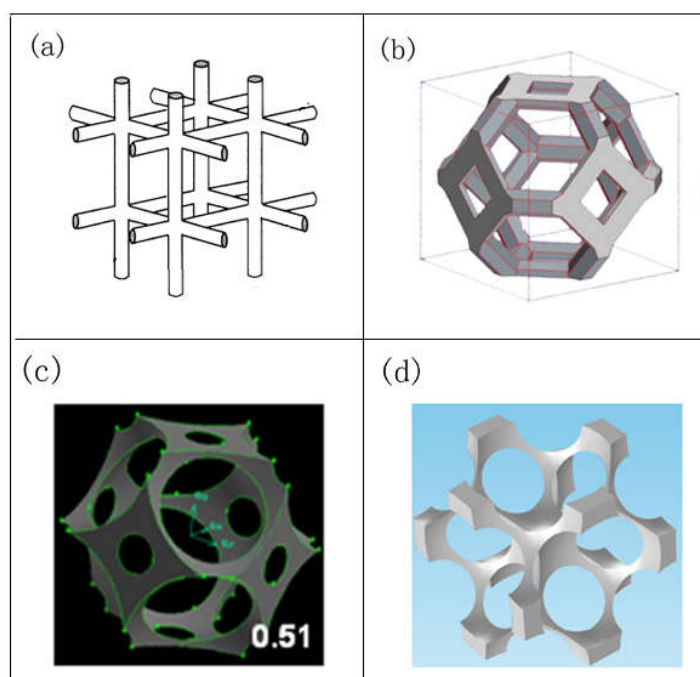


Fig. 1.15. Some common micro models of open cell metal foam

The research works using the micro model could demonstrate clearly the heat transfer in the metal foam and the heat exchange between metal and PCM. When the pore of metal foam is small, the natural convection is suppressed by metal foam and could be neglected. However, as the pore size increasing, the natural convection of liquid PCM will develop in the composite and contribute to the

melting process. In this case, the micro model could not meet the requirement of the analysis of the heat transfer in the composite. Thus, the macro model should be used to reveal the flow characteristics of the PCM embedded in metal foam.

1.5.2 Macro model of metal foam

In order to better understand the heat transfer process in porous structure, the heat convection in the metal foam is a vital part of the research task. As discussed above, due to the complex structure of the metal foam, the connective heat transfer in the whole region is difficult to be analyzed by micro model. In this condition, the macro model is applied by the researchers. For the macro model, there is no microscopic structure of the metal foam, and the fluid flow in the pores is neglected. The representative elementary volume is employed to represent the metal foam/PCM composite, which is a continuous and homogeneous region. The characteristics of the porous structure are realized by integrating the constitutive equations with some proper parameters and source terms. Therefore, the macro model could be used to investigate the heat transfer process in the composite, which is based on the comprehensive consideration of effect of both the thermal convection in the macroscopic zone and heat exchange in the microscopic pore.

In the macro model, the metal foam is supposed to homogeneous and isotropic. The liquid phase is treated as incompressible liquid, and the void volume of metal foam is assumed to be fulfilled with PCM in the simulation. The finite volume method (FVM) is always employed to discretize the governing equations of the macro model, which include continuity equation, momentum equation and energy equation.

Continuity equation:

$$\nabla \cdot \mathbf{U} = 0 \tag{1-8}$$

Momentum equation:

$$\frac{\partial \mathbf{U}}{\partial t} + \frac{1}{\varepsilon} (\mathbf{U} \cdot \nabla) \mathbf{U} = \frac{\mu}{\rho} \nabla^2 \mathbf{U} - \frac{\varepsilon}{\rho} \nabla P - \frac{\varepsilon}{\rho} \frac{\mu}{K} \mathbf{U} + \varepsilon g \gamma (T - T_0) + S \quad (1-9)$$

Where, \mathbf{U} represents the velocity field of liquid; ρ is the density; ε is the porosity of the foam; μ is the viscosity; K is the permeability; γ is the thermal expansion factor. The third term in the right side is based on Darcy law, which is used to analyze the suppression of the convective motion in the porous medium. The fourth term is deduced by Boussinesque approximation, and it is the driving force of the flow. The addition of the source term S in Eq. (1-9) is to calculate the flow velocity in the mushy zone. The source term is followed as:

$$S = \frac{C(1-\beta^2)}{\alpha + \beta^3} \quad (1-10)$$

Where, α is a constant; C is consecutive number for the mushy zone, and the value is fixed at 10^6 ; β is the liquid fraction.

For the energy equation, there are two kinds of methods applied in the investigation of heat transfer process of the metal foam/PCM composite, which are defined as equilibrium model and non-equilibrium model. The equilibrium equation model considered the metal foam/PCM composite as a single material, and the parameters in the equation are the effective value of two phases. This model is reliable when the temperature difference between the metal foam and PCM is small, and it is relatively simple and could shorten the calculation time [93]. The expression is as following:

$$(\varepsilon \rho_p c_p + (1-\varepsilon) \rho_s c_s) \frac{\partial T}{\partial t} + \rho_p c_p (\mathbf{U} \cdot \nabla T) = k_{\text{eff}} \nabla^2 T - \varepsilon \rho_p L \frac{\partial \beta}{\partial t} \quad (1-11)$$

Where, L is the latent heat; β is the volume fraction of the liquid; k_{eff} is the effective thermal conductivity.

Another model is non-equilibrium model. Because the thermal properties of metal foam and PCM are very different, the temperature difference between these two materials could not be neglected in some conditions [19]. In this case, the non-equilibrium model applies two energy equations for the PCM and metal foam, as described in Eq. (1-12) and Eq. (1-13). The interior surface area (A) and the heat transfer coefficient (h) in this model are utilized to calculate the heat exchange between the metal foam and PCM. This model could better reflect the temperature variation of different materials, thus it is always used in the investigations of the thermal convection in the composite [94, 95].

Energy equation for paraffin:

$$\varepsilon\rho_p c_p \frac{\partial T_p}{\partial t} + \varepsilon\rho_p c_p (\mathbf{U} \cdot \nabla) T_p = k_{pe} \nabla^2 T_p + hA(T_s - T_p) - \varepsilon\rho_p L \frac{\partial \beta}{\partial t} \quad (1-12)$$

Energy equation for metal foam:

$$(1 - \varepsilon)\rho_s c_s \frac{\partial T_s}{\partial t} = k_{se} \nabla^2 T_s + hA(T_p - T_s) \quad (1-13)$$

Where, h is the heat transfer coefficient; A is interfacial area density. k_{pe} and k_{se} are effective thermal conductivity of paraffin and metal foam.

1.5.3 Model of phase transition process

The phase transition process of PCM in this study mainly focuses on the melting and solidification process. During these processes, the phase and the properties of PCM will change as well as the position of the solid-liquid interface. The absorption or release of the latent heat also occurs accompanying with the evolution of the interface at the fixed temperature or the temperature range. For the analysis method, phase transition process is described by a particular kind of boundary value problem for partial differential equations [96, 97], while the

boundary in the equation will move with time. This question is called Stefan problem, and it is especially complicated due to many variable factors in phase change process. Evans [98] and Douglas [99] proved the existence and uniqueness of the solution, respectively. However, the analytical solutions are few in closed form and mainly for the one-dimensional case [100].

As research continues, an enthalpy formulation is proposed by Voller and Prakash [101] to make the moving boundary problem much simple. In this method, the solid-liquid interface is not tracked explicitly. Instead, a mushy zone is created between solid and liquid phase, in which the value of liquid fraction is between 0 and 1. The introduction of the mushy zone leads to a continuous computational region, which could be calculated by enthalpy method. The enthalpy (H) of the PCM is consists of sensible heat (h) and latent heat (ΔL), and the expression is as follow:

$$H = h + \Delta L \quad (1-14)$$

and where

$$h = \int_{T_m}^T \rho_p c_p dT \quad (1-15)$$

$$\Delta L = \beta \rho_p L \quad (1-16)$$

where, T_m is the melting temperature; L is the latent heat of PCM; β is the liquid fraction and it could be determined by Eq. (1-17)

$$\beta = \begin{cases} 0 & T_p < T_{m1} \\ (T_p - T_{m1}) / (T_{m2} - T_{m1}) & T_{m1} \leq T_p < T_{m2} \\ 1 & T_p \geq T_{m2} \end{cases} \quad (1-17)$$

For the phase change process, it is found that the enthalpy is the function of temperature, and the expression is defined in Ref. [102] as:

$$\frac{\partial H}{\partial t} = k \nabla^2 T \quad (1-18)$$

If the Eq. (1-15) and Eq. (1-16) are substituted in Eq. (1-18), an alternate form could be obtained in two dimensions, which could be taken as the basic of energy equation.

$$\rho c \frac{\partial T}{\partial t} = k \frac{\partial^2 T}{\partial x^2} + k \frac{\partial^2 T}{\partial y^2} - \rho L \frac{\partial \beta}{\partial t} \quad (1-19)$$

The enthalpy formulation is widely applied in the research about phase change problem [103, 104]. With the development of the finite element method and finite volume method, some simulation software also integrates this method into the model of melting and solidification. In this work, the model in ANSYS Fluent is taken as an example. In order to analyze the velocity on the interface, the mushy zone in this software is assumed to a porous medium whose porosity varies from 0 and 1. If the PCM is solid, the porosity is equal to zero and the flow is restricted. And, when the PCM totally melts, the value is equal to one. Based on this method, the flow velocity and the convective heat transfer of the interface could be obtained.

1.6 Conclusion

The open-cell metal foam is a promising material in the thermal energy storage. The metal foam/PCM composite, which is prepared by inserting metal foam into PCM, could enhance significantly the thermal conductivity of the energy storage system. As the skeleton material, the metal foam plays a critical role in the metal foam/PCM composite. A review of the investigation of metal foam is performed in this section, including manufacturing method, thermal properties, modeling method and the research progress in energy storage. It is found that the structure characteristics of metal foam, which is determined by the

manufacturing method, could directly affect the thermal properties. In the previous studies, the researcher mainly concerned the heat transfer process in the metal foam and the heat exchange between metal foam and PCM. The further researches of the effect of the structure of metal foam on the efficiency of energy storage are still needed. Thus, the work in this study aims at improving the efficiency of energy storage by optimizing the structure of metal foam. Both of the experimental and numerical methods are applied to analyze the thermal conduction and convection of the PCM embedded in metal foam.

Chapter 2.

Numerical analysis of the defects in aluminum foam

Chapter 2. Numerical analysis of the defects in aluminum foam

2.1 Introduction.....	37
2.2 Manufacturing process of the aluminum foam	38
2.2.1 Materials and equipment	38
2.2.2 Process of infiltration casting method	39
2.2.3 Common defects in aluminum foam	40
2.3 Modeling method of manufacturing process	41
2.3.1 Theory of infiltration process	42
2.3.2 Description of the model	45
2.3.3 Governing equations.....	46
2.3.4 Boundary condition and validation of the model	48
2.4 Numerical analysis of the causes of defects	50
2.4.1 Cause of the defect	50
2.4.2 Effect of the manufacturing parameters on the defect.....	53
2.4.3 Prevention of the defect.....	57
2.5 Conclusion	61

2.1 Introduction

In this section, the manufacturing process of aluminum foam is investigated by experimental and numerical methods to improve the quality of the products. As discussed above, there are several manufacturing methods for open-cell metal foam. According to the experiment conditions in our laboratory, the infiltration casting method is applied in this study to prepare the open-cell aluminum foam.

In the sample of aluminum foam, some defects are found occasionally at several special positions, which will deteriorate the properties of aluminum foam. In order to reduce the defects in the material, the investigation is conducted from three aspects. The first part is the preparation of aluminum foam with infiltration casting method. The materials, equipment and the experiment parameters are presented, and the positions of the casting defects in the samples are summarized. The second part concerns the modeling method of the manufacturing process, which is based on the theory of infiltration and three conservation equations. In last part, each stage of manufacturing process is analyzed numerically to find out the cause of the defects in the aluminum foam. And, the effects of the experiment parameters in manufacturing process on the defects are also investigated, like temperature, pressure, and particle size of salt.

The numerical results reveal the causes and the influencing factors of these defects. Based on these conclusions, several remedy methods are proposed for each stage to reduce the defects. Finally, the numerical and experimental results indicate that these methods are efficient for improving the quality of aluminum foam.

2.2 Manufacturing process of the aluminum foam

2.2.1 Materials and equipment

For the infiltration casting method, the interconnected structure in aluminum foam is generated by the preform, and the shape and size of the pore are based on the preform particle. Thus, the preform is very important for the structure and quality of final product. There are two requirements of the properties for the preform: high melting temperature and good solubility. In this study, the salts particles are chosen as the preform, and the type of aluminum matrix is AS7G. The casting mold is made of stainless steel. The thermal properties of the material used in the experiment are listed in Table 2.1.

Table 2.1 Thermal properties of the materials [105, 106]

Material	Property	Value	Unit
AS7G	Density of liquid	2380	kg m ⁻³
	Specific heat	963	J kg ⁻¹ K ⁻¹
	Thermal conductivity of liquid	85	W m ⁻¹ K ⁻¹
	Thermal conductivity of solid	160	W m ⁻¹ K ⁻¹
	Latent heat	389	kJ kg ⁻¹
	Solidus temperature	555	°C
	Liquidus temperature	615	°C
Mold	Density	8030	kg m ⁻³
	Thermal conductivity	502	W m ⁻¹ K ⁻¹
	Specific heat	16	J kg ⁻¹ K ⁻¹
Salt	Density	2185	kg m ⁻³
	Thermal conductivity	1030	W m ⁻¹ K ⁻¹
	Specific heat	4.6	J kg ⁻¹ K ⁻¹

In order to obtain the uniform size of salt particles, the screening machine AS 200 basic Retsch® is applied. Seven kinds of particle sizes could be acquired by this screening machine, including 1.9; 1.6; 1.25; 1.01; 0.81; 0.58; 0.365 mm. The

aluminum ingots are melted in a tilting furnace Labotherm K4/10. This kind of furnace allows the fast heating and it could be controlled easily. The pump is produced by Busch, which could generate the maximum negative pressure of 70k Pa. Moreover, an infrared camera (VarioCAM®) is also used to observe the temperature distribution of the mold during the manufacturing process.

2.2.2 Process of infiltration casting method

Before the casting process, the pretreatment of the mold with preform is important, because the bulk density of the preform plays a vital role in the final porosity of aluminum foam. Thus, the salt particles should be filled in the mold with the proper volume and density. After that, the mold will be heated to 650°C and kept at this temperature for 3 hours. This process aims at keeping the fluidity of molten aluminum and avoiding the solidification during the filling process. It is worth to note that the temperature rise rate could not be very large; otherwise the salt particle will crack due to the variation of the temperature.

The process of infiltration casting consists of three steps: injection, infiltration and solidification. The schematic diagram of these steps is presented in Fig. 2.1. In the injection process, the molten aluminum (700°C) is poured into the mold. Due to the existence of surface tension force, the liquid could not fill into the preform by gravity. Thus, the negative pressure should be conducted immediately to make the aluminum infiltrate into the space between the salt particles. The infiltration process is quick when the viscosity of the molten aluminum is small. The final step is the solidification, and the mold with sample will be cooled at ambient temperature. After taking out from the mold, the aluminum/salt composite, as illustrated in Fig. 2.2 (a), will be placed in the water to remove the salt. At last, the aluminum foam with open cell is obtained and cut into pieces, as shown in Fig. 2.2(b).

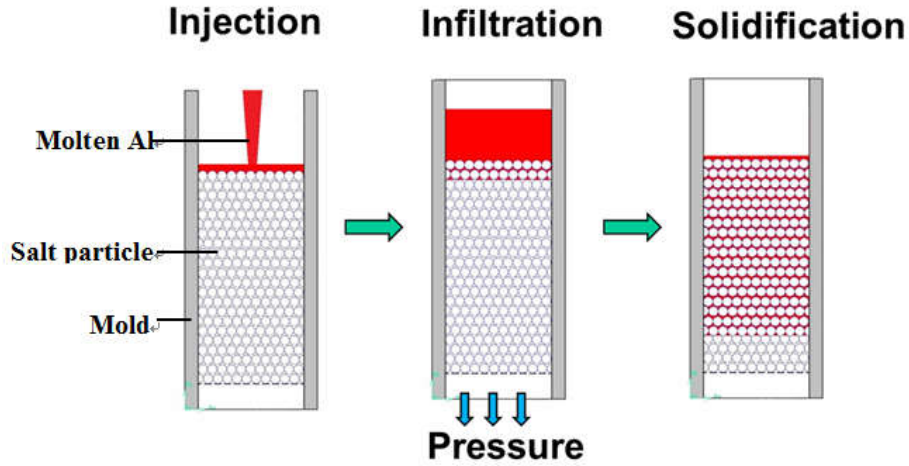


Fig. 2.1. Schematic diagram of infiltration casting method

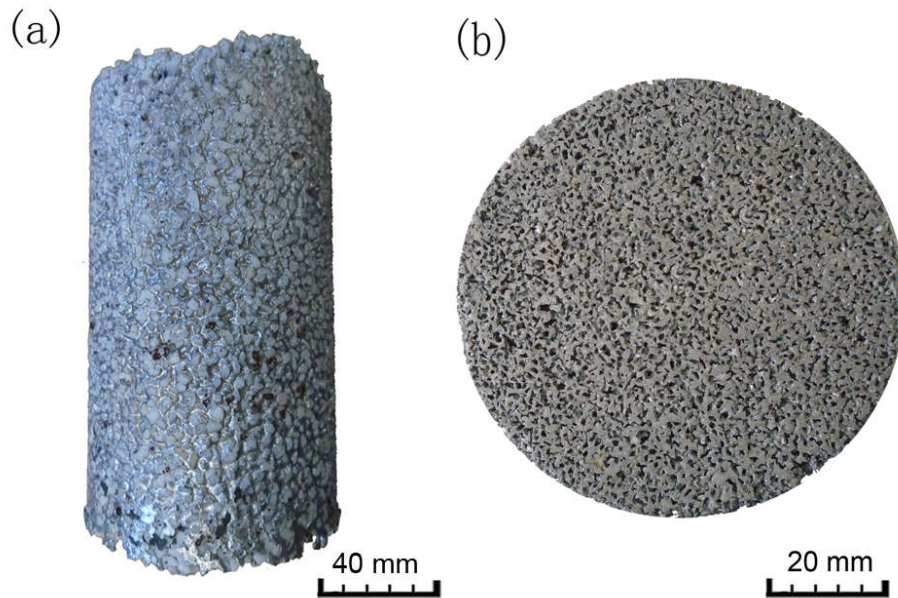


Fig. 2.2. Photograph of samples (a) aluminum/ salt composite (b) open-cell aluminum foam

2.2.3 Common defects in aluminum foam

For the porous material, the pore size is always uniform or fluctuates in a narrow range. Thus, the defect in metal foam is defined as the void cavity that is much larger than the normal pore. In the manufacturing process, the defects are usually found in the sample and these defects mainly appear at some special positions. As presented in Fig. 2.3, the defects could appear in the center of the sample (both at the top and bottom), or on the surface of the cylinder. These

defects will reduce the yield of the product and deteriorate significantly the properties of the metal foam. Through observing the positions of these defects, it is considered that the causes of these defects in aluminum foam have the relationship with the preparation process. Therefore, each step of manufacturing process should be analyzed and optimized to reduce the defects. Due to the complexity of the infiltration process, the numerical method is applied in this study, and the details of modeling method are described in the following section.

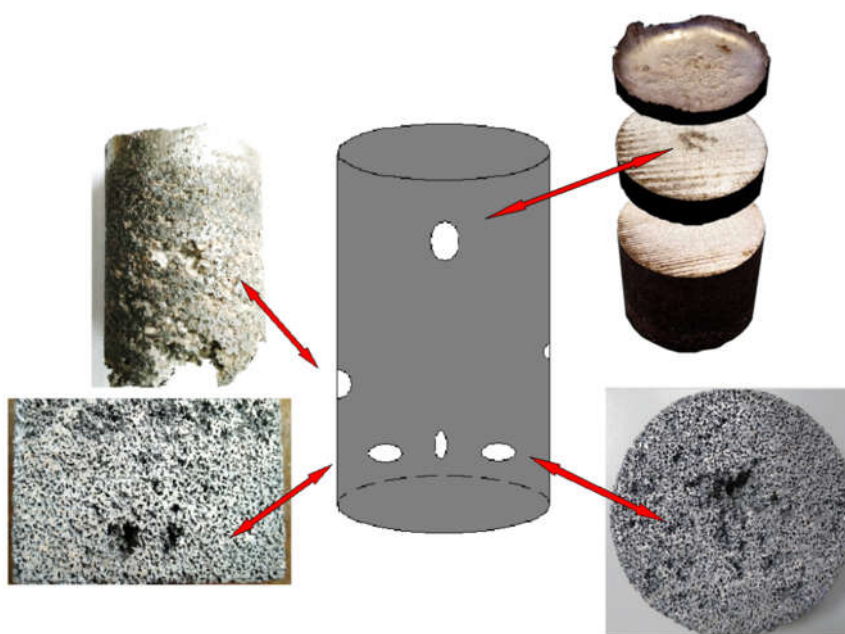


Fig. 2.3. Defects in the sample of aluminum foam

2.3 Modeling method of manufacturing process

Infiltration casting method is one of the traditional technologies to prepare metal matrix composite. In the previous simulations of the manufacturing process of composite [107, 108], it is found that the infiltration process is the most important step, which could be treated as the problem of fluid through porous medium. For the preparation of aluminum foam, the condition and principle of flow are similar to the manufacturing process of composite. Therefore, like the numerical analysis of composite, the modeling method in this study follows the

theory of infiltration and three conservation equations. And, the numerical analysis of the whole manufacturing process, including injection, infiltration and solidification, is based on the volume of fluid (VOF) and k-epsilon model in non-isothermal condition.

2.3.1 Theory of infiltration process

The infiltration of molten aluminum through the stacked salt particles is a complex process, because it involves the multiphase flow (air and liquid) in the porous media. Besides, the infiltration process could also be affected by several factors: size of preform, temperature, pressure and surface tension. Until now, the infiltration processes in common conditions could be well explained [109-111]. These research works are mostly according to capillary law and Darcy law, which are two useful theories for the infiltration process.

(a) Capillary law

For the infiltration process, it is noted that the molten aluminum is non-wetting for the salt particles. There is an upward force (F) generated by surface tension in the liquid, which prevents the liquid from filling in the void space by gravity, as presented in Fig. 2.4. Thus, in order to overcome the surface tension, a minimum pressure should be conducted which is called threshold pressure, P_0 . The determination method of threshold pressure is proposed by Garcia et.al [112]. If the preform particles are treated as sphere, the expression of threshold pressure is as following:

$$P_0 = 6\gamma \cos\theta \frac{V_p}{d_p(1-V_p)} \quad (2-1)$$

where, γ is the surface tension of aluminum liquid; θ is the contact angle at liquid/solid interface; V_p is the particle volume fraction; d_p is the average diameter of particle.

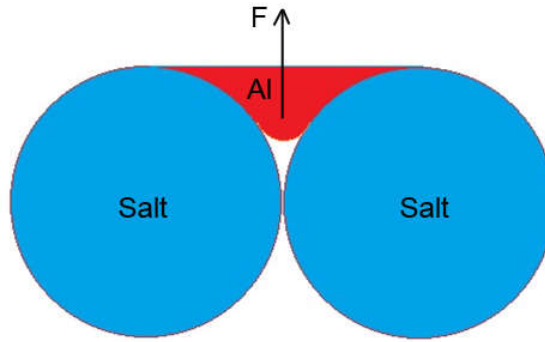


Fig. 2.4. Schematic of the non-wetting phenomenon between molten aluminum and salt particles

In the manufacturing process, the value of threshold pressure is estimated firstly, and the negative pressure should be large than this value. In our experiment, it is found that the value of V_p has no relationship with the particle size, and it is always at about 0.52 without compaction. Thus, if V_p is fixed at a constant value, the threshold pressure is the function of pore size. The surface tension γ and contact angle is 0.85 N m^{-1} [113] and 152° [114], respectively. The calculation results of P_0 are shown in Fig. 2.5. It is seen that the threshold pressure reduces as the increase of the salt size. Thus, for the small particle, a large negative pressure should be performed to make the liquid penetrate into the porous media.

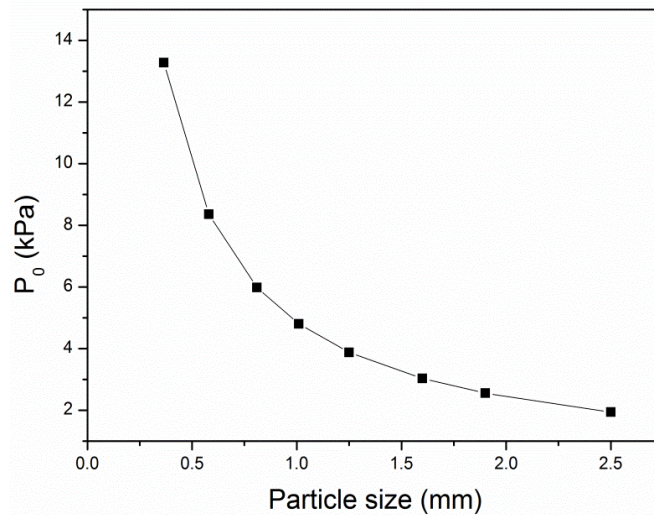


Fig. 2.5. Threshold pressure (P_0) as a function of the particle size

(b) Darcy law

Darcy's law is utilized to describe the relation between velocity and pressure drop for the infiltration in the porous zone. However, the classical form of Darcy's law, as shown in Eq. (1-5), is deduced in the condition that the porous region is fulfilled with liquid. In fact, the infiltration process could be treated as the process that the liquid replaces the position of air in the porous media. This process involves the movement of the two-phase flow in the preform. Due to the surface tension and non-wetting phenomenon, the void space could not be occupied totally by liquid. In order to analyze the infiltration process of the non-saturated flow, the relative permeability is introduced in Darcy's law [115] and the new equation is called Extended Darcy's law, as given by:

$$\mathbf{v} = -\frac{K_s K_r}{\mu} \nabla P \quad (2-2)$$

where, K_s is the specific preform permeability and it is a physical property of material; K_r is relative permeability. The relative permeability is a scalar with the value between 0 and 1, and it is depended on the saturation of two flows. The relationship between relative permeability and saturation could be described by Eq. (2-3).

$$K_r = A s^B \quad (2-3)$$

where, A and B are constant and s is the saturation which is equal to the ratio of the liquid volume to the initial void space. T. Dopler et.al [116] studied the infiltration process of metal-matrix composite and found that the numerical results have the best agreement with experimental results when A and B equal to 1. Besides, for the saturation, S.Y. HE [117] considered the surface tension of the molten aluminum will prevent the liquid from filling all the void space. He established a geometry model to calculate the volume of air, as presented in Fig. 2.6. Finally, he found that

the air fraction is the function of particle size (d_s) and negative pressure (P).

$$V_{air} = \int_0^a \pi(kY^2 + d)^2 dY - \int_0^a \pi [R^2 - (Y - R)^2] dY \quad (2-4)$$

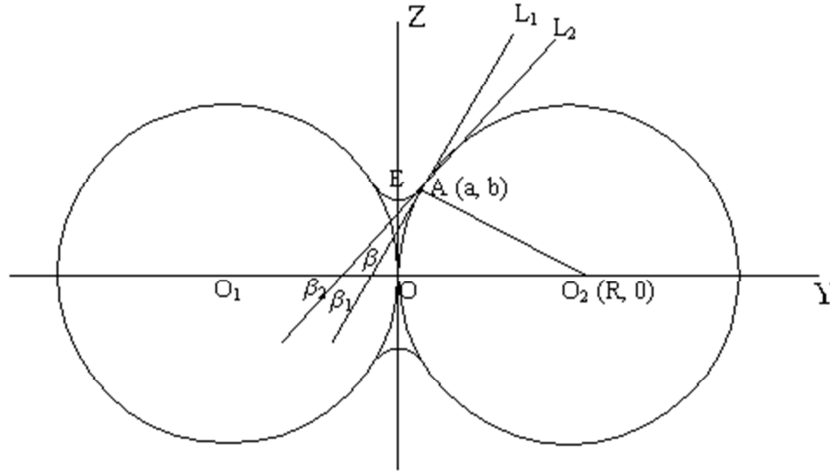


Fig. 2.6. Geometry model of the air distribution between two particles

As a result, the saturation could be calculated by the equation $s = 1 - V_{air}/V_{void}$. The relative permeability could be determined by their results and the relationship between K_r , d_s and P is shown in Fig. 2.7.

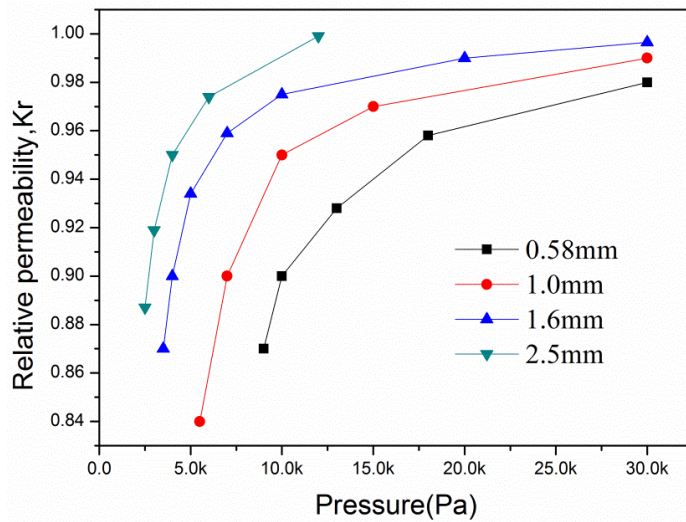


Fig. 2.7. Relative permeability as a function of pressure for different particle sizes

2.3.2 Description of the model

Fig. 2.8 shows the dimension of the cylinder mold (the black part) filled with

preform (the green part). The height (H) and diameter (D) of the mold are 240 mm and 100 mm, respectively. For the preform, the height (h) is 160 mm and the diameter (d) is 80 mm. The aluminum alloy chosen for this study is AS7G and the mold is made of stainless steel.

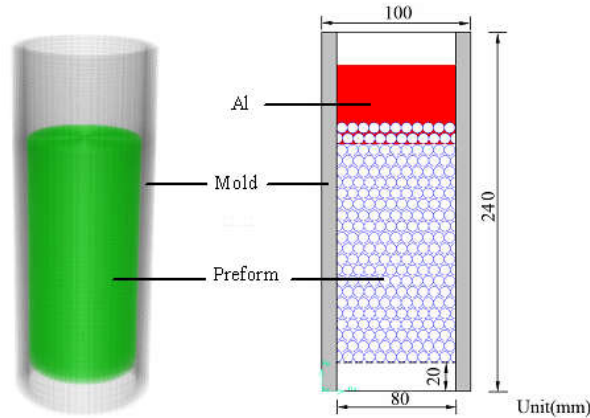


Fig. 2.8. Dimension of the model

The phenomena governing infiltration is always complex, particularly the penetration and heat transfer in the porous preform. In order to simplify the analysis, some assumptions are adopted in the simulation: (1) The part of the preforms is uniform and isotropic without defects; (2) During the processes of injection and infiltration, the deformation of the preform will not occur; (3) The thermal properties of molten aluminum are the function of temperature.

2.3.3 Governing equations

For the simulation of the manufacturing process, the molten aluminum will be considered as the incompressible viscous liquid. The following conservation equations can be applied:

(1) Continuity equation:

$$\frac{\partial \rho}{\partial t} + \frac{\partial(\rho u)}{\partial x} + \frac{\partial(\rho v)}{\partial y} + \frac{\partial(\rho w)}{\partial z} = 0 \quad (2-5)$$

where, ρ is density; u, v, w are dimensional velocities in x, y and z direction, respectively.

(2) Momentum conservation equation:

$$\rho \left(\frac{\partial u}{\partial t} + u \frac{\partial u}{\partial x} + v \frac{\partial u}{\partial y} + w \frac{\partial u}{\partial z} \right) = \mu \left(\frac{\partial^2 u}{\partial x^2} + \frac{\partial^2 u}{\partial y^2} + \frac{\partial^2 u}{\partial z^2} \right) - \frac{\partial p}{\partial x} - \frac{\mu}{K_s K_r} u + \frac{1}{2} C_i \rho u |u| \quad (2-6)$$

$$\rho \left(\frac{\partial v}{\partial t} + u \frac{\partial v}{\partial x} + v \frac{\partial v}{\partial y} + w \frac{\partial v}{\partial z} \right) = \mu \left(\frac{\partial^2 v}{\partial x^2} + \frac{\partial^2 v}{\partial y^2} + \frac{\partial^2 v}{\partial z^2} \right) - \frac{\partial p}{\partial y} - \frac{\mu}{K_s K_r} v + \frac{1}{2} C_i \rho v |v| \quad (2-7)$$

$$\rho \left(\frac{\partial w}{\partial t} + u \frac{\partial w}{\partial x} + v \frac{\partial w}{\partial y} + w \frac{\partial w}{\partial z} \right) = \mu \left(\frac{\partial^2 w}{\partial x^2} + \frac{\partial^2 w}{\partial y^2} + \frac{\partial^2 w}{\partial z^2} \right) - \frac{\partial p}{\partial z} - \frac{\mu}{K_s K_r} w + \frac{1}{2} C_i \rho w |w| \quad (2-8)$$

where, μ is dynamic viscosity; C_i is inertial resistance factor; K_s is the specific preform permeability and it is obtained by Eq.(1-6); K_r is according to the results in Fig. 2.7.

(3) Energy equation:

$$\frac{\partial T}{\partial t} \left[(1-\varepsilon) \rho_s c_s + \varepsilon \rho_f c_f \right] + \rho_f c_f \left(u \frac{\partial T}{\partial x} + v \frac{\partial T}{\partial y} + w \frac{\partial T}{\partial z} \right) = k_{eff} \left(\frac{\partial^2 T}{\partial x^2} + \frac{\partial^2 T}{\partial y^2} + \frac{\partial^2 T}{\partial z^2} \right) + \varepsilon \rho_f L \frac{\partial \beta}{\partial t} \quad (2-9)$$

where, ε is porosity; ρ_s and ρ_f are densities of solid matrix and fluid material; c_s and c_f are specific heats of solid matrix and fluid material; L is latent heat; β is volume fraction of the liquid; k_{eff} is the total thermal conductivity and it is determined by the equation:

$$k_{eff} = \varepsilon k_f + (1-\varepsilon) k_s \quad (2-10)$$

$$\varepsilon = 1 - \frac{V_{salt}}{V_{preform}} \quad (2-11)$$

where, V_{salt} is the volume of salt; $V_{preform}$ is the volume of packed bed of preform.

2.3.4 Boundary condition and validation of the model

(a) Initial and boundary conditions

Based on the experimental values, the initial temperature of the mold and preform are $T=630$ °C. The volume fraction of the aluminum in the mold is equal to zero. For the boundary conditions, in the processes of injection and infiltration, because these processes are conducted at ambient temperature, the heat of the mold escapes into surrounding air by convection and radiation with following equations:

For the mold bottom:

$$\frac{\partial T_m}{\partial y} = 0 \quad (2-12)$$

For the mold surface:

$$k_m \left(\frac{\partial T_m}{\partial x} + \frac{\partial T_m}{\partial z} \right) = h(T_{amb} - T_m) + e\sigma(T_{amb}^4 - T_m^4) \quad (2-13)$$

where, T_m is the temperature of the mold; h is heat transfer coefficient, e is emissivity of stateless and σ is Stefan-Boltzmann constant.

The entrance of injection is located at the center of the mold top and its diameter is 8 mm. The injection velocity and temperature are:

$$v_x=v_z=0, v_y=-1 \text{ m s}^{-1} \ \& \ T_{al}= 700 \text{ °C}; \quad (2-14)$$

The infiltration pressure is applied on the mold bottom and the value is:

$$P_x=P_z=0, P_y=-P \quad (2-15)$$

(b) Validation

In order to check the model and the thermal parameters, the infrared camera is used to measure the temperature change of the mold during the manufacturing process, and the results are depicted in Fig. 2.9. Four detected points will be placed in the real mold and numerical model at the same positions, as shown in Fig. 2.10.

Because the periods of the injection and the infiltration are relatively short, the obtained results mainly show the temperature change during the solidification. Fig. 2.11 presents the comparison of the experimental and numerical results. It is obviously that the numerical results are in agreement with the experimental dates. The model could reflect the real manufacturing process and it could be used to optimize the parameters in the manufacture. The deviation is to blame for using the law of mixtures to determine the effective thermal conductivity and the neglect the gap that generates between the mold and aluminium during solidification.

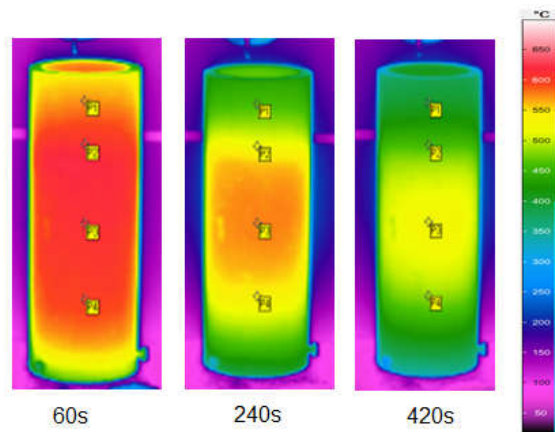


Fig. 2.9. Temperature distributions of the mold during

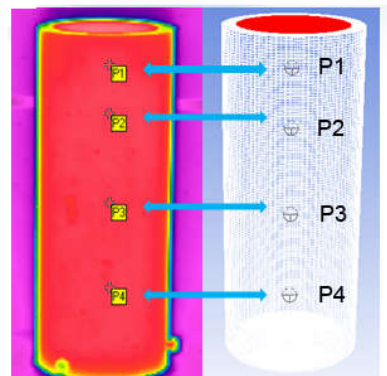


Fig. 2.10. Position of the detected points on the surface of the mold

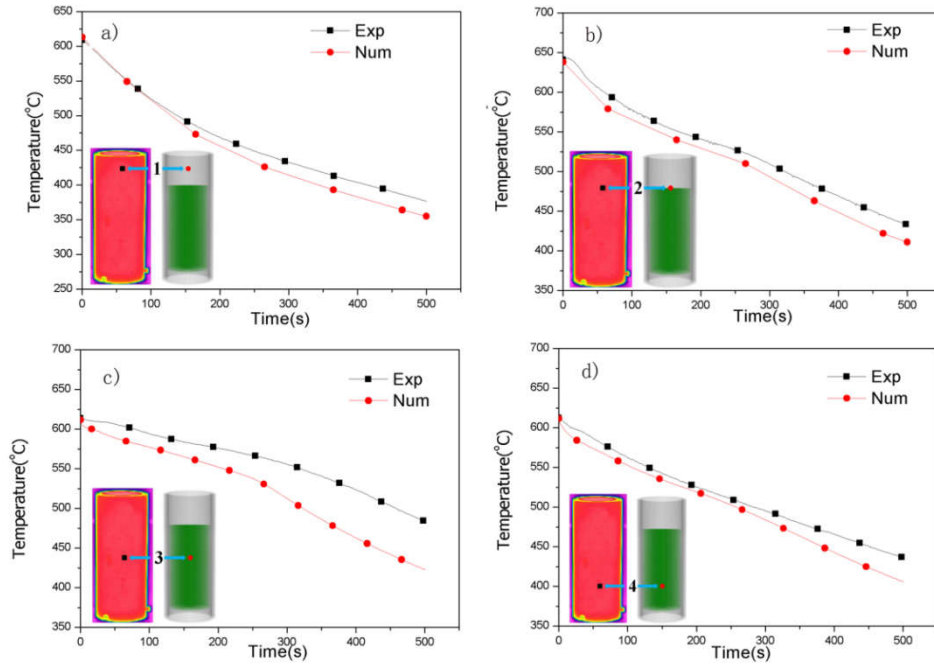


Fig. 2.11. Comparison between the experimental and simulation results

(a) Point 1 (b) Point 2 (c) Point 3 (d) Point 4

2.4 Numerical analysis of the causes of defects

2.4.1 Cause of the defect

The defects in aluminum foam may occur in all the casting process, thus we should analyze numerically each step of the manufacturing process: the injection, infiltration and solidification. In these simulations, certain phenomena should be concerned, such as the motion of liquid and bubbles, the distance of infiltration and the solidification sequence.

(a) Injection

Many casting simulations have neglected the injection process due to its short duration [118]. However, when the liquid aluminum at 700 °C is poured directly on the top of the porous preform at 630 °C, the temperature, velocity and viscosity of the molten liquid will change dramatically. Therefore, the investigation of the injection process is significant. Fig. 2.12(a) shows the process that the molten

aluminum is injected in the mold with preform. It is seen that the molten aluminum is poured from the center of the entrance, and then the surface of liquid rises steadily. At this moment, only a small part of aluminum penetrates in the preform, which is attributed to the surface tension. In this process, it is obvious that some bubbles would mix in the molten aluminum as shown in Fig. 2.12(b). Because of the temperature difference between the mold and the molten aluminum, the liquid viscosity will increase when the molten metal contacts the preform. In this case, some bubbles will be trapped in the liquid. In the top view of the mold, most of the bubbles distribute in the interior surface of the mold. These bubbles will become a disturbance for the following process, as shown in Fig. 2.13.

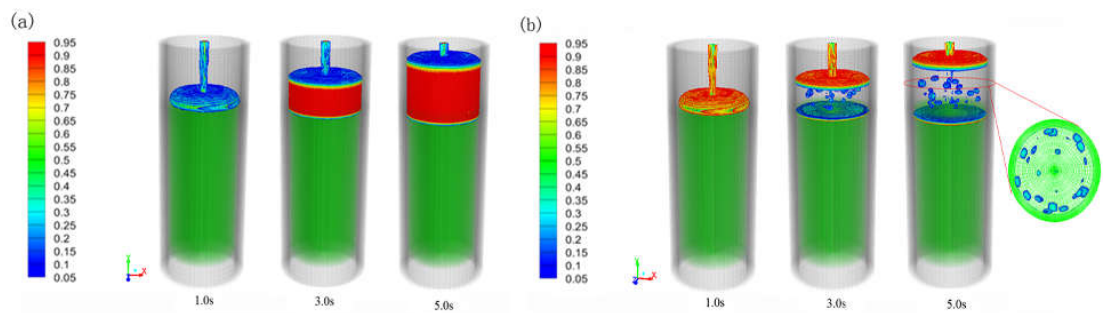


Fig. 2.12. Injection process (a) aluminum liquid distribution, (b) air distribution



Fig. 2.13. Defects in the sample generated in injecting process

(b) Infiltration

After injection process, the viscosity of molten aluminum increases, so the negative pressure should be applied immediately. The pressure used in this study is -30 kPa, and the duration of the infiltration process is 0.5 s. As shown in Fig. 2.14(a),

the aluminum liquid infiltrates gradually into the preforms with the help of the negative pressure. It is obviously that some bubbles remained in the aluminum will also enter into the preform accompanied with the liquid as presented in Fig. 2.14(b). In this process, if the infiltration distance and value of the negative pressure could not be controlled properly, the bubble will remain in the production and become the defects after the solidification, just like the condition in Fig. 2.15.

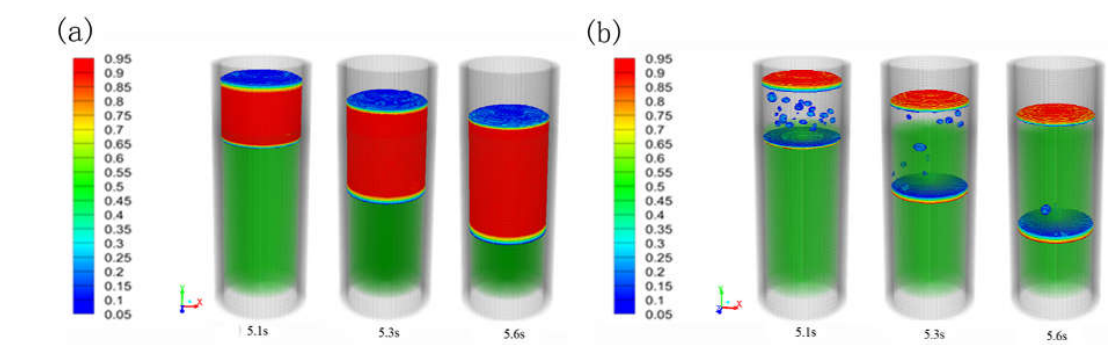


Fig. 2.14. Infiltration process (a) aluminum liquid distribution (b) air distribution

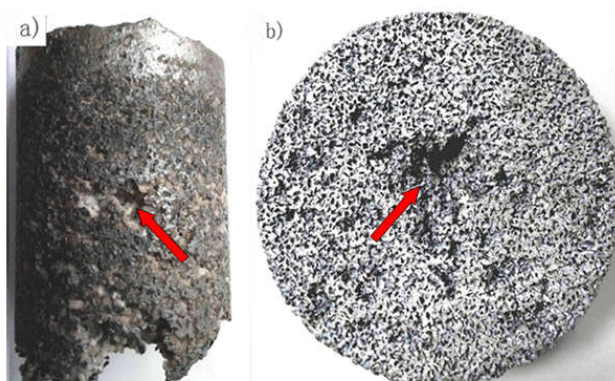


Fig. 2.15. Bubbles remained in aluminum foam

(c) Solidification

In the casting process, the solidification sequence is very important to analyse the location of the shrinkage in the product. However, this phenomenon is rather difficult to be observed by experiment. With the help of the numerical method, the solidification sequence is obtained, as shown in the Fig. 2.16. It is obviously that the bottom of the metal solidifies firstly because the flow distance of the infiltration front is larger than the other parts, which induces a serious temperature drop.

Besides, during the solidification, the heat escapes from the mold surface into the surrounding air by convection and radiation. For these reasons, the solidification follows from external edge to centre part and the centre molten metal near the top surface solidifies lastly. When the infiltration distance is large and there is not enough metal remained on the preform, the defect is often found in the centre of the top part of the sample. This part is just the location where the metal solidifies finally, as shown in Fig. 2.17.

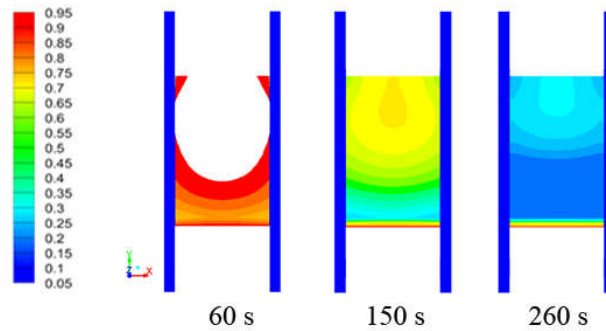


Fig. 2.16. Solidification sequence of the aluminum foam

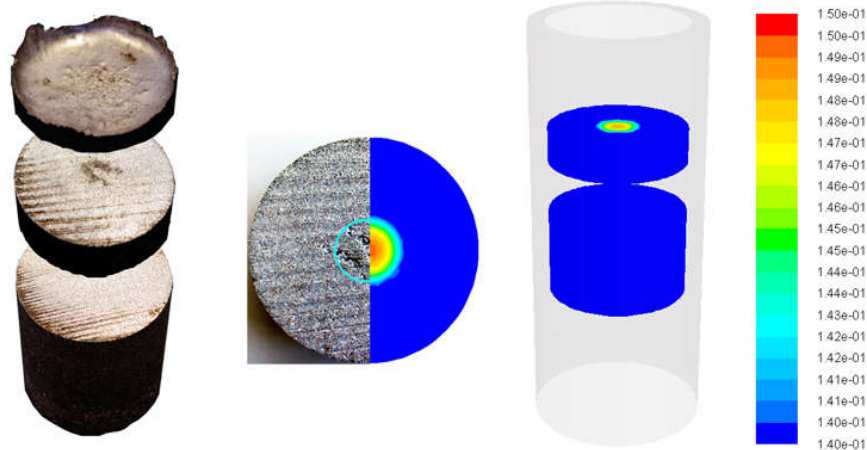


Fig. 2.17. Shrinkage location in the aluminum foam for real sample and numerical model

2.4.2 Effect of the manufacturing parameters on the defect

As mentioned above, some defects in aluminum foam are caused by the

bubbles remained in the sample during the manufacturing process. It is considered that the movement characteristic of these bubbles varies with different conditions. In the manufacturing process, some manufacturing parameters could affect directly the movement of liquid and air, such as temperature, pressure, particle size. Thus, to reduce the defects, the effect of these parameters on the bubbles is studied in this section.

(a) Temperature of molten aluminum

The temperature of molten aluminum could affect directly the viscosity of the liquid. To study the effect of the liquid temperature on the injection process, three different temperatures of liquid are applied in the simulation. The results are illustrated in Fig. 2.18. It is found that the bubbles still exist in the liquid and the numbers of bubbles are similar for three conditions, indicating that the variation of the temperature has little effect on the injection process.

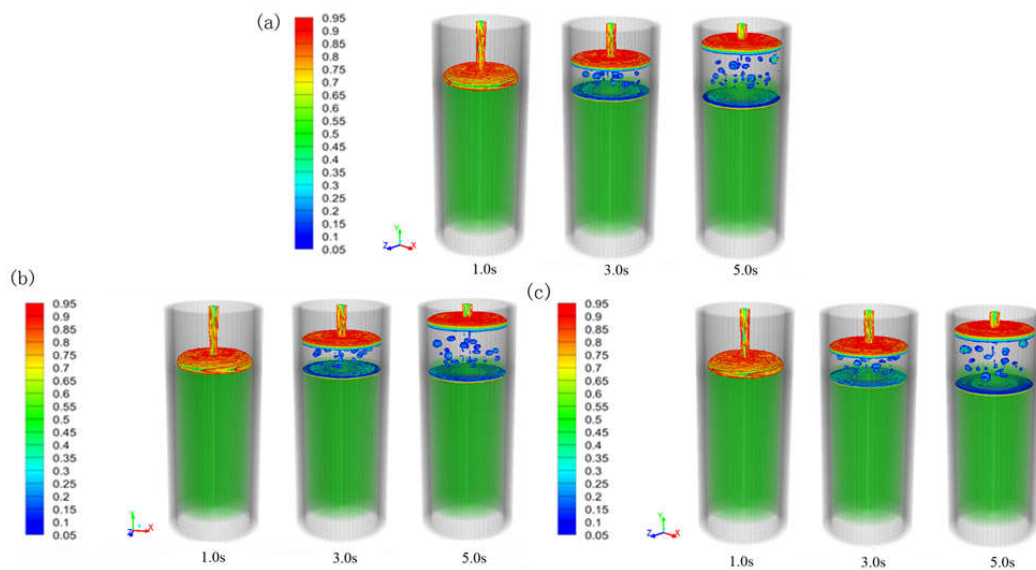


Fig. 2.18. Injection process at different temperatures (a) 650°C (b) 700°C (c) 750°C

(b) Particle size

Particle size is one of the critical parameters for the pressure infiltration casting, because it could not only control the pore size but also affect the

penetration in the porous preform. In order to investigate the effect of particle sizes on the motion of bubbles, three kinds of sizes (0.58mm, 1.60mm, 2.50mm) are used in our work. Their injection approaches are according to the process shown in Fig. 2.12, and the initial bubble numbers trapped in the liquid are approximate. The porosity of preform is 0.47 and the negative pressure is -20kPa. Fig. 2.19 presents the gas distribution during the infiltration process. It is obvious that the number of the trapped bubbles increases with the increase of the particle size. When the porosity is constant, the large particle size could lead to high permeability and large infiltration velocity (in Fig. 2.20), which is responsible for the entrance of bubbles. On the contrary, for the size of 0.58mm, the infiltration duration is long and the liquid could penetrate in the preform at a low velocity. In this condition, only a few bubbles could enter in the gaps between the particles. As a result, if negative pressure applied is constant, the particle with small size should be selected to make the molten metal infiltrates steady, which contributes to reducing the bubbles trapped in the preform.

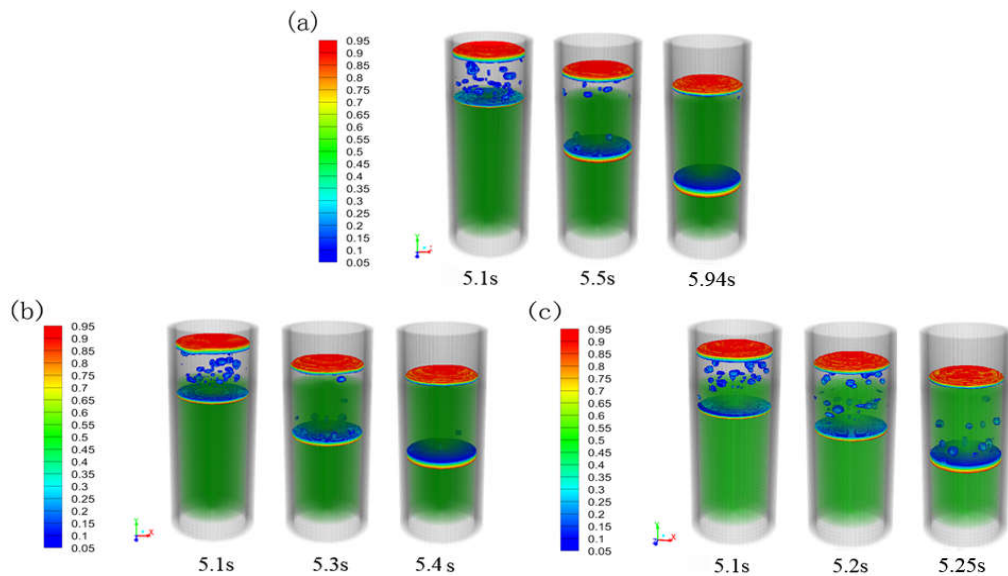


Fig. 2.19. Infiltration process in different particle sizes: (a) 0.58 mm, (b) 1.60 mm, (c) 2.50 mm

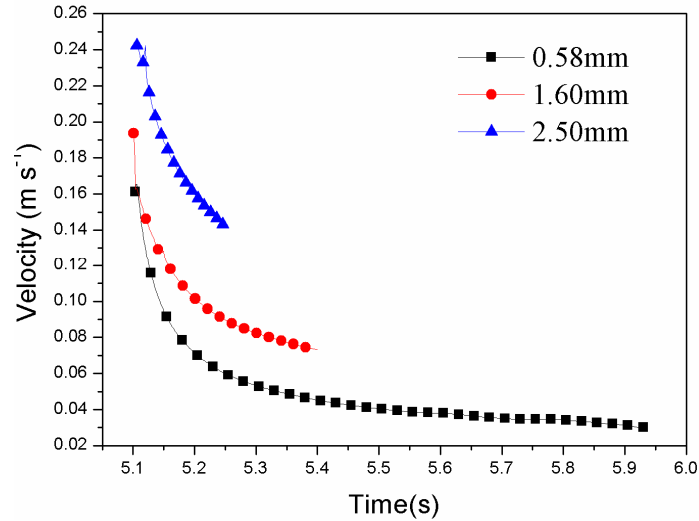


Fig. 2.20. Infiltration velocity as a function of time for different particle sizes

(c) Negative pressure

In order to overcome the surface tension, negative pressure is applied in the manufacturing process. As the main driving force, the pressure could control the infiltration velocity and the porosity of the aluminum foam. In addition, it could also affect the motion of the gas bubbles in molten metal. Fig. 2.21 shows the gas distribution during the infiltration with three different pressures (particle size is 1.0mm). When the pressure increases, the number of the trapped bubbles improves. This phenomenon could be attributed to the velocity of infiltration, as depicted in Fig. 2.22. When the infiltration is performed under 10kPa, the liquid could penetrate in the preform slowly. In this condition, most of them could escape from the liquid with the help of buoyancy force. However, as the pressure increasing, the infiltration velocity will become large and it induces that the bubbles enter in the preform by suction force, as shown in Fig. 2.21 (c). Therefore, the decrease of the pressure could help to reduce the defect in the manufacturing process.

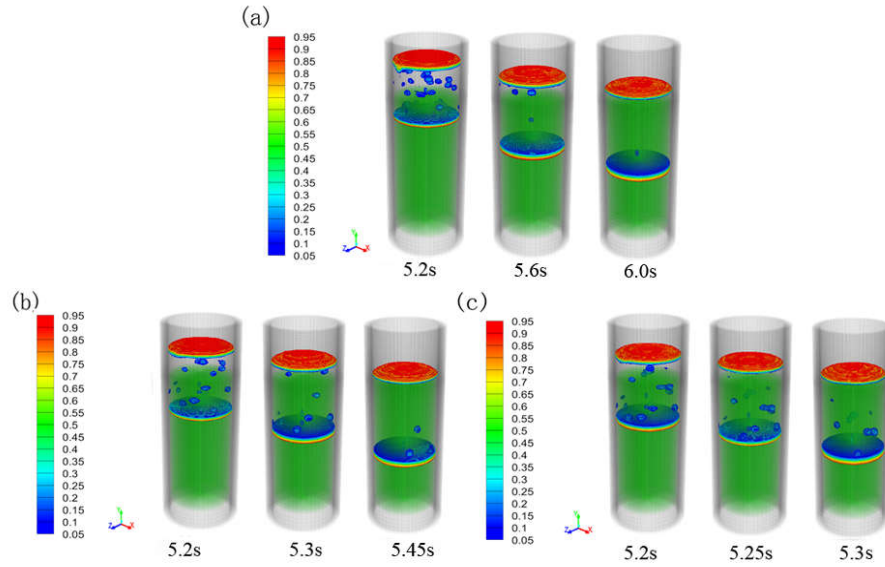


Fig. 2.21. Infiltration process with different negative pressure: (a) 10kPa, (b) 50kPa, (c) 90kPa

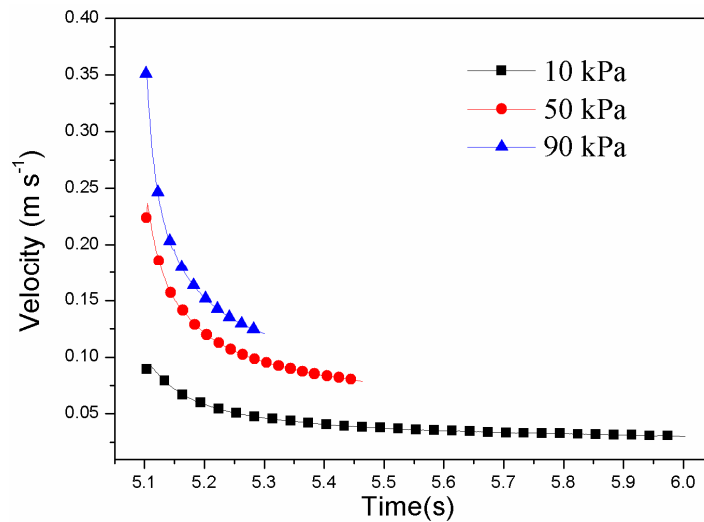


Fig. 2.22. Infiltration velocity as a function of time for different negative pressures

2.4.3 Prevention of the defect

As discussed above, the defects in the aluminum foam produced in our laboratory are caused by the mixing bubbles or volume shrinkage of metal during the solidification. In the different manufacturing steps, the kinds of the defects formed in the aluminum foam are various. For the mixing bubbles, they exist in injection and infiltration processes, and the particle size and negative pressure could influence the motion of the bubbles. While, the shrinkage in the center

occurs in the solidification and it has the relationship with the liquid volume remained on the preform top. Thus, to reduce the defect in the products, several methods are proposed in this study for the different procedures.

(a) In injection process

The most effective way to prevent the bubbles from entering in the preform is to reduce the turbulent extent during the injection process. For the casting operation, the optimization of the gate size or geometry could improve the casting quality [119]. Therefore, the injection process with a large gate is simulated and the result shows in Fig. 2.23(a). As increasing the gate size, it is obvious that the duration of the injection decreases and the number of bubbles trapped in the liquid reduces. However, it is noteworthy that the volume of metal liquid injected on the preform surface is increasing due to the change of the gate size, which tends to induce the deformation of the preform. The other method to reduce the bubbles is adjusting the injection angle, as shown in Fig. 2.23(b). The molten metal is injected on the interior surface of the mold instead of the surface of preform, and the liquid fills in the mold along the wall. This method could reduce the turbulent extent effectively so that the number of trapped bubbles in the liquid decreases.

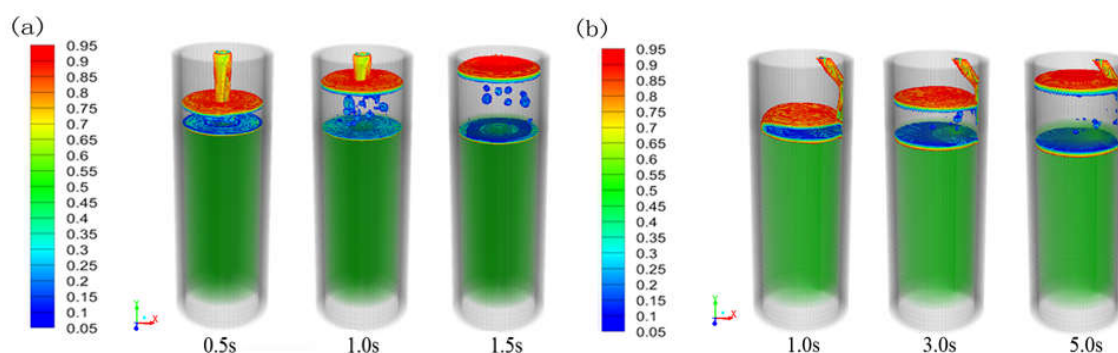


Fig. 2.23. Optimized injection process (a) changing the gate size, (b) changing the injection angle

(b) In infiltration process

The motion of bubbles is determined by particle size and negative pressure,

which is the conclusion in Section 2.4.2. However, changing the particle will affect the shape and size of the pore in the final product. Thus, it is considered that adopting a proper negative pressure is a better method for the fabrication. Even for the large size particle, the effect of negative pressure is also remarkable. For example, in Fig. 2.19(c), it is seen that many bubbles remain in the preform with 2.5 mm salt particle under -20 kPa. As the decrease of the pressure, the number of bubbles could be reduced obviously, as shown in Fig. 2.24. As a result, decreasing the negative pressure could make the liquid penetrate into the preform steady, which is an effective method to reduce the defects in the aluminum foam.

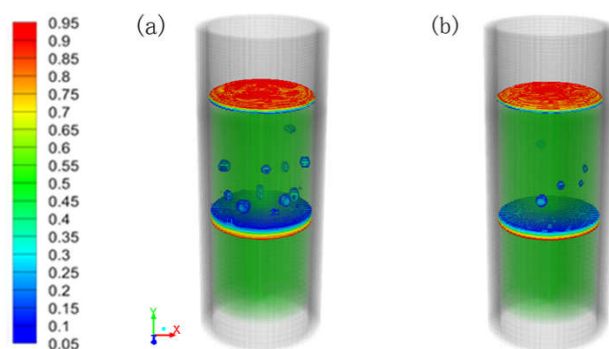


Fig. 2.24. Infiltration condition in the preform with 2.5 mm particles under different pressures (a) -20kPa (b) -3kPa

(c) In solidification process

The shrinkage is a kind of common defects in the traditional casting process. Due to the reduction of liquid volume, the caves always exist in the center of the sample, where the liquid solidifies lastly. The remedy of the shrinkage is adding a riser on the top of the product. In this case, the molten aluminum mold could be supplemented by the redundant liquid in the riser. This method may be also applied in the manufacturing of aluminum foam. Through controlling the infiltration length certain liquid could be remained on the top of the preform. And, this part of liquid could play the role of riser. The related simulation is performed and the numerical result is presented in Fig. 2.25. It is found that the top surface

becomes curving after solidification, indicating that the liquid in the riser solidifies lastly. Thus, the shrinkage in the preform could be avoided. This method is confirmed by experiment results, as shown in Fig. 2.26. It is observed that the top of the sample is sunken, which conforms to the simulation results. After cutting the piece, the section of the sample is continuous and homogenous. Therefore, the remedy of the shrinkage is effective for the aluminum foam produced by infiltration casting method.

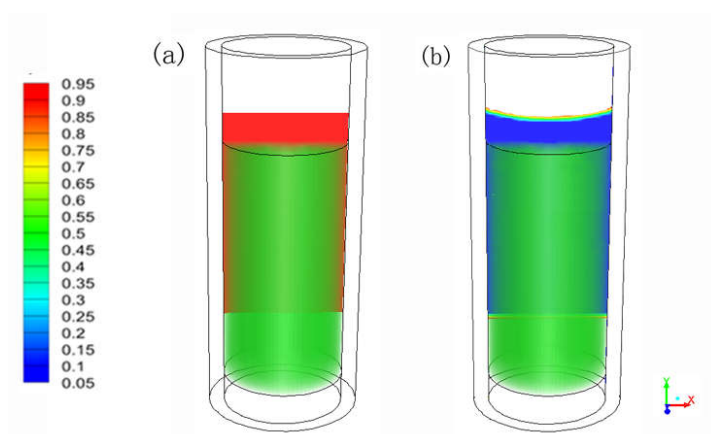


Fig. 2.25. Solidification process of the casting with a riser (a) before solidification (b) after solidification



Fig. 2.26. Photos of the sample with a riser

2.5 Conclusion

The process of the infiltration casting method for preparing aluminum foam is investigated experimentally and numerically. The infrared camera is applied to measure the variation of the temperature of the mold during the manufacturing process. A 3D model is established based on Darcy law, VOF model and k-epsilon model. The relative permeability is taken into account to study the flow of liquid and air in porous preform during infiltration process. The model is validated by comparing the numerical results with experimental data obtained from the camera.

The 3D model is adopted to analyze the cause of the defects in open-cell aluminum foam. It is found that the bubbles could mix and remain in the liquid in injection process. The defects in the surface and bottom of the aluminum foam are due to gas entrapment. Under the negative pressure, the bubbles could be trapped in the preform and become the defects after the solidification. The cave in the center is the shrinkage, and it will occur when the volume of molten aluminum remained on the preform top is not enough.

The prevention of the defect is proposed and analyzed based on the manufacturing step. For injection process, adjusting injection angle could reduce the turbulent extent and results in fewer bubbles trapped in the molten aluminum. The motion of the bubbles is affected by particle size and negative pressure during the infiltration process. The small particle and low negative pressure could lead to a low infiltration velocity, which could reduce the bubbles remained the porous zone. Through controlling the infiltration length, the molten aluminum remained on the top of the preform could fill into the preform during solidification process thus the shrinkage in the center of the sample could be avoided.

Furthermore, the infiltration time, flow velocity and solidification sequence

could be obtained from the simulation results. Therefore, the model established in this section is meaningful for the manufacturing process of aluminum foam, especially for the improvement of the quality and yield of the aluminum foam.

Chapter 3.
**Experimental and numerical
investigation of thermal
performance of LPAF/PCM
composite**

Chapter 3. Experimental and numerical investigation of thermal performance of LPAF/PCM composite

3.1 Introduction.....	65
3.2 Heat transfer characteristic of paraffin	66
3.2.1 Thermal property of paraffin	66
3.2.2 Melting process of paraffin.....	68
3.3 Heat transfer characteristic of LPAF.....	70
3.3.1 Micro model of LPAF.....	71
3.3.2 Simulation of effective thermal conductivity	71
3.4 Thermal performance of LPAF/paraffin composite	74
3.4.1 Preparation of LPAF/ paraffin composite	74
3.4.2 Test apparatus	75
3.4.3 Uncertainty analysis	76
3.4.4 Heat transfer characteristic of LPAF/paraffin composite	77
3.4.5 Effect of the porosity on the heat transfer in composite.....	81
3.5 Numerical analysis of heat transfer in the LPAF/ paraffin composite	87
3.5.1 Modeling method.....	88
3.5.2 Determination of the structural parameters	89
3.5.3 Numerical procedure and boundary conditions.....	90
3.5.4 Comparison of the equilibrium model and non-equilibrium model	91
3.5.5 Flow characteristics for different heat source locations	93
3.6 Conclusion	94

3.1 Introduction

In thermal energy storage domain, the phase change material (PCM), as the critical material of system, always suffers from the low thermal conductivity. In order to solve this problem, inserting metal foam into PCM is a promising and efficient method. Owing to the metal matrix and porous structure, this kind of metal foam/PCM composite could not only increase the effectiveness thermal conductivity of the composite [120] but also make the temperature more homogeneous[78]. As the skeleton material, the aluminum foam plays a vital role in composite during the energy storage and release process. At present, there are several kinds of open cell aluminum foams as commercial products. Base on their porosities (ϵ), open-cell aluminum foam could be classified into two groups: high porosity aluminum foam (HPAF, $\epsilon > 85\%$) [19] and low porosity aluminum foam (LPAF, $50 < \epsilon < 85\%$). These two kinds of aluminum foam have different structures, as shown in Fig. 3.1.

In this study, HPAF is defined as the aluminum foam by the replication casting method, while LPAF is prepared by infiltration casting method. For HPAF, the high void volume and high permeability are two major advantages, while LPAF has the high thermal conductivity and large surface area to volume ratio. Until now, many research works are performed to study the thermal transport HPAF/PCM composite. However, due to the limit of manufacture technology, the research of the thermal performance of LPAF is relatively rare at present. Therefore, in order to further understand the effect of LPAF on the thermal performance of the composite, the investigations of thermal behavior of LPAF/PCM composite should be performed.

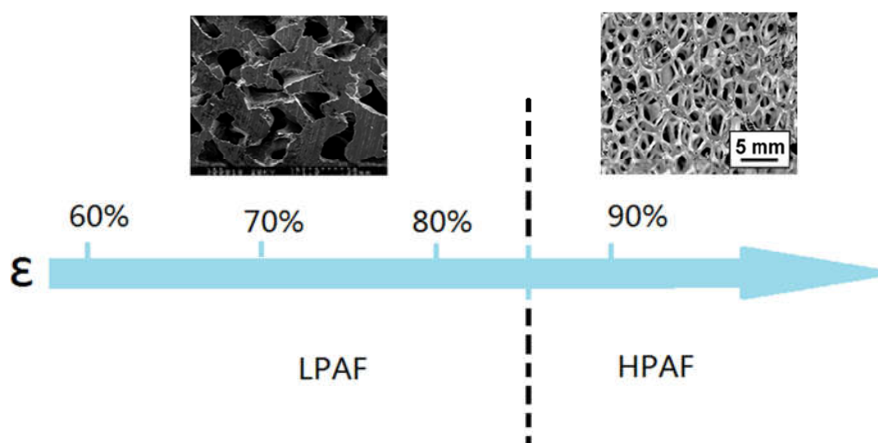


Fig. 3.1. Structure characteristics of LPAF and HPAF

Paraffin is chosen as PCM in this section. Firstly, the heat transfer characteristics of paraffin and LPAF are studied separately. The melting process of paraffin is observed, and the thermal conductivity of LPAF is predicted by numerical method. After that, the LPAF/paraffin composite is prepared by immersing LPAF into liquid paraffin. The heat transfer process of the composite is recorded by infrared camera. The effects of the porosity of LPAF and the locations of heat source on the melting process are investigated. Finally, to analyze numerically the heat transfer in the composite, the 3D macro models are also established by using equilibrium model and non-equilibrium model, respectively.

3.2 Heat transfer characteristic of paraffin

3.2.1 Thermal property of paraffin

Paraffin is a kind of common organic PCMs and is widely applied in thermal energy storage due to its low cost and large latent heat. Paraffin consists of a mixture mostly straight chain n-alkanes $\text{CH}_3-(\text{CH}_2)_n-\text{CH}_3$ [121], and the length of the hydrocarbon chain could determine the thermal properties of paraffin. For instance, the melting temperature and latent heat will increase with the increase of

the chain length. The paraffin could be classified according to the number of carbon atoms, like C18, C20-C33, C21-C50, etc. or the melting temperature, such as R54, R56, R58, etc. Some investigations of the thermal properties of different kinds of paraffin have been conducted in Ref.[122-124]. Thus, the proper paraffin could be chosen to make a good match between the melting temperature and operating temperature.

The paraffin used in this study is R56-58 (produced by Merck Millipore, Malaysia). The latent heat and melting point of paraffin are measured by differential scanning calorimeter (DSC) with the heat and cooling rate of $5^{\circ}\text{C min}^{-1}$. The DSC result is displayed in Fig. 3.2. The minor peak represents the solid-solid phase transition, and the main peak is the solid-liquid phase transition. It is found that the melting process occurs at a temperature range, not at a constant temperature. By analyzing the boundary and area of the main peak, it is determined that the melting range of paraffin is $50.6\text{-}66.5^{\circ}\text{C}$ and the latent heat is 120.7 J g^{-1} . Some other parameters of the paraffin are listed in Table 3.1.

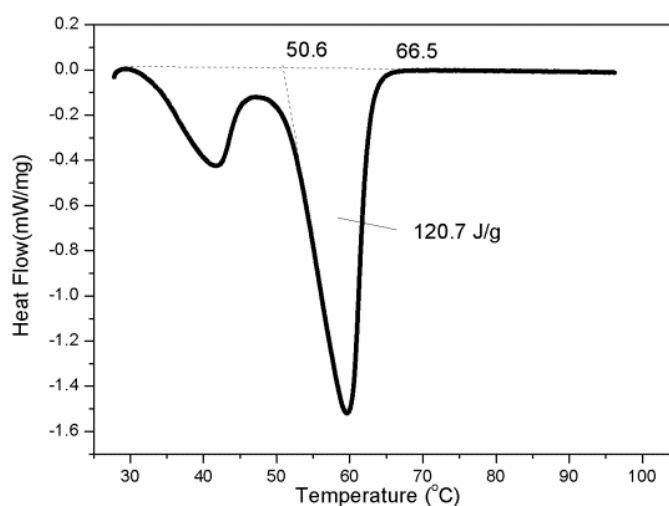


Fig. 3.2. DSC result of the paraffin

Table 3.1 Thermal properties of paraffin

Property	Value
Density, ρ (kg m^{-3})	840
Specific heat, C ($\text{J kg}^{-1} \text{K}^{-1}$)	2100
Thermal conductivity, λ ($\text{W m}^{-1} \text{K}^{-1}$)	0.2
Viscosity, μ ($\text{kg m}^{-1} \text{s}^{-1}$)	0.003
Thermal expansion coefficient, γ (K^{-1})	0.0004
Latent heat, L (kJ kg^{-1})	120.7
Solidus temperature, T_{m1} ($^{\circ}\text{C}$)	50.6
Liquidus temperature, T_{m2} ($^{\circ}\text{C}$)	66.5

3.2.2 Melting process of paraffin

During phase transition process, the evolution of the solid-liquid interface could reflect the heat transfer mechanism of paraffin. Thus, the melting processes of paraffin heated by two different heat sources are observed, as presented in Fig. 3.3 and Fig. 3.4. The paraffin is enclosed in an acrylic box, and it is heated by a heat source with 3500 W m^{-2} . In these pictures, the white parts represented the solid paraffin, while the transparent parts are the liquid paraffin. The experiment is conducted in the ambient temperature, and the paraffin is all solid at beginning. For the horizontal heat source, when the paraffin is solid, the heat transfer in paraffin is governed by heat conduction. Due to the low thermal conductivity, the heat is accumulated near the heat source, leading to the appearance of liquid in this position. At 600 s in Fig. 3.3, it is observed that the interface is wavy, which indicates that the natural convection prevails at this stage. The wavy interface is referred to the formation of Benard convection cells in liquid paraffin[125]. When the temperature difference in the liquid reaches a critical value, the buoyant force develops and overcomes the viscous force. In this condition, the hot liquid rises up at first. After arriving at the interface, the liquid will fall down around. The circulation of this process results in several Benard convection cells in the liquid,

which could contribute to the heat transfer between heat source and interface. As time progressed, the interface rises gradually and the shape becomes smooth. This phenomenon demonstrates that the circulating flows seem to merge with each other, which may be due to the appearance of the turbulent natural convection in liquid [126]. Finally, the center at the top of paraffin melts firstly, and the existence of shrinkage in paraffin maybe accounts for this phenomenon.

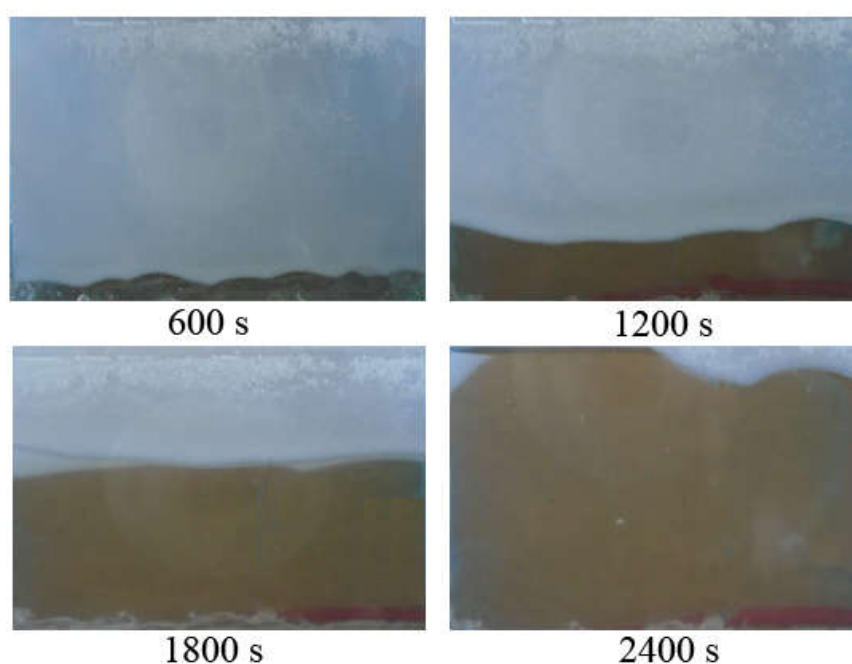


Fig. 3.3. Interface evaluation of paraffin heated by horizontal heat source

The melting process of the paraffin heated by vertical heat source is different. As shown in Fig. 3.4, the interface is sloping and the shape of liquid paraffin at top parts is convex at 1200 s. This melt characteristic is the typical phenomenon of natural convection dominated melting [127]. This phenomenon could be explained that the hot liquid adjacent to the heat source rises up with the development of buoyant force. After being impeded by the top surface of the container, the liquid starts to flow forward. In this case, the solid phase at the top part will be heat by the hot liquid. Then the liquid flows down along the interface and the temperature in liquid decreases gradually. This kind of circulating flow make the paraffin at the

top parts melts more quickly than that at the bottom parts, so that the solid paraffin in the right bottom corner melts at last, as presented at 4800 s in Fig. 3.4.

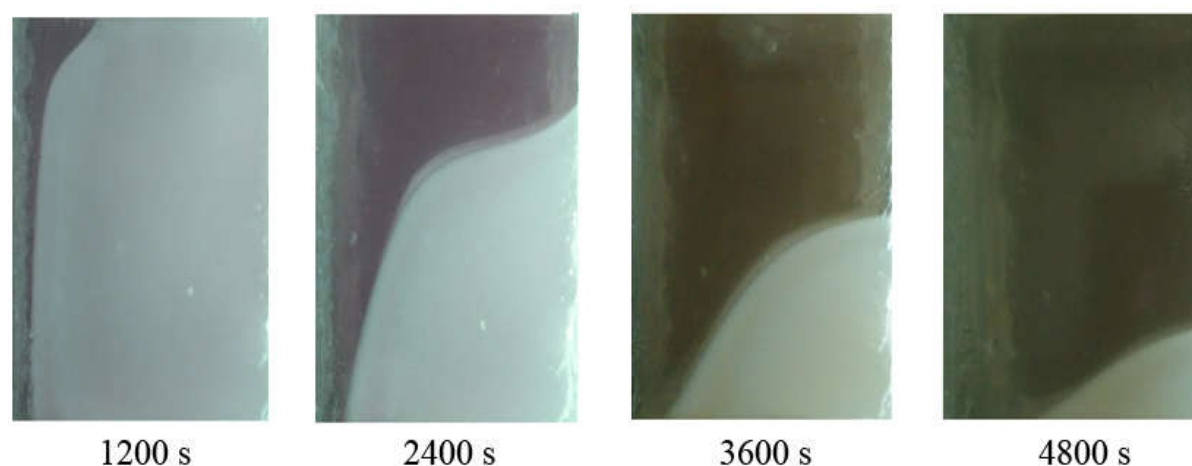


Fig. 3.4. Interface evaluation of paraffin heated by vertical heat source

Although the heat transfers of paraffin for two heat conditions are both governed by thermal convection, it is found that the melting process of paraffin heated by vertical heat source is slow, which is confirmed by comparing the liquid fractions for two heat conditions at the same moment. This is due to the different forms of natural convection for two heat conditions. As discussed above, there are many 3D Benard convection cells for the horizontal heat source. However, for the vertical heat source, there is only one regular circulating flow in the liquid, and some researchers treated it as a 2D flow. Kamkari et al. [128] found that the Nusselt number for horizontal heat source is twice than that for vertical source. Thus, the circulating flow for vertical heat source weakens the effect of the natural convection on the heat transfer and slows down the melting process.

3.3 Heat transfer characteristic of LPAF

The heat transfer of PCM could be greatly improved by inserting metal foam into it, because the thermal conductivity of metal is much higher than that of PCM. For the metal foam without filler, it could be treated as the composite made of

metal and air. In this case, the effective thermal conductivity (k_{eff}) becomes one of the most important parameters of metal foam. In this section, the determination method of the effective thermal conductivity of low porosity aluminum foam (LPAF) is studied by numerical method.

3.3.1 Micro model of LPAF

The structure characteristic of LPAF prepared by infiltration casting method is affected by the arrangement of the preform particles. In the previous work of our laboratory, Su [9] treated the salt particle as a tetradehedron, and the model of the aluminum foam unit is obtained by subtracting tetradehedron from a cube, as presented in Fig. 3.5. This micro model is defined as the modified Kelvin model. It has been confirmed that the modified Kelvin model could be used to analyze the compression property of metal foam, indicating that it could reflect the property of the real structure. Therefore, according to the modified Kelvin model and Fourier law, the determination of k_{eff} of LPAF is attempted in the following section.

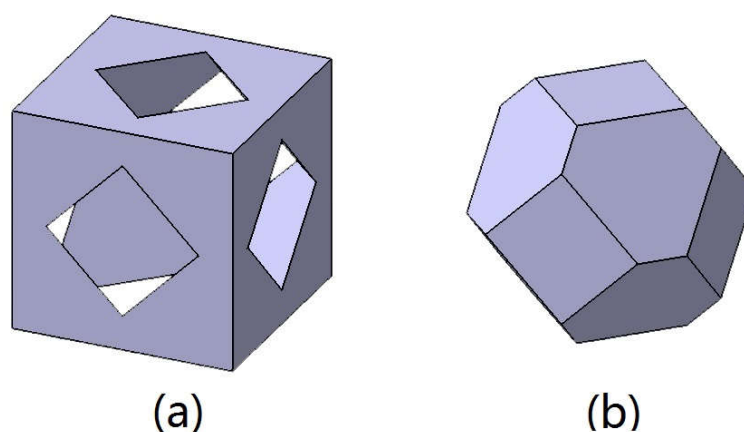


Fig. 3.5. Modified Kelvin model (a) metal part and (b) pore part (tetrakaidehedron)

3.3.2 Simulation of effective thermal conductivity

The modified Kelvin model represents only one unit of LPAF, so that the

thermal convection of the air in the pore could be neglected. The solid part of the model is governed by energy conservation equation:

$$\rho c \frac{\partial T}{\partial t} = k \left(\frac{\partial^2 T}{\partial x^2} + \frac{\partial^2 T}{\partial y^2} + \frac{\partial^2 T}{\partial z^2} \right) \quad (3-1)$$

The equation is solved by finite volume method in the software Fluent®. The temperature difference between top and bottom surface is 50K. The heat flux density will approach a constant number when the system arrives at steady state, as shown in Fig. 3.6. Therefore, by using the Fourier law, the thermal conductivity could be obtained and the detail process is based on Ref.[129].

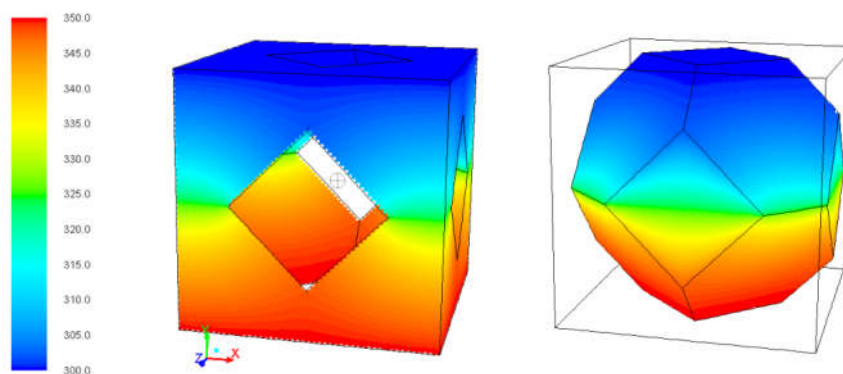


Fig. 3.6. Temperature distribution of the model at steady state

The model grid used in this analysis is the tetrahedral mesh. In order to confirm the grid number, the model with different grid numbers is simulated at the condition discussed above. The heat flux density of middle surface is detected during the process. Fig. 3.6 shows the heat flux density as a function of grid number. It obvious that the value of the heat flux become steady as the grid number increasing. As a result, considering both the precision and calculate time, the grid number is set to 785257.

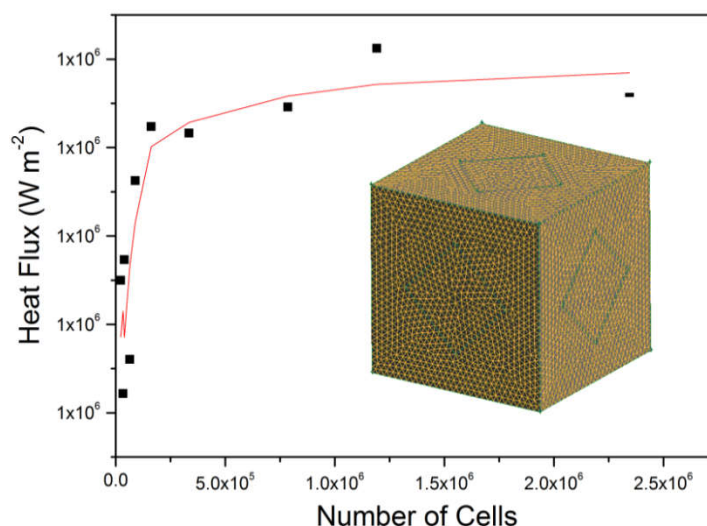


Fig. 3.7. Mesh dependence analysis

To verify the modified Kelvin model, a comparison between experimental data [21] and numerical results is conducted. The porosity range is from 57 to 69%, and the average pore size is 1.43 mm. As depicted in Fig. 3.8, it is found that the numerical results are consistent with the experimental ones. Therefore, the modified Kelvin model could be applied in the determination of k_{eff} for the LPAF. Furthermore, it is obvious that the value of k_{eff} has a linear relation with the porosity. Due to the reduction of metal fraction, the effective thermal conductivity decreases as the porosity increasing. Except for porosity, the pore size is also one of the critical structural parameters. The effect of the pore size on the effective thermal conductivity is investigated and the results are presented in Fig. 3.9. It is seen that the pore sizes of aluminum foam have little influence on the k_{eff} , which agrees with the results of Peak et.al [130]. As a result, it is concluded that the value of k_{eff} is only determined by the porosity of aluminum foam.

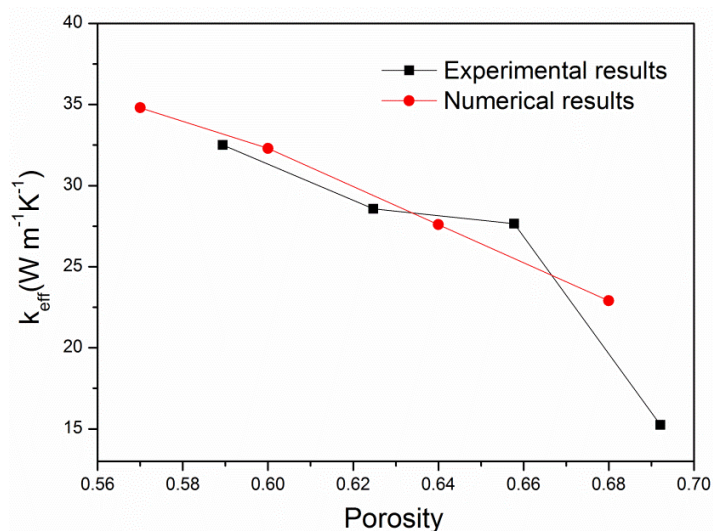


Fig. 3.8. Comparison between experimental and numerical results

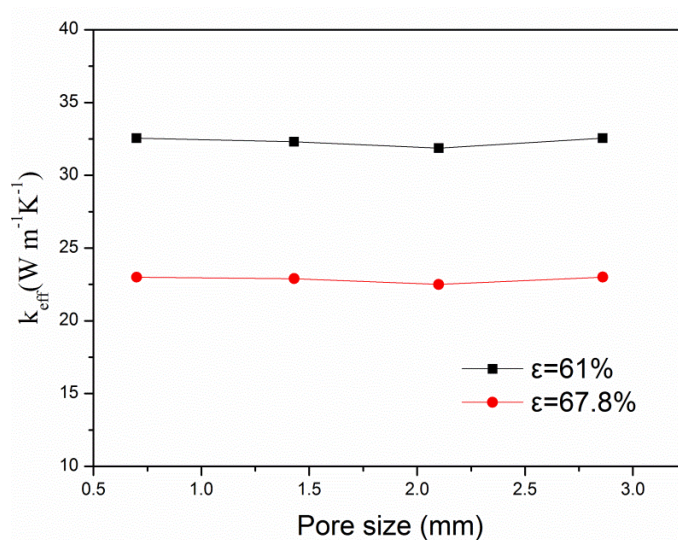


Fig. 3.9. Effect of pore size on the effective thermal conductivity of aluminum foam

3.4 Thermal performance of LPAF/paraffin composite

3.4.1 Preparation of LPAF/ paraffin composite

The low porosity aluminum foam (LPAF) is prepared by infiltration casting method with the particle size of 2.5 mm. The type of aluminum matrix is AS7G. Fig. 3.10 presents the structures of LPAFs with different porosities. The pores are produced by the preform, thus the shapes and sizes of these pores are depended on

the salt particles. It is observed that these interconnected open pores are surrounded by aluminum ligaments. As the increase of the porosity, the fraction of aluminum decreases and the void parts increase, as shown in Fig. 3.10 (a)-(c).

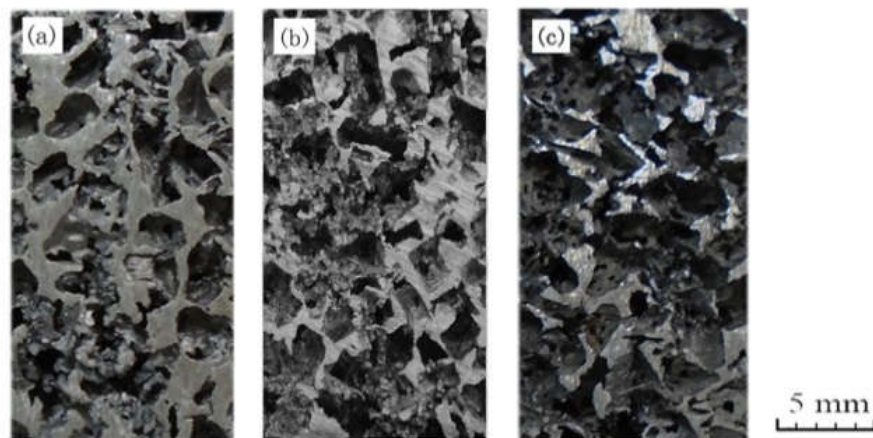


Fig. 3.10. LPAFs with different porosities (a) 67% (b) 75% (c) 84%

The LPAF/PCM composite is prepared by impregnation method. The aluminum foam should be preheated to the temperature above the melting point of paraffin, so that it could be avoided that the paraffin solidifies on the surface of the metal ligaments during the infiltration process. After that, the aluminum foam is immersed into the liquid paraffin gradually. In order to remove the bubble remained in the pores, the container with the composite is placed in a vacuum device after impregnation process. The sample should be cooled for 24h before it is taken out from the container.

3.4.2 Test apparatus

The test apparatus designed to observe the melting process and measure the temperature variation of composite is illustrated in Fig. 3.11. The sample of the composite is placed in a rectangle container with inside dimension 60mm×24 mm×45 mm. The bottom of the container is the aluminum plate attached with an electric heating film, which is applied as the heat source. The constant heat flux

density is realized by DC power. The top plate is an aluminum sheet contacting the ambient air. In order to observe the interface evolution during the melting process, the other four walls are made of the transparent acrylic glasses with the thickness of 2 mm. To avoid the leak of paraffin, these plates are all fixed by glue and sealed by glass cement. The aluminum foam has the same dimension as the container, and it is attached on the heat source by conductive silicon paste to reduce the thermal contact resistance. Three T type thermocouples are placed in the center of the sample to measure the temperature variations, and their specific locations are presented in Fig.3. The data are collected by an indicator every 1 second and transferred to the computer simultaneously. An infrared camera (VarioCAM[®]) is also used to observe the temperature distribution of the composite.

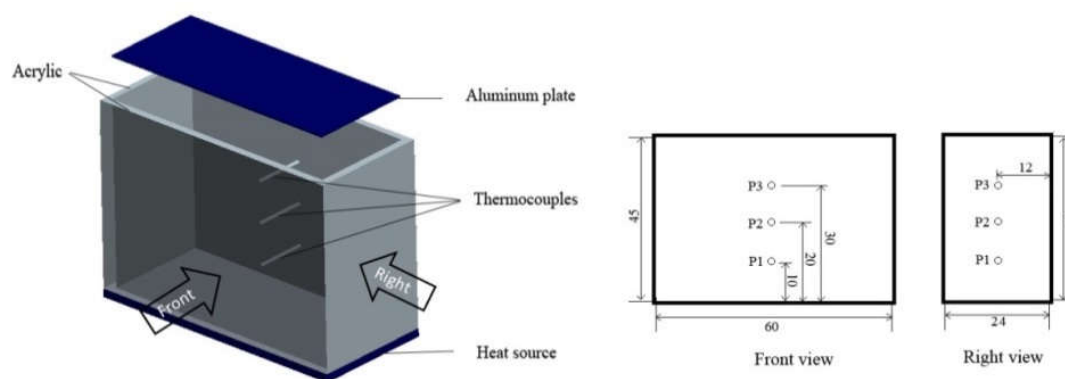


Fig. 3.11. Schematic illustration of test apparatus and specific locations of thermocouples

3.4.3 Uncertainty analysis

The experimental errors always exist in the investigation due to the design of the test apparatus and the accuracy of the measurement equipment. The experiment results in this study could be affected by these following factors: (1) The errors of paraffin filling rate, V (%); (2) The heat loss from the acrylic glass surfaces to the ambient, ΔQ (J); (3) The temperature uncertainty of the thermocouples, ΔT (K); (4) The error of the DC power supply, E_{power} (%). Neglecting the left and right surfaces

which are isolated by grass fibers, the heat loss from the front and back acrylic surfaces could be calculated by the equation:

$$\Delta Q = 2 \int_0^t h_w a_w (T_{ave} - T_{amb}) dt \quad (3-2)$$

where, h_w is the convective heat transfer coefficient of the front wall, a_w is the surface area of the front wall, T_{ave} is the average temperature of the wall, T_{amb} is the ambient temperature. For the melting process of composite with $\varepsilon = 75\%$, the input power is 5 W. The heat loss of the front and the back surface is 1050J. Besides, the values of V and ΔT are 4.1% and 0.1°C, respectively. The E_{power} is 3.2% in this condition. As a result, the total uncertainty is based on the method in the Ref.[131], and the formula is as follow:

$$E_{total} = \sqrt{V^2 + \left(\frac{\Delta Q}{Q_{in}}\right)^2 + \left(\frac{\Delta T}{T_{tc}}\right)^2 + E_{power}^2} = 8.06\% \quad (3-3)$$

where, Q_{in} is the total input heat quantity, which is the product of input power and total melting time; T_{tc} is the average temperature of three thermocouples.

3.4.4 Heat transfer characteristic of LPAF/paraffin composite

In order to analyze the effect of aluminum foam on the heat transfer of paraffin, the temperature distributions of the pure paraffin and the composite are detected by the infrared camera. The constant heat flux density 3500 W m⁻² is imposed at the bottom surfaces. Fig. 3.12 presents the temperature distributions of pure paraffin during the melting process, in which the white part and red part represent the liquid phase and solid-liquid interface, respectively. In Fig. 3.12(a), the interface is parallel to the bottom surface, indicating that the thermal conduction prevails in the liquid. As the liquid fraction increasing, the Benard

convection cells caused by the buoyance force develop in the liquid phase, which is confirmed by the wavy form of the solid-liquid interface in Fig. 3.12(b). At this moment, the heat transfer in pure paraffin is predominated by thermal convection.

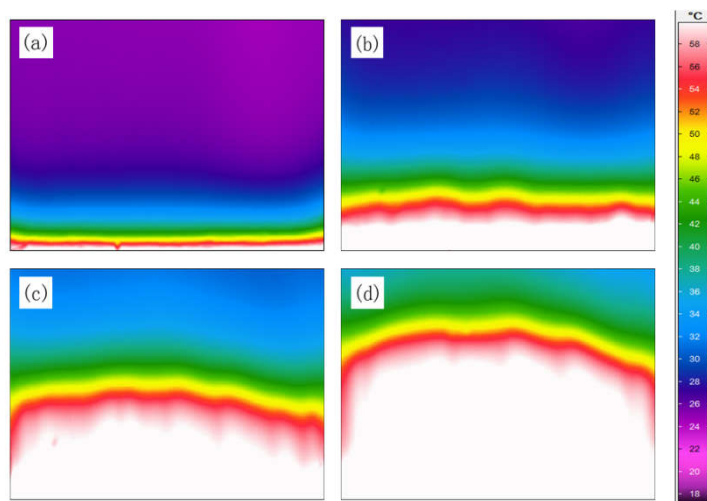


Fig. 3.12. Temperature distributions of pure paraffin (right view) (a) 800 s (b) 1800 s (c) 2600 s (d) 3300 s

Fig. 3.12 presents the temperature variation of the detected points in pure paraffin. For the pure paraffin, the temperatures of the detect points keep increasing during the melting process, but the temperature rise rate are various at different temperature ranges. From 20°C to 40°C, the temperatures increase slowly due to the low thermal conductivity of paraffin. After that, because of the development of natural convection, the heat transfer efficiency is enhanced and temperature rise rates between 40°C and 66.5°C are largest during the melting process. When the temperature reaches 66.5°C, the paraffin totally melts. Because of the existence of the circulations in the liquid, the curve of temperature variation begins to fluctuate, and the temperature values of three points tend to be uniform, as shown in Fig. 3.13. Moreover, the flat zone for latent heat could not be observed in the temperature range of phase transition, which is attributed to the strong natural convection in pure paraffin [132].

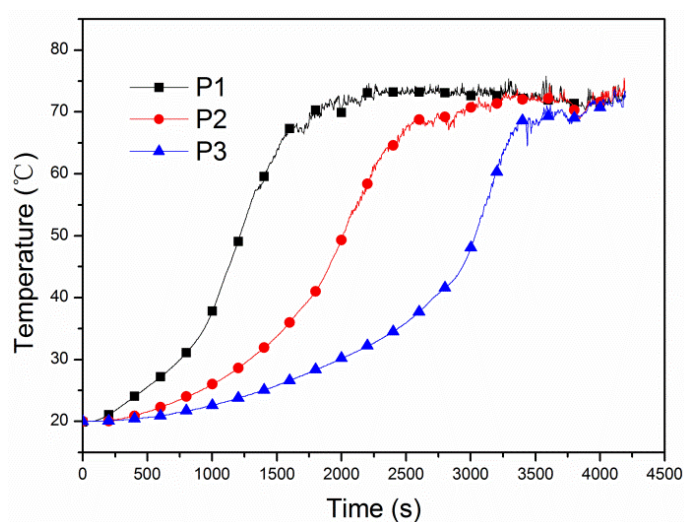


Fig. 3.13. Temperature variation of three detected points for pure paraffin

After inserting the aluminum foam in the paraffin, the paraffin is divided into many cells by metal ligaments, as shown in Fig. 3.14(a). Because of the high thermal conductivity of aluminum, the aluminum foam is heated firstly and the heat flux is transferred along the structure of metal ligaments, which could be observed in Fig. 3.14 (b)-(d). In this condition, the paraffin in the cellular units could be warmed by the metal matrix and the paraffin far from the heat source could be heated quickly.

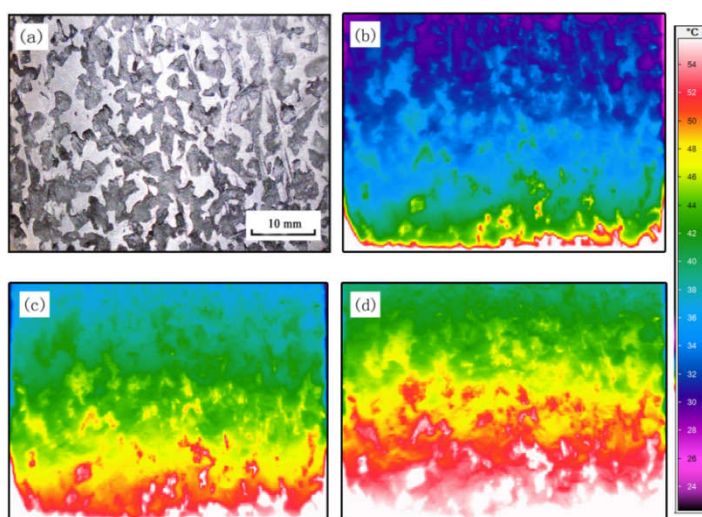


Fig. 3.14. Morphology (a) and temperature distributions of LPAF/PCM composite (right view) (b) 500 s (c) 750 s (d) 1000 s

Fig. 3.15 shows the temperature variations of composite. It is seen that the curves of temperature variations are different with pure paraffin. According to the characteristic of temperature variation, the curves could be divided into three regions: solid, mush and liquid [133]. During the melting process, the temperature rises of three points are synchronized and the temperature differences between the points are small. These characteristics are because of the high thermal conductivity of LPAF. In addition, the fluctuations of temperature are disappeared and the flat zones at the temperature of melting range are distinct, indicating that the natural convection is suppressed by aluminum foam. Therefore, the addition of the LPAF changes the heat transfer process in paraffin, and the melting process of composite is controlled by thermal conduction.

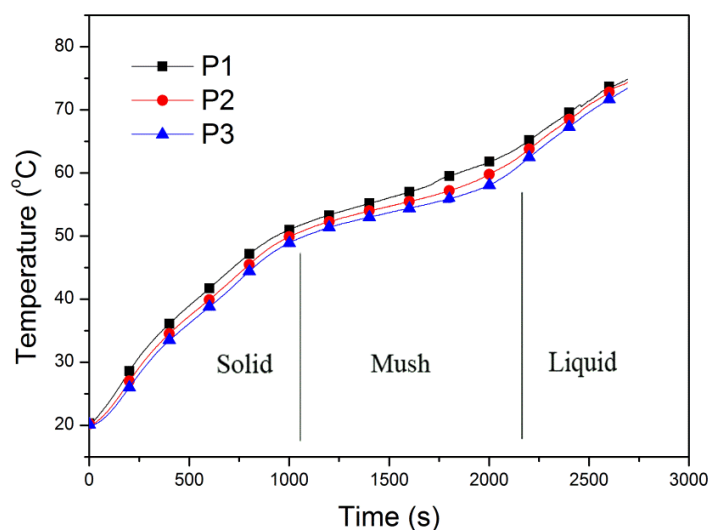


Fig. 3.15. Temperature variation of three detected points for LPAF/paraffin composite

Combining the results in Fig. 3.13 and Fig. 3.15, a comparison of temperature variations for composite and pure paraffin is obtained, as presented in Fig. 3.16. For the composite, the overall average temperature of three points reaches 70°C at about 2500 s, which is much faster than that of pure paraffin (>4000 s). The reason includes two aspects: one is the less volume paraffin; the other is the large thermal conductivity of composite. In a word, the addition of the aluminum foam could

improve the heat transfer in PCM, while the existence of aluminum reduces quantity of the paraffin and affects the latent heat stored in the system. In order to balance these two factors, the aluminum foam with an optimum value of porosity should be used in the composite, which will be studied in the following section.

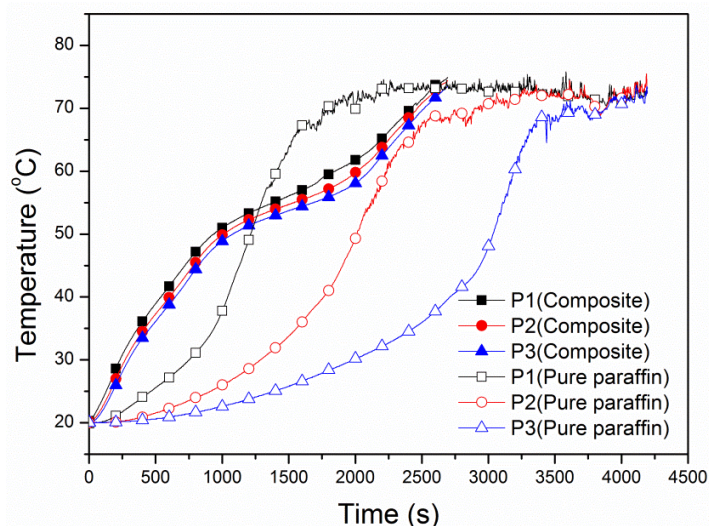


Fig. 3.16. Comparison of temperature variations for composite and pure paraffin

3.4.5 Effect of the porosity on the heat transfer in composite

The porosity is one of the critical parameters of aluminum foam, which could determine the effective thermal conductivity and permeability. Lafdi et al. [76] found that the heat transfer in composite is also affected by the porosity of aluminum foam. Therefore, to study the effect of porosity on the thermal behavior of LPAF/paraffin composite, the melting process and the temperature variation of the composite with different porosities are recorded for two different heat conditions.

(a) Melting process of composite heated by horizontal heat source

Fig. 3.17 shows the melting evolution of the composites with different porosities. The horizontal heat source is at the bottom and it provides the constant heat flux 3500 W m^{-2} . Liquid phase is transparent and the solid zone is shiny white.

For the composite with $\varepsilon = 67\%$, the solid-liquid interfaces are not distinct during the melting process, as presented in Fig. 3.17(a). The evolution of the interface is very quick and the total melting time is short, which demonstrates the temperature of the whole region rises synchronously. The melting processes of composites with $\varepsilon = 75\%$ and $\varepsilon = 84\%$ are displayed in Fig. 3.17 (b) and (c), respectively. The solid-liquid interface is obvious and it keeps rising horizontally. Besides, it is seen that the interface shapes of two composites are wavy, which is maybe attributed to the natural convection in liquid phase.

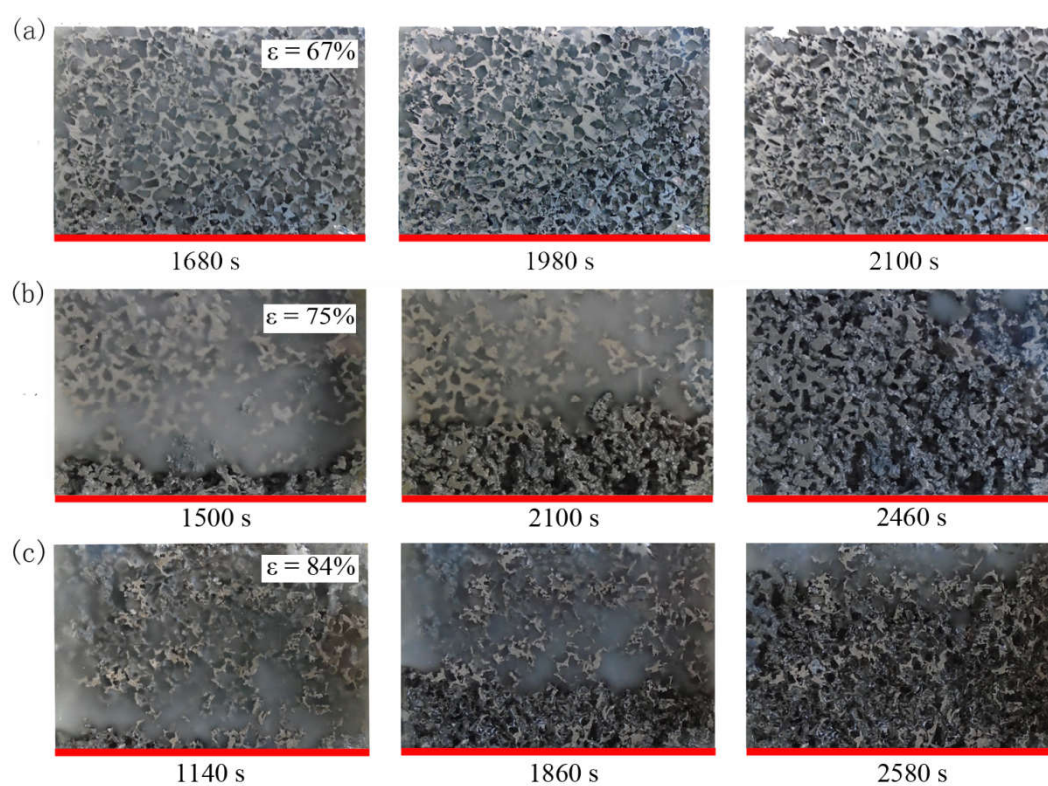


Fig. 3.17. Melting evolution of the composite with different porosities for horizontal heat source (a) 67% (b) 75% (c) 84%

In order to analyze quantitatively the effect of the porosity, the temperature variations of detected points are recorded and the results are shown in Fig. 3.16. It is seen that the temperature differences between the adjacent detect points increase as the porosity increasing. This is because the large effective thermal conductivity (k_{eff}) of the composite with low porosity could improve the heat transfer process

and make the temperature homogenous. Besides, it is noted that the mushy region of the composite with $\varepsilon = 67\%$ is distinct, while this region tends to be vague for composite with $\varepsilon = 84\%$. It is considered that the phenomenon is as a result of the change of the heat transfer mode. The permeability of aluminum foam with $\varepsilon = 67\%$ is small, which suppresses the natural convection of the liquid paraffin. In this case, the paraffin is restricted in the pores of aluminum foam and the heat transfer is governed by thermal conduction. In contrast, the aluminum foam with $\varepsilon = 84\%$ has the large permeability, and the motion of liquid paraffin in aluminum foam is less limited by metal ligaments. The natural convection of liquid phase will develop in the composite, leading to the uniform variation of temperature [134]. Therefore, it is inferred that the heat transfer in the composite with $\varepsilon = 84\%$ is affected by both thermal conduction and convection.

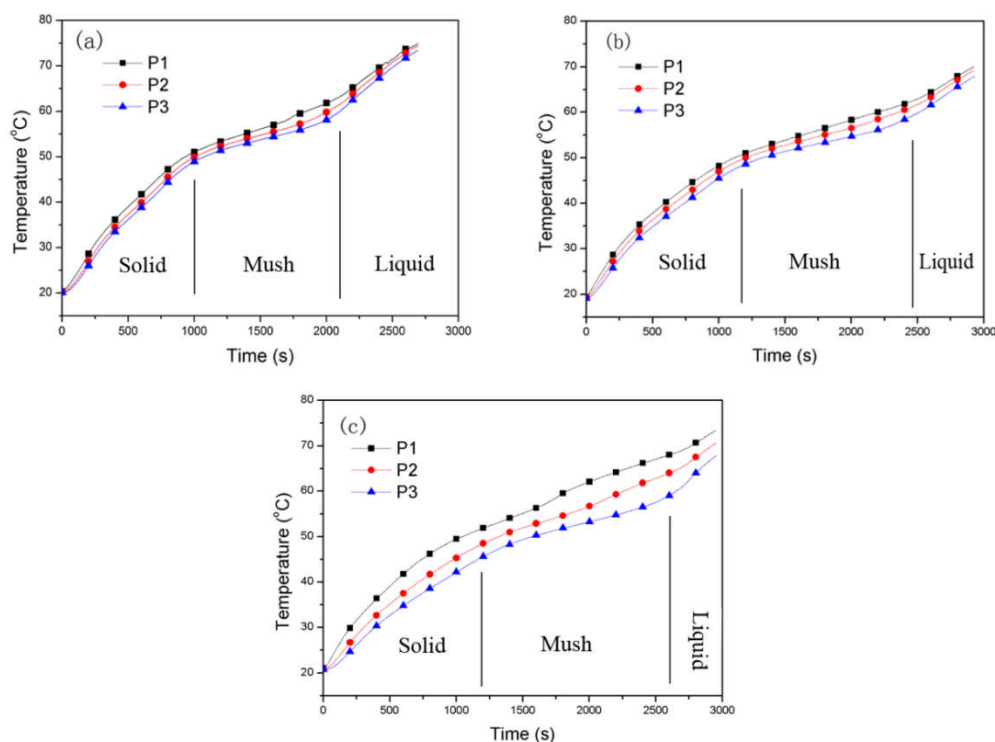


Fig. 3.18. Temperature variations of composite with different porosities for horizontal heat source (a) 67% (b) 75% (c) 84%

(b) Melting process of composite heated by vertical heat source

As concluded above, the natural convection could affect the melting process

of LPAF/paraffin composite. According to the melting process of pure paraffin, the circulation flows in the liquid are different with varying the heat directions. In order to further understand the effect of the natural convection on the heat transfer, the composites with different porosities are heated by vertical heat source, and the results are shown in Fig. 3.19. Similar to the horizontal heat source, the evolution of solid-liquid interfaces of the composite with $\varepsilon = 67\%$ are parallel to the heat source due to the thermal conduction. For the composite with $\varepsilon = 75\%$, the interface is straight at beginning. As the liquid volume increasing, the natural convection develops at 2180 s, which is confirmed by the sloping interface. However, the circulation flow does not always exist in liquid and it tends to disappear at 2700 s. This is because the thermal conduction still prevails in heat transfer, and the natural convection is suppressed during the melting process. The melting process of composite with $\varepsilon = 84\%$ is similar to pure paraffin. The sloping interface appears early, and the paraffin at the top melts quickly than that at the bottom, which is a typical phenomenon of the development of natural convection. As time progressed, the paraffin in the right corner melts lastly, as presented at 3420 s in Fig. 3.19(c). Thus, it is confirmed that the natural convection exists in the composite and the effect becomes more and more important as the increase of the porosity.

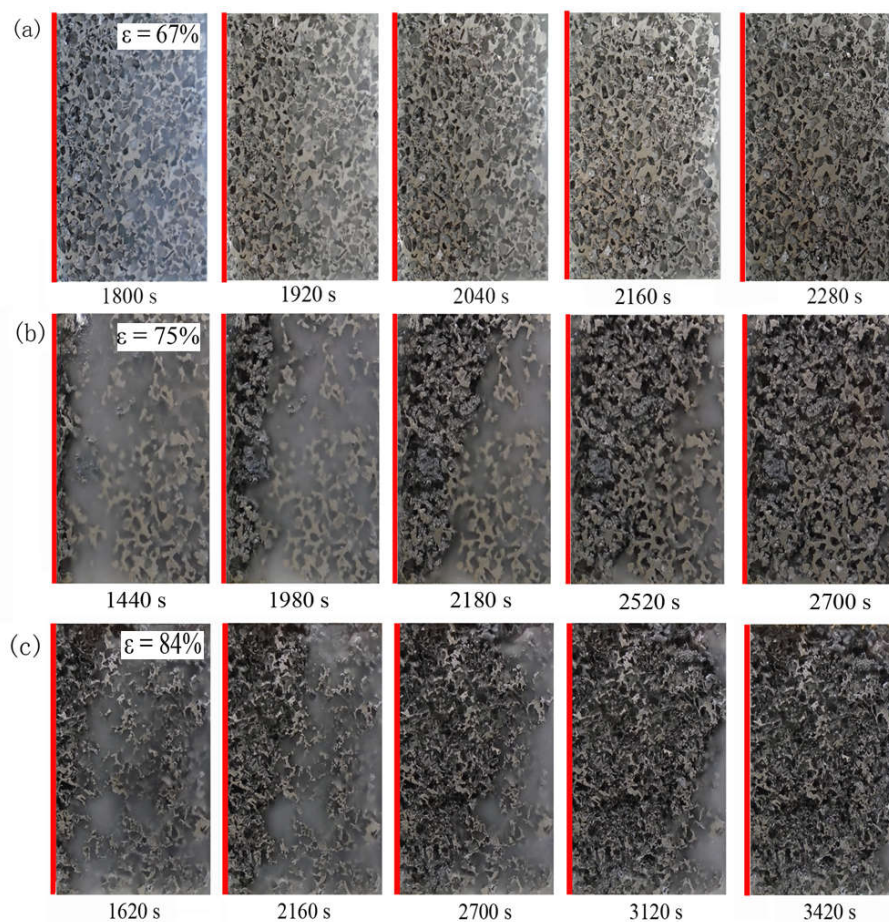


Fig. 3.19. Melting evolution of the composite with different porosities for vertical heat source (a) 67% (b) 75% (c) 84%

Fig. 3.20 displays temperature variations of composite with different porosities for vertical heat source. It is found that, although the flow patterns are different for two heating conditions, the shapes and feature of the curves for vertical heat source are similar to the horizontal heat source. This is because the thermal conduction always plays an important role in the heat transfer in spite of the heating directions, which affects the temperature distribution in whole region. However, the effect of natural convection will be influenced by the position of the heat source. Thus, the temperature rising rate for vertical heat source is slow than that for horizontal heat source.

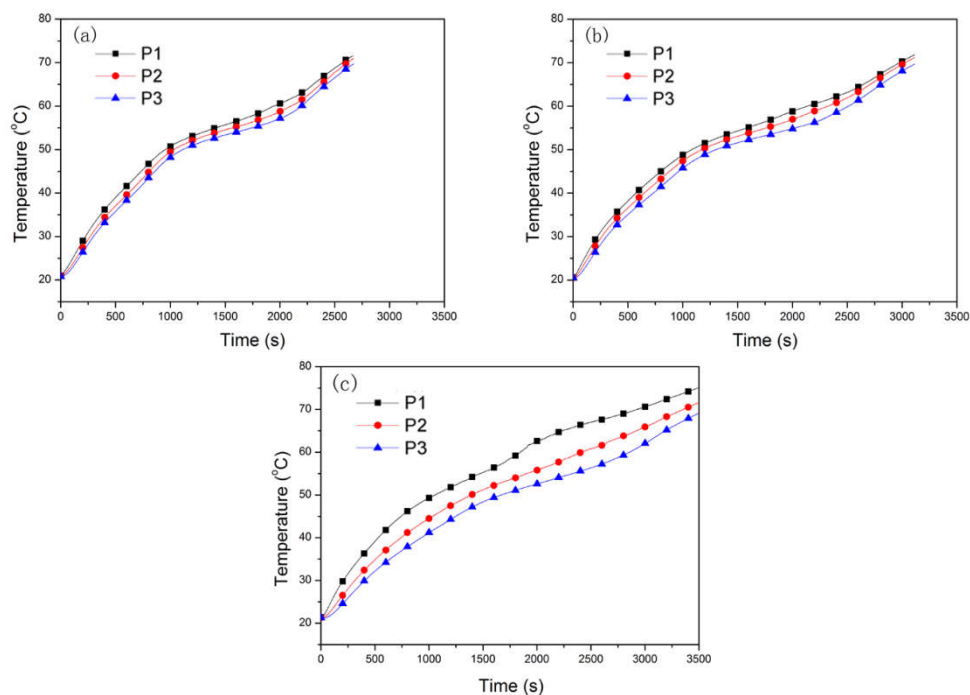


Fig. 3.20. Temperature variations of composite with different porosities for vertical heat source (a) 67% (b) 75% (c) 84%

Fig. 3.19 presents the total melting time as the function porosity for different heating conditions. The total melting time increases as the increase of the porosity, because the composite with large porosity need more energy to melts the paraffin. Besides, the composites heated by horizontal source have the shorter melting times than that of vertical heat source, and the time differences between two heating conditions become more and more distinct with the increase of the porosity. It could be explained that the effect of convective heat transfer is more and more pronounced as the porosity increasing. The different circulations caused by heating direction lead to the different melting orders. In horizontal heating condition, the natural convection could be developed well so that it accelerates the heat transfer process. For the vertical heat source, the natural convection makes the solid paraffin in the bottom right corner melts lastly, which is responsible for the longer melting time.

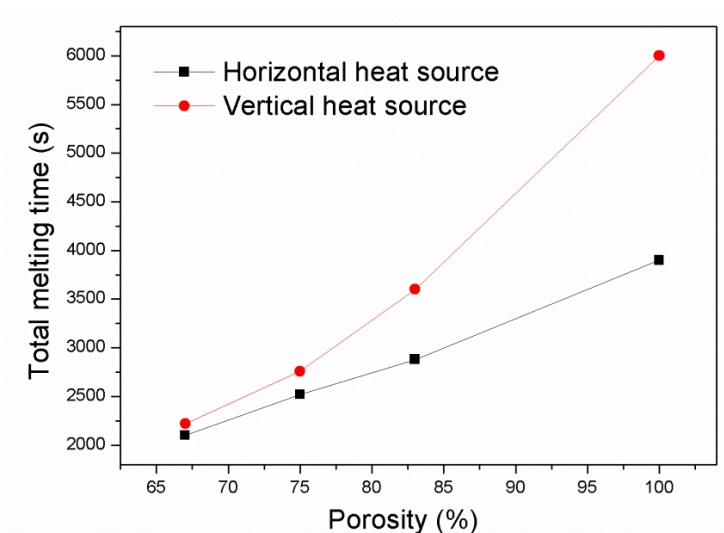


Fig. 3.21. Variations of total melting time versus porosity for different locations of heat source

In the applications of the thermal energy storage (TES) system, the heat source is always vertical, such as waste heat recovery, energy storage radiator, and solar energy equipment. Besides, in order to store more energy, the volume of the phase change material should be as much as possible. In this condition, the problem of the natural convection for the vertical heat source will deteriorate the efficiency of TES system. Thus, this factor should be noted and studied further in the design of TES system.

3.5 Numerical analysis of heat transfer in the LPAF/ paraffin composite

In the experiments, the temperature variations and melting process of LPAF//paraffin composite could be obtained. However, it is difficult to observe some transient results and interior phenomena by experiment. In order to further understand the thermal performance of LPAF, the macro models are established according to the experiment conditions.

3.5.1 Modeling method

The cube represents the paraffin embedded in LPAF, whose dimension is 60mm×45mm×24mm. The bottom surface is the heat source with constant heat flux 3500 W m⁻². The left and right surfaces are isolated, and the top surface is the aluminum plate. For melting process of the composite, because the heat transfer and phase transition process are complex, some assumptions need to be applied in the calculation process: (1) The aluminum foam is considered as homogeneous and is full filled with paraffin; (2) The thermal properties of paraffin are constant during the phase transition process; (3) The thermal radiation on the model sample is neglected (4) The crystal transition in solid paraffin is not considered.

The governing equations of the model are based on mass, momentum and energy conservation equations, and the expressions are described as follows:

Continuity equation:

$$\frac{\partial \rho_p}{\partial t} + \nabla \cdot (\rho_p \mathbf{U}) = 0 \quad (3-4)$$

Momentum equation:

$$\frac{\rho_p}{\varepsilon} \frac{\partial \mathbf{U}}{\partial t} + \frac{\rho_p}{\varepsilon^2} (\mathbf{U} \cdot \nabla) \mathbf{U} = \frac{\mu}{\varepsilon} \nabla^2 \mathbf{U} - \nabla P - \left(\frac{\mu}{K} \mathbf{U} + \frac{C_i \rho_p \mathbf{U} |\mathbf{U}|}{2} \right) + \rho_p g \gamma (T - T_0) + S \quad (3-5)$$

Energy equation:

$$(\varepsilon \rho_p c_p + (1 - \varepsilon) \rho_s c_s) \frac{\partial T}{\partial t} + \rho_p c_p (\mathbf{U} \cdot \nabla T) = k_{\text{eff}} \nabla^2 T - \varepsilon \rho_p L \frac{\partial \beta}{\partial t} \quad (3-6)$$

where, \mathbf{U} represents the velocity field of liquid paraffin; ρ is the density, and the subscript p and s represent paraffin and aluminum foam, respectively; ε is the porosity of the foam; μ is the viscosity of the paraffin; c is specific heats; γ is the thermal expansion factor; L is the latent heat; β is the volume fraction of the liquid; S is the source term; k_{eff} is the effective thermal conductivity and it is calculated by Eq. (1-1).

The Eq. (3-6) is called equilibrium model in some research works, which regards the metal foam and PCM as a whole. The equilibrium model is relatively simple and it could shorten the calculation time. Recently, another model is developed which is named non-equilibrium model. This model applies two energy equations for the PCM and metal foam, as described in Eq. (3-7) and Eq. (3-8). The non-equilibrium model is always used in the investigations of the natural convection in the composite with high porosity.

Energy equation for paraffin:

$$\varepsilon\rho_p c_p \frac{\partial T_p}{\partial t} + \varepsilon\rho_p c_p (\mathbf{U} \cdot \nabla) T_p = k_{pe} \nabla^2 T_p + hA(T_s - T_p) - \varepsilon\rho_p L \frac{\partial \beta}{\partial t} \quad (3-7)$$

Energy equation for metal foam:

$$(1 - \varepsilon)\rho_s c_s \frac{\partial T_s}{\partial t} = k_{se} \nabla^2 T_s + hA(T_p - T_s) \quad (3-8)$$

where, k_{pe} and k_{se} are effective thermal conductivity of paraffin and metal foam; h is the heat transfer coefficient; A is interfacial area density.

3.5.2 Determination of the structural parameters

Several parameters in the equations are critical for the simulation, such as k_{se} , h , K and A . and their values always have the relationship with the structure of aluminum foam. As mentioned above, the structures of LPAF and HPAF are different, leading to the different determination methods for these parameters. For the k_{se} of LPAF, it is based on the results in Fig. 3.8 while the porosity range is only from 57% to 68%. For HPAF, the equation deduced by Boomsma and Poulikakos [25] is a popular method. Combining the results of these two numerical methods, the curve of k_{se} as a function of ε could be fitted, as shown in Fig. 3.22. It is obvious that the numerical results have good agreement with the experiment data [21, 135, 136]. Therefore, the value of k_{se} used in this study could be acquired according to the fitting curve.

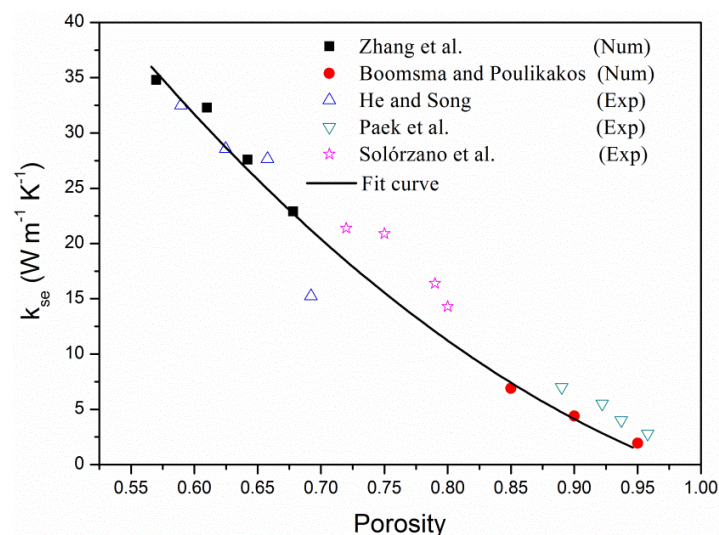


Fig. 3.22. Effective thermal conductivity determined by numerical and experimental methods

Furthermore, the determination methods for h , K and A are followed by empirical formulas, as listed in Table 3.2. The expressions of K and A are deduced according to the structure of LPAF, and the correlation of h has a wide application range. Thus, these equations are chosen in this study.

Table 3.2 Correlations of LPAF parameters

Parameter	Correlation	No.	Ref.
Permeability, K	$K = \frac{\varepsilon r^2}{\pi} \left[\frac{\varepsilon - \varepsilon_0}{3(1 - \varepsilon_0)} \right]^{3/2}$	(3-9)	[137]
Heat transfer coefficient, h	$h = \frac{k_p}{d_f} \left[\left(1 + \frac{4(1 - \varepsilon)}{\varepsilon} \right) + 0.5(1 - \varepsilon)^{0.5} Re^{0.6} Pr^{1/3} \right]$	(3-10)	[138]
Interfacial area density, A	$A = \frac{281}{d_p} \left[(1 - \varepsilon)^{1/2} - (1 - \varepsilon) \right] (1 - \varepsilon)^{0.4}$	(3-11)	[139]

3.5.3 Numerical procedure and boundary conditions

The equilibrium model and non-equilibrium model are calculated in Fluent[®] software, and the governing equations are solved by finite volume method with SIMPLE algorithm. Due to the existence of natural convection, PRESTO method is recommended as the discretization method for pressure. The UDF (user defined

functions) is also applied in simulation to realize the heat transfer between the metal foam and phase change material. Based on the geometrical shape of the sample, the hexahedral cell with uniform size is suitable for the simulation. The mesh independence is tested by comparing the total melting time obtained in three different meshes: 1.5×10^5 , 3×10^5 and 6×10^5 grids. The results indicate that the mesh with 3×10^5 grids could balance both the time and accuracy with less than 2 % time differences of three meshes.

In initial, the sample is at ambient temperature (20 °C). The boundary conditions are based on the experiment. The heat source has the constant heat flux 3500 W m^{-2} . The surface conditions are mentioned above in section 3.4.2, and they could be presented as equations in Table 3.3.

Table 3.3 Initial and boundary conditions

	Positions	Conditions
Initial condition	$0 \leq x \leq 60, 0 \leq y \leq 45,$ $0 \leq z \leq 25$	$T_s = T_p = T_0$
Boundary condition	$x = 0 \ \& \ x = 60$	$\frac{\partial T}{\partial x} = 0$
	$z = 0 \ \& \ z = 25$	$k_{eff} \frac{\partial T}{\partial z} + h_{eff}(T_{amb} - T) = 0$
	$y = 45$	$k_{eff} \frac{\partial T}{\partial y} + h_{eff}(T_{amb} - T) = 0$
	$y = 0$	$q_h = q_s + q_p = (1 - \varepsilon)q_h + \varepsilon q_h$

3.5.4 Comparison of the equilibrium model and non-equilibrium model

The comparison is carried out between the results of two models and experimental data. Fig. 3.23 presents the temperature variation results, and the average errors are listed in Table 3.4. It could be found that both of the models agree well with the experiment for the composite with $\varepsilon = 67\%$, and the average

error of equilibrium model is small than that of non-equilibrium model. As discussed above, the heat transfer process of the composite with $\varepsilon = 67\%$ is dominated by thermal conduction. In this condition, the non-equilibrium model which is developed for natural convection does not show its advantages. Consequently, the equilibrium model could satisfy the simulation of the composite with $\varepsilon = 67\%$. For the composite with $\varepsilon = 84\%$, the results of two kinds of models have the same tendency with the experimental data. The deviations between numerical and experimental results are due to the neglect of the thermal radiation, crystal transition in paraffin, and filling rate of paraffin. In Table 3.4, the average error of non-equilibrium model is smaller than that of equilibrium model, because it considers the development of natural convection. Besides, non-equilibrium model could reflect the temperature stratification in the composite, as shown in Fig. 3.23 (d). As a result, the non-equilibrium model is more suitable to the composite with $\varepsilon = 84\%$.

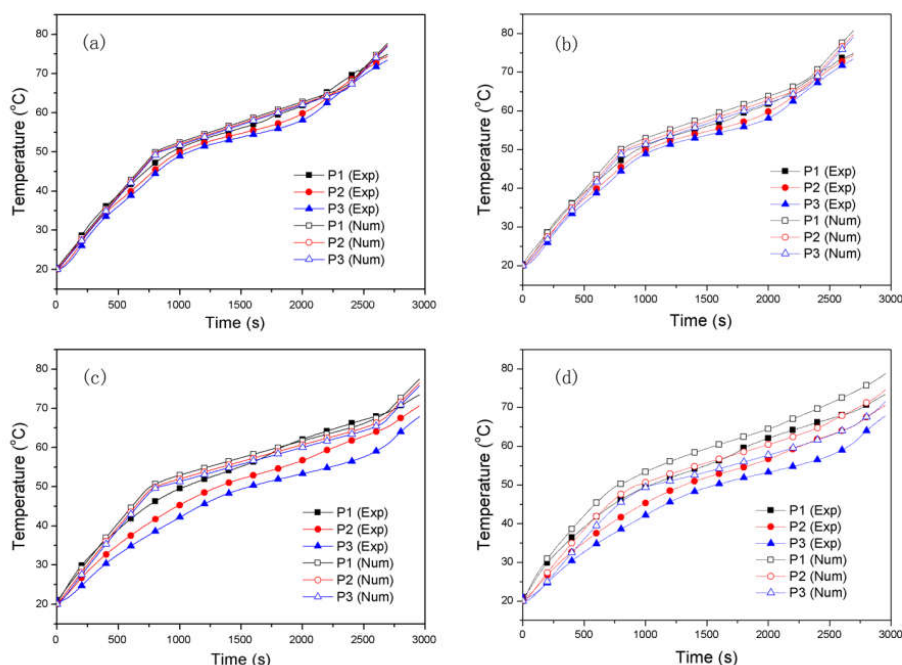


Fig. 3.23. Comparison of temperature variations between numerical results and experiment data (a) equilibrium model with $\varepsilon=67\%$ (b) non-equilibrium model with $\varepsilon=67\%$ (c) equilibrium model with $\varepsilon=84\%$ (d) non-equilibrium model with $\varepsilon=84\%$

Table 3.4 Average errors between experimental data and numerical results

Model	$\varepsilon=67\%$	$\varepsilon=84\%$
Equilibrium model	3.4%	8.6%
Non-equilibrium model	4.1%	7.5%

3.5.5 Flow characteristics for different heat source locations

With the help of the simulation results, the natural convection of paraffin embedded in aluminum foam could be visualized. Fig. 3.24 depicts the liquid phase distributions and stream lines under different heat source locations for the composite with $\varepsilon = 84\%$. When the heat source is placed horizontally, the interface is parallel with the bottom, which agrees with the experiment process. Temperature gradient leads to the circulations in the liquid, and the stream lines demonstrate that the flow rises from the center and decreases to the bottom along with the front and back surfaces, as displayed in Fig. 3.24 (a). The interface of the vertical heat source is sloped as the result of the natural convection. It is noted that the circulation flows are uniform and large. The liquid near the heat source rises up due to high temperature and buoyancy force. After reaching the top surface, the liquid paraffin changes the flow direction and moves forward. When it touches the solid phase, the liquid releases energy to the solid paraffin and flows down along with the interface. In this process, the interface becomes inclined, and the top part melts more rapidly than the bottom part.

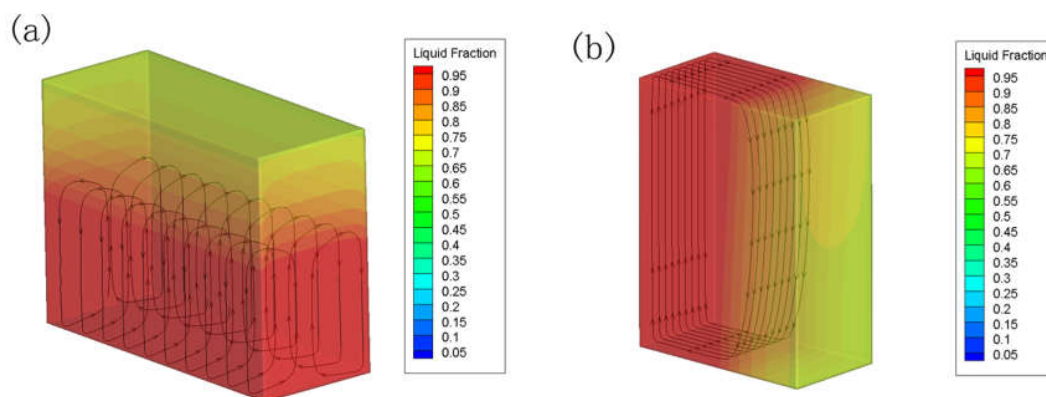


Fig. 3.24. Liquid phase distributions and stream lines under different heat source locations at 2600s for the composite ($\varepsilon=84\%$). (a) horizontal heat source (b) vertical heat source

3.6 Conclusion

The melting process of pure paraffin is predominated by thermal convection, and the flow pattern in the liquid is based on the location of the heat source. Comparing with the vertical heat source, the Benard convection cells could contribute to the heat transfer when the paraffin is heated by horizontal heat source. The modified Kelvin model could be used to analyze the effective thermal conductivity of the low porosity aluminum foam, and the numerical results agree well with the experimental data.

The phase transition process of LPAF/paraffin composite is investigated by adopting both experimental and numerical methods. Comparing with the pure paraffin, the addition of aluminum foam with low porosity could remarkably enhance the heat transfer of the paraffin and make the temperature distribution of the composite more uniform. Both thermal conduction and thermal convection contribute to the melting process of paraffin embedded in the aluminum foam. As increase of porosity, the effect of natural convection on the heat transfer is enhanced while the thermal conduction becomes weak. The horizontal location of heat source could reduce the total melting time, especially for the composite with ε

= 84%, while the effect of the location is not significant for the composite with $\varepsilon = 67\%$.

The 3D models are established by using equilibrium model and non-equilibrium model to study the melting process and natural convection in the composite. The numerical results show reasonable agreement with experimental results, and it could be applied in the analysis of the heat transfer in the composite. The equilibrium model could satisfy the simulation of the composite with $\varepsilon = 67\%$. As the porosity increasing, the non-equilibrium model owns the advantages in reflecting the natural convection and temperature stratification.

Chapter 4.
**Numerical analysis of thermal
performance of HPAM/PCM
composite**

Chapter 4. Numerical analysis of thermal performance of HPAM/PCM composite

4.1 Introduction.....	99
4.2 Model of HPAM/PCM composite	100
4.2.1 Modeling method.....	100
4.2.2 Boundary conditions and validation.....	103
4.3 Determination of the optimized porosity of aluminum foam	106
4.3.1 Melting process of the composite with different porosities.....	106
4.3.2 Evaluation of the thermal efficiency of the composite.....	108
4.4 Enhancement methods of the effective thermal efficiency of composite	111
4.4.1 Description of methods and conditions	111
4.4.2 Melting characteristics of the enhancement methods.....	114
4.4.3 Comparison among three enhancement methods	118
4.4.4 Proposition of optimization methods.....	122
4.4.5 Comprehensive evaluation of enhancement methods.....	123
4.5 Conclusion	124

4.1 Introduction

Embedding PCM in metal foam to make metal foam/PCM composite is considered so efficient that it becomes a popular area of research in thermal energy storage [75, 140]. In the study of metal foam/PCM composite, it is found that the porosity of aluminum foam is a vital parameter, because it could not only affect heat transfer mode in the melting process of PCM [141], but also determine the final energy storage efficiency of the system. However, for the composite with LAPF and HPAF, the problem that which one possesses the best thermal performance is still not clear until now.

In the past ten years, the high porosity aluminum foam (HPAF) draws the attention of many researchers, because its high void volume and high permeability could benefit the energy storage system [19]. But these works mainly focus on the heat transfer mechanism of the composite. In this section, a 2D model of HPAM/PCM composite is established with non-equilibrium equation. Combining the model of LPAM/PCM composite obtained in Section 3, the energy storage efficiencies of composites with the porosity ranging from 65% to 95% could be calculated and compared. The effective thermal efficiency (η_e) of the system is defined as the evaluation parameter to obtain the optimized porosity of the composite.

After determining the optimized porosity, three enhancement methods are proposed and compared to further enhance the energy storage efficiency of the composite with optimized porosity, including changing the value of pores per inch (PPI), changing the shape of the cold wall and using the discrete heat sources. The melting process, heat loss, average velocity of natural convection and the total melting time are analyzed and discussed. Finally, an optimization method realized by combining the advantages of these methods is also presented.

4.2 Model of HPAM/PCM composite

The schematic representation of the 2D model is illustrated in Fig. 4.1. The dimension of the model is 40mm×90mm. The left surface and right surface is heat source and cold wall, respectively. The top and bottom surfaces are isolated. The metal foam used in this study is made by aluminum alloy AS7G, and paraffin wax is chosen as PCM, whose thermal properties are available in Ref.[79].

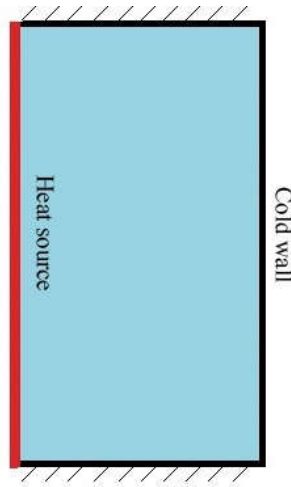


Fig. 4.1. Schematic diagram of the 2D model

In order to simplify the simulation, several assumptions should be adopted in the 2D model: (1) The liquid is considered as incompressible and the flow in the liquid region is laminar; (2) The natural convection caused by buoyancy is subject to the Boussinesque approximation; (3) Because the operation temperature is below 373K, the thermal radiation in the aluminum foam could be neglected during the melting process; (4) The thermal properties of the paraffin are the constant and the volumetric expansion due to the phase transition is negligible; (5) The aluminum foam is considered as homogeneous and isotropic.

4.2.1 Modeling method

The melting process of PCM in the porous metal includes heat conduction and convection. In the early study, the metal foam and PCM are assumed to have

the same temperature [127], and the natural convection is neglected. In fact, the natural convection could increase the melting rate in the latent heat storage system. In order to analyze its effect on the phase transition process, the non-equilibrium equation should be employed in energy conservation equation. As discussed above, the governing equations applied in this study can be written as follow:

Continuity equation:

$$\frac{\partial \rho}{\partial t} + \rho \left(\frac{\partial u}{\partial x} + \frac{\partial v}{\partial y} \right) = 0 \quad (4-1)$$

Momentum equation:

$$\frac{\rho}{\varepsilon} \frac{\partial u}{\partial t} + \frac{\rho}{\varepsilon^2} \left(u \frac{\partial u}{\partial x} + v \frac{\partial u}{\partial y} \right) = \frac{\mu}{\varepsilon} \left(\frac{\partial^2 u}{\partial x^2} + \frac{\partial^2 u}{\partial y^2} \right) - \frac{\partial P}{\partial x} - \left(\frac{\mu}{K} u + \frac{C_i \rho u |u|}{2} \right) + S(u) \quad (4-2)$$

$$\frac{\rho}{\varepsilon} \frac{\partial v}{\partial t} + \frac{\rho}{\varepsilon^2} \left(u \frac{\partial v}{\partial x} + v \frac{\partial v}{\partial y} \right) = \frac{\mu}{\varepsilon} \left(\frac{\partial^2 v}{\partial x^2} + \frac{\partial^2 v}{\partial y^2} \right) - \frac{\partial P}{\partial y} - \left(\frac{\mu}{K} v + \frac{C_i \rho v |v|}{2} \right) + \rho g \gamma (T - T_0) + S(v) \quad (4-3)$$

Energy equation for PCM:

$$\varepsilon \rho_p c_p \frac{\partial T_p}{\partial t} + \varepsilon \rho_p c_p \left(u \frac{\partial T_p}{\partial x} + v \frac{\partial T_p}{\partial y} \right) = k_{pe} \left(\frac{\partial^2 T_p}{\partial x^2} + \frac{\partial^2 T_p}{\partial y^2} \right) + hA(T_s - T_p) - \varepsilon \rho_p L \frac{\partial \beta}{\partial t} \quad (4-4)$$

Energy equation for metal foam:

$$(1 - \varepsilon) \rho_s c_s \frac{\partial T_s}{\partial t} = k_{se} \left(\frac{\partial^2 T_s}{\partial x^2} + \frac{\partial^2 T_s}{\partial y^2} \right) + hA(T_f - T_s) \quad (4-5)$$

The addition of the third term on the right side of Eq. (4-2) is based on Darcy-Forchheimer law, which is an empirical equation for studying liquid flow in porous zone. The fourth term on the right side of Eq. (4-3) represents the Boussinesque approximation. If there is a temperature difference in the liquid zone during the melting process, the density gradients lead to the buoyancy force, which is the driving force of natural convection. The utilization of the source term S in the momentum conservation equation is due to the mushy zone during the phase transition. The source term is followed as:

$$S = \frac{C(1-\beta^2)}{\alpha + \beta^3} \quad (4-6)$$

where, α is a constant and C is consecutive number for the mushy zone which could make PCM static before melting. Shmueli et al. [142] found that the numerical result has the best agreement with experimental data when C is 10^8 . The last term in the energy equation for PCM is applied to account for the absorption of latent heat in PCM during the melting process, and the liquid fraction is based on the enthalpy method.

To obtain the accurate results, some parameters related to the structure of aluminum foam are important, such as permeability (K), heat transfer coefficient (h) and interfacial area density (A). There are several determination methods of these parameters, which are commonly used in literature [29, 31, 34, 35, 137, 138, 143-145]. According to the application range of these expressions, three equations are chosen in this study and listed in Table 1.

Table 4.1 Common correlations of HPAM parameters

Parameter	Correlation	No.	Ref.
Permeability, K and inertial coefficient, C_i	$\frac{K}{d_p^2} = 0.00073(1-\varepsilon)^{-0.224} \left(\frac{d_f}{d_p}\right)^{-1.11}$	(4-7)	[31]
	$C_i = 0.00212(1-\varepsilon)^{-0.132} \left(\frac{d_f}{d_p}\right)^{-1.63}$		
Heat transfer coefficient, h	$h = \frac{k_f}{d} \left[\left(1 + \frac{4(1-\varepsilon)}{\varepsilon}\right) + 0.5(1-\varepsilon)^{0.5} \text{Re}^{0.6} \text{Pr}^{1/3} \right]$	(4-8)	[138]
Interfacial area density, A	$A_{PPI10} = 349.15 \ln(1-\varepsilon) + 1667.99$	(4-9)	[145]
	$A_{PPI20} = 442.2 \ln(1-\varepsilon) + 2378.62$		
	$A_{PPI40} = 694.57 \ln(1-\varepsilon) + 3579.99$		

The Eq. (4-7) is applied to determine the value of K, because the effect of porosity and structure of metal foam is taken into account. The Eq. (4-8) could represent well the heat conduction and convection during the phase transition. Thus, h could be calculated by this formula. The interfacial area density (A) is the rate of surface area to volume. The value of A is calculated by Eq. (4-9), which is derived from experimental data. In addition, the relation between d_f and d_p is based on Eq. (4-14)

$$\frac{d_f}{d_p} = 1.18 \sqrt{\frac{1-\varepsilon}{3\pi}} \quad (4-10)$$

The effective thermal conductivities of solid and liquid phase have a significant impact on the energy equation. The determination method of these two parameters proposed by Boomsma and Poulikakos [25] has been adopted widely to describe the heat transfer in metal foam. Thus, this method is applied in this study and the expression is described as follow:

$$\begin{aligned} k_e &= \frac{1}{\sqrt{2}(R_A + R_B + R_C + R_D)} \\ R_A &= \frac{4\lambda}{(2e^2 + \pi\lambda(1-e))k_s + (4 - 2e^2 - \pi\lambda(1-e))k_f} \\ R_B &= \frac{(e - 2\lambda)^2}{(e - 2\lambda)e^2k_s + (2e - 4\lambda - (e - 2\lambda)e^2)k_f} \\ R_C &= \frac{(\sqrt{2} - 2e)^2}{2\pi\lambda^2(1 - 2\sqrt{2}e)k_s + 2(\sqrt{2} - 2e - \pi\lambda^2(1 - 2\sqrt{2}e))k_f} \\ R_D &= \frac{2e}{e^2k_s + (4 - e^2)k_f} \\ \lambda &= \sqrt{\frac{\sqrt{2}(2 - (5/8)e^3\sqrt{2} - 2\varepsilon)}{\pi(3 - 4\sqrt{2}e - e)}}, e = 0.339 \\ k_{je} &= k_{eff} \Big|_{k_m=0}, k_{se} = k_{eff} \Big|_{k_p=0} \end{aligned} \quad (4-11)$$

4.2.2 Boundary conditions and validation

The paraffin and aluminum foam are initially both at the ambient temperature. The heat source has a constant heat flux density q_w . The cold wall is in contact with

air so that it could release the heat to the environment. The top and bottom walls are both adiabatic. The initial condition and boundary condition are described by the following expressions:

$$\text{Initial condition: } 0 \leq x \leq 50, 0 \leq y \leq 90, u = v = 0, T_{Al} = T_p = T_0$$

$$x = 0, 0 \leq y \leq 90, u = v = 0, q_{Al} + q_p = (1 - \varepsilon)q_w + \varepsilon q_w;$$

$$0 \leq x \leq 50, y = 0, u = v = 0, \frac{\partial T}{\partial y} = 0;$$

$$\text{Boundary conditions: } 0 \leq x \leq 50, y = 90, u = v = 0, \frac{\partial T}{\partial y} = 0;$$

$$x = 50, 0 \leq y \leq 90, u = v = 0, k_{\text{eff}} \frac{\partial T}{\partial x} + h_{\text{eff}} (T_{\text{amb}} - T) = 0$$

The mesh in the computational domain is the uniform quadrilateral element. The mesh independence is examined, and the result is presented in Fig. 4.2. The coarse mesh (5000 elements), medial mesh (10000 elements) and fine mesh (20000 elements) are tested. Comparing with the result of the fine mesh, the differences of liquid fraction of medial meshes are less than 2 %. Considering the accuracy of the results and computational time, 10000 elements can ensure the mesh independence.

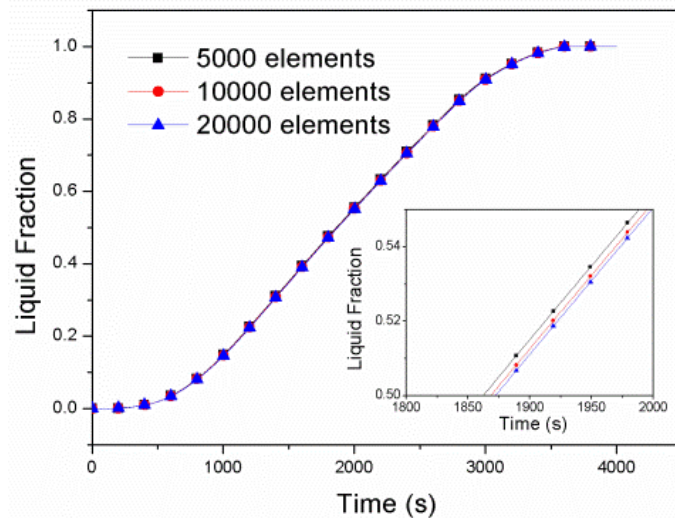


Fig. 4.2. Mesh dependence analysis.

The model used in this study is validated against the experimental results of Zhao et al. [78] and Lafdi et al. [76]. Fig. 4.3 shows the comparison of temperature variations between the numerical and experimental results. It is obvious that these two temperature rising curves predicted by the model show a good agreement with the experimental data. The comparison of the interface locations between the experimental photos and numerical results is shown in Fig. 4.4. The predicted locations of solid/liquid phases agree well with the locations in experimental photos. As a result, the model could be applied to investigate the heat transfer and phase transition process of the paraffin embedded in aluminum foam.

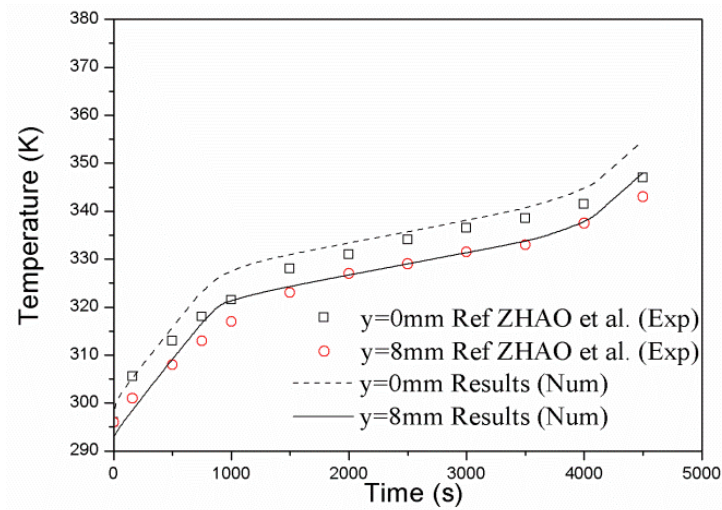


Fig. 4.3. Comparison of temperature variations between the experimental data [78] and numerical results

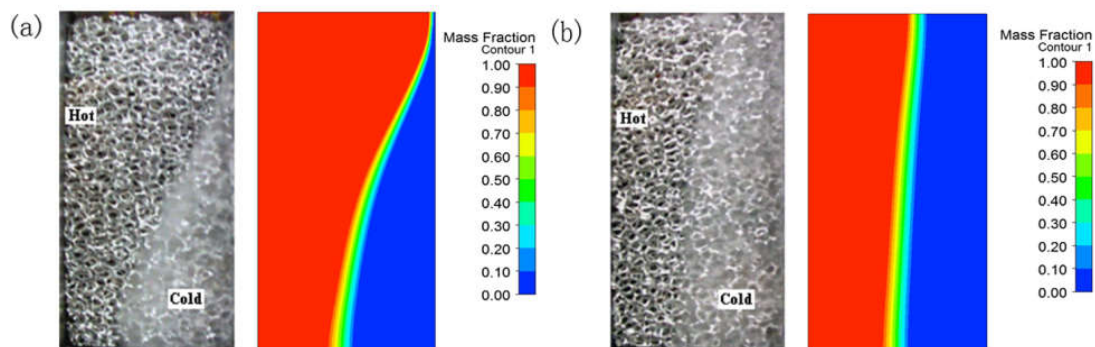


Fig. 4.4. Comparison of the interface locations between the experimental photos [76] and numerical results (a) 96.6% porosity and 10PPI (b) 93.4% porosity and 10PPI.

4.3 Determination of the optimized porosity of aluminum foam

In fact, it is found that the main difference between LPAF model and HPAF model is the determination methods of the structural parameters. In this case, if we combine the two models that have been obtained in the same condition, the thermal behavior of the aluminum foam with the porosity (ϵ) range from 65% to 95% could be analyzed numerically. In this section, the geometric dimension and boundary conditions are according to the model in Section 4.2. Considering the effect of the heat conduction and convection in the composite, it is speculated that there is an optimized porosity in the composite, which could balance two heat transfer modes and optimize the performance of thermal energy storage system. To obtain the optimized porosity, the melting process, variation of liquid fraction and thermal efficiency of the composite are studied and compared.

4.3.1 Melting process of the composite with different porosities

Fig. 4.5 shows the melting processes of the composites with $\epsilon = 70\%$, 80% and 90% . It is seen that the liquid- solid interface becomes more and more sloping with the increase of the porosity, indicating that the effect of natural convection is enhanced. In addition, the thickness of the mushy zone decreases as the porosity increasing. Shyy and Chen [146] considered that the reduction of temperature difference between PCM and aluminum foam could make the mushy zone thick. Comparing the thickness of mushy zone for different composites, it is concluded that temperature different in the composite with low porosity is smaller than that in composite with high porosity. The results of liquid fractions are presented in Fig. 4.6. It is found that, for the composite with $\epsilon = 70\%$ and 80% , the liquid fraction

seems to be a linear function of time and the paraffin in these composites melts quickly. Although the liquid phase appears early in the composite with $\varepsilon=90\%$, the melting rate of the paraffin reduces with the elapse of the time, especially for the period after 3000 s. As discussed above, the natural convection plays a critical role in the melting process of the composite made of HPAF. Due to the flow pattern, the solid paraffin in the right bottom corner of the composite will melt at the last stage, as displayed in Fig. 4.5(c). This corner is far away from the heat source and the length of the interface of the paraffin decreases gradually, which weakens the convective heat transfers. Therefore, the reduction of melting rate at last period is a problem for the composite with high porosity.

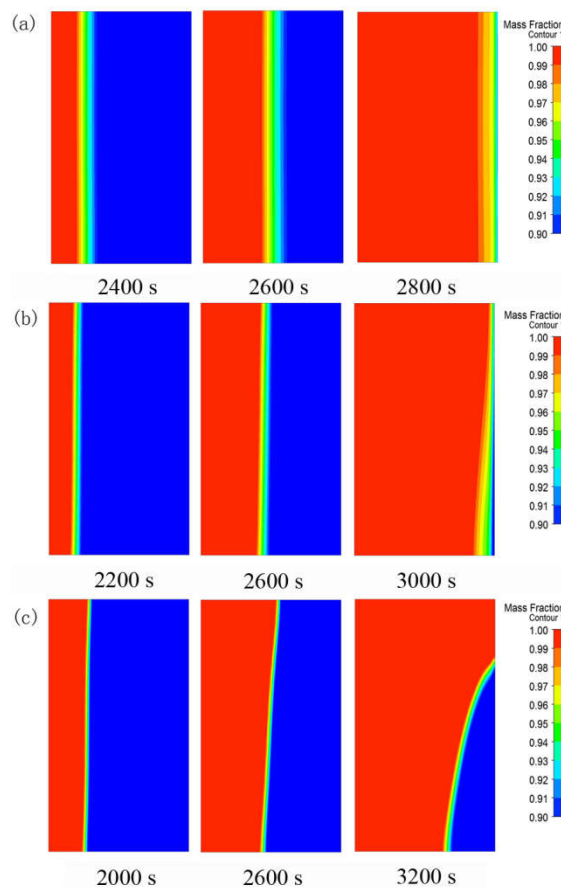


Fig. 4.5. Melting processes of the composites with different porosities. (a) 70%
(b) 80% (c) 90%

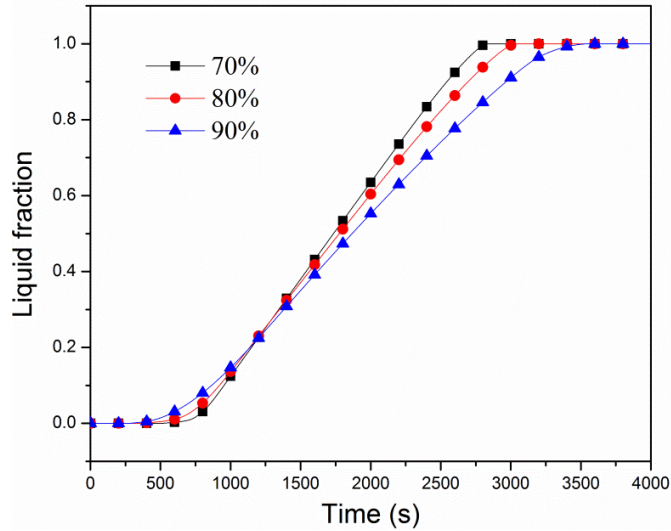


Fig. 4.6. Variations of liquid fractions as the function of time for the composites with different porosities

4.3.2 Evaluation of the thermal efficiency of the composite

Although the composite with low porosity has the fast melting process, the low fraction of PCM maybe reduces the total quantity of the energy stored in the composite. To obtained the optimized porosity in the composite, the efficiency of the energy storage is a vital evaluation standard. Thus, the thermal efficiency (η) of the system is defined as the ratio between the energy stored in composite and the amount of input energy. The expression is as follow:

$$\eta = \frac{E_{store}}{E_{in}} \times 100\% \quad (4-12)$$

where, E_{in} represents the amount of input energy, E_{store} is the energy stored in composite, including the energy stored in the PCM and aluminum foam. The energy in PCM consists of two parts: sensitive energy and latent energy. Thus, the formula of E_{store} is based on Eq.(4-13):

$$\begin{aligned}
E_{store} &= E_{PCM} + E_{al} \\
&= m_p Lf + \sum_{i=1}^M \sum_{j=1}^N \Delta m_p c_p [(T_p)_{ij} - T_0] + \sum_{i=1}^M \sum_{j=1}^N \Delta m_{al} c_{al} [(T_{al})_{ij} - T_0] \quad (4-13)
\end{aligned}$$

where, the subscript p and al represent PCM and aluminum foam, respectively; m is mass of material; L is the latent heat of PCM; f is liquid fraction; c is specific heat; M and N represent the numbers of the mesh in x and y axis; T_0 is the initial temperature. Because the composite is heated by constant power, the value of E_{in} could be calculated by the equation: $E_{in} = qS_h t$, where q is heat flux density; S_h is the surface area of heat source; t is the time. As a result, the final expression of thermal efficiency of the system is as follow:

$$\eta = \frac{m_p Lf + \sum_{i=1}^M \sum_{j=1}^N \Delta m_p c_p [(T_p)_{ij} - T_0] + \sum_{i=1}^M \sum_{j=1}^N \Delta m_{al} c_{al} [(T_{al})_{ij} - T_0]}{qS_h t} \times 100\% \quad (4-14)$$

Fig. 4.7 presents the variation of η as the function of time. The initial value of η is 100%. As time progressed, the temperature of the composite increases gradually, leading to an augment of heat loss from the cold wall and the decrease of the thermal efficiency. In the period from 1000 s to 3000 s, it is found that the descent rate of η reduces and there is a flat zone in the curve. This is because the majority of paraffin melts in this period and the input energy is stored in the composite as the form of latent heat. When the paraffin melts totally, the thermal efficiency of the composite will decrease greatly again. Besides, comparing η of different composites at the same moment, the composite with high porosity possesses the large thermal efficiency. The reason could be due to the low thermal conductivity, so that the heat loss from the cold wall is less than others. But, these results do not mean that the composite with high porosity is the best for the system, because the total melting time of the composite will be increased as the increase of the porosity, as presented in Fig. 4.8.

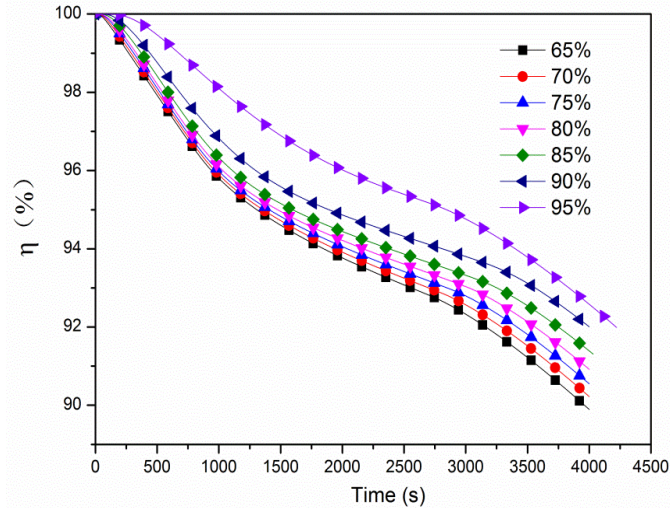


Fig. 4.7. Thermal efficiency (η) as the function of time for the composites with different porosities

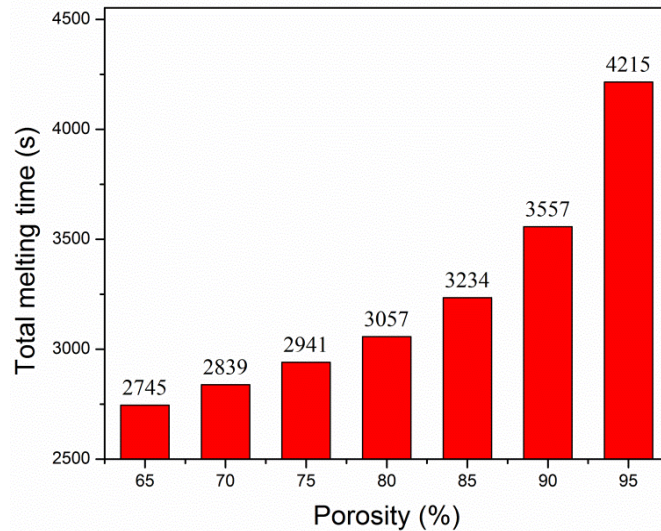


Fig. 4.8. Total melting times of the composites with different porosities

The composite could not be heated too long. When the paraffin becomes liquid, the continuous heating could lead to the increase of the temperature. At this moment, the form of energy stored in paraffin becomes sensitive heat again. The purpose of the utilization of phase change material is that the amount of energy could be stored in the material during phase change process. Thus, we defined the value of η at the moment when the paraffin totally melts as the effective thermal efficiency (η_e) of the system. In this condition, the relationship of effective thermal efficiency and porosity could be obtained, as shown in Fig. 4.9. It is found that the

value of η_e is the highest when the porosity is from 85% to 90%. Thus, the optimized porosity could be determined in this range, which could balance the energy storage quantity and the melting time. The composite with the optimized porosity could own the largest thermal efficiency in the condition of safety and stability.

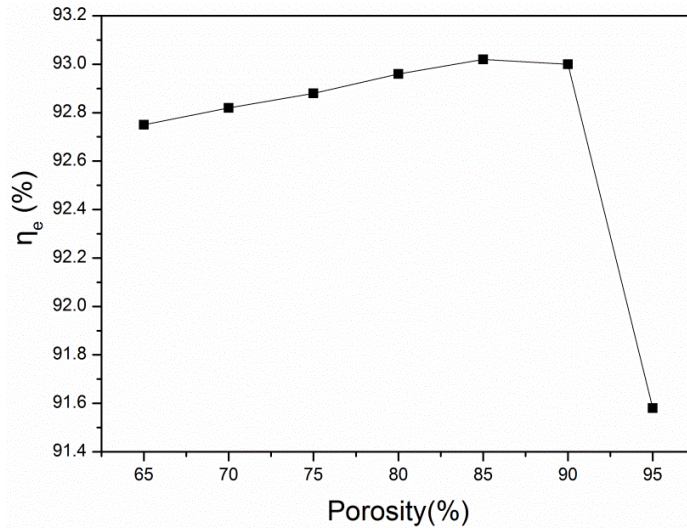


Fig. 4.9. Effective thermal efficiency as the function of porosity

4.4 Enhancement methods of the effective thermal efficiency of composite

Although the composite with $\varepsilon=90\%$ has the largest value of effective thermal efficiency, there is still a problem for this composite that the melting rate will decrease at the last stage. To further enhance the melting rate of paraffin, three methods are investigated and compared in this section for the composite with $\varepsilon=90\%$. Finally, an optimization method is also proposed by combining the advantages of these methods

4.4.1 Description of methods and conditions

Among the parameters of the physical model, the aluminum foam, cold wall and heat source are critical factors because they could affect the melting process of

the paraffin embedded in aluminum foam. In order to improve the melting rate of paraffin, three enhancement methods are proposed based on these factors. Meanwhile, the different conditions in each method will be studied to obtain the most suitable structure and parameter. The characteristic conditions and schematic representation of the enhancement methods are presented in Table 4.2 and Fig. 4.10. Method I is changing the value of pores per inch (PPI). Cond.1, 2 and 3 represent the metal foam with 5, 10 and 20 PPI. Method II consists to changing the shape of the cold wall. In order to adapt the evolution of the liquid-solid interface, the cold walls of Cond.4 and 5 are sloped with respect to the horizontal surface, as shown in Fig. 4.10(b). Based on the form of liquid-solid interface, the cold wall with curved surface in Cond.6 is designed to optimize the heat transfer process. Method III is using the discrete heat sources. The total length of heat sources is 60 mm, and the number of the heat source is 2, 3 and 4 for Cond.7, 8 and 9, as shown in Fig. 4.10(c). The heat sources of each condition have the same length and the gaps between them are the same. The first heat sources contacts to the bottom surface and the others are arranged in order. Moreover, all the conditions have the same porosity and volume. The top and bottom surfaces are thermal insulation, and the heat in the sample is released to the atmosphere from cold wall with the heat transfer coefficient $10 \text{ W m}^{-2} \text{ K}^{-1}$. The heat flux density of Method I and II is constant 3800 W m^{-2} , but the value of Method III is 5700 W m^{-2} , which is calculated based on the ratio of power to area.

Table 4.2 Characteristic conditions of three enhancement methods

Method	Condition	PPI	Angle of cold surface (degree)	Heat flux of hot surface ($W m^{-2}$)
Method I	Cond.1	5	90	3800
	Cond.2	10	90	3800
	Cond.3	20	90	3800
Method II	Cond.4	5	83	3800
	Cond.5	5	77	3800
	Cond.6	5	—	3800
Method III	Cond.7	5	90	5714 (2 parts)
	Cond.8	5	90	5714 (3 parts)
	Cond.9	5	90	5714 (4 parts)

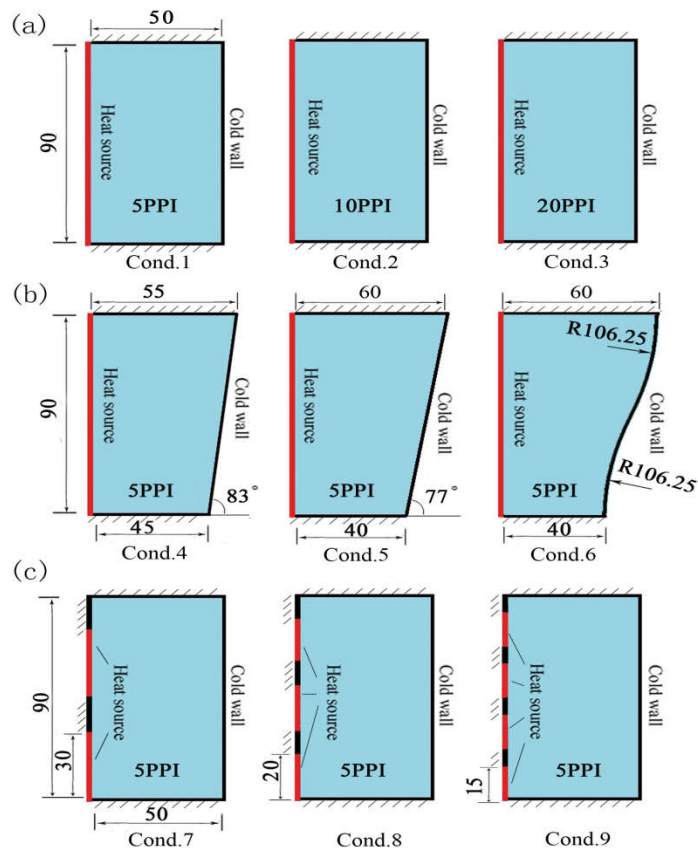


Fig. 4.10. Schematic representation of three enhancement methods
 (a) Method I (b) Method II (c) Method III.

4.4.2 Melting characteristics of the enhancement methods

(a) Method I

Fig. 4.11 shows the melting process of paraffin embedded in aluminum foam in Method I. It is obvious that, at the beginning of melting process, the liquid-solid interface is in parallel with the heat source because the heat conduction plays a dominant role at this time. At 2400s, the interfaces of Cond.1 and Cond.2 are curved, and this phenomenon is due to the development of natural convection. However, for Cond.3, the interface is always in parallel with the heat source before 2400s, because the heat conduction governs the melting process and the heat convection is suppressed due to its low permeability. Fig. 4.12 presents the variations of liquid fraction of Cond.1, 2 and 3. It turned out that the liquid fractions of three conditions are almost the same before 3000 s. This result indicates that, although the predominant mode of heat transfer of Cond.1 and Cond.3 is thermal convection and thermal conduction respectively, the enhancement effects of them on the melting process are similar. The difference of three conditions becomes obvious at last stage. In Fig. 4.11, it is also found that the solid fraction of Cond.3 is less than that of Cond.1 and Cond.2 at 3400 s. Based on Eq.(4-9), the large PPI could result in a large interfacial area density, which could accelerate the heat conduction process between metal foam and PCM. As a result, although the natural convection is suppressed, Cond.3 could enhance the melting process significantly.

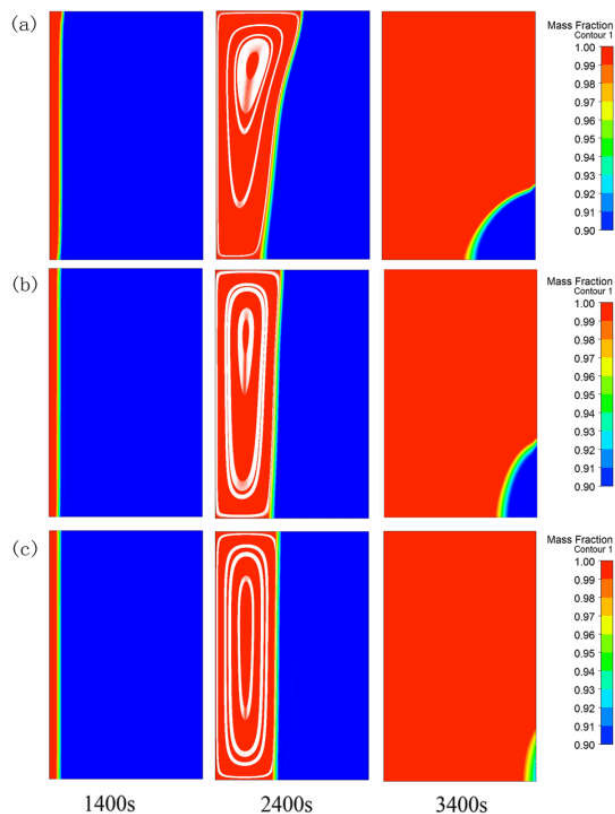


Fig. 4.11. Melting process of Method I at different times. (a) Cond.1 (5 PPI) (b) Cond.2 (10 PPI) (c) Cond.3 (20 PPI)

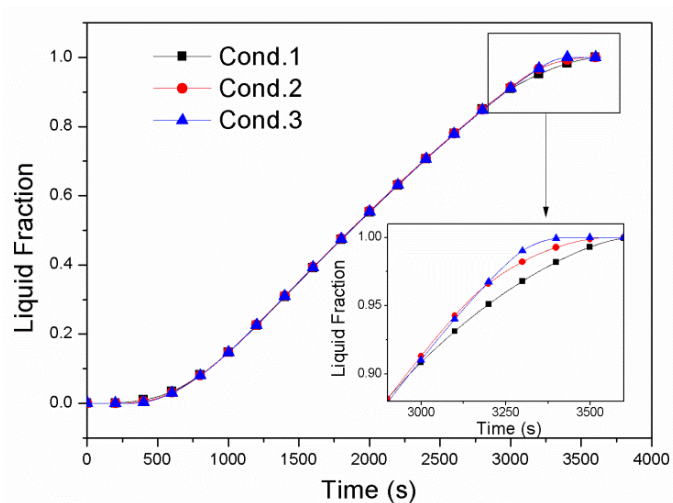


Fig. 4.12. Variation of liquid fraction with time for method I

(b) Method II

The melting processes of Method II with three different conditions are presented in Fig. 4.13. The aluminum foams with 5 PPI are used in Method II,

thus the large diameter of pore leads to a high permeability. At 1400 s, the natural convection is not evident due to the small liquid fraction. As time progresses, the natural convection develops gradually and the melting processes of three conditions are all dominated by heat convection at 2400 s, which is proved by the forms of the interfaces and the streamlines. From the locations of the interfaces at 1400 s and 2400 s, the change of the cold wall does not affect the melting process in this period. The distinction of the liquid fractions of three conditions occurs at 3400 s, which is also observed in Fig. 4.14. Comparing with the interface location of Cond.1 at 3400 s, it turns out that these modified shapes could contribute significantly to improve the melting rate. Besides, although the area of the cold wall in Cond.6 is the largest, its melting rate is faster than others. This is because the shape of the cold wall could affect the heat loss and the natural convection during the melting process. The detailed reason will be discussed in the following section.

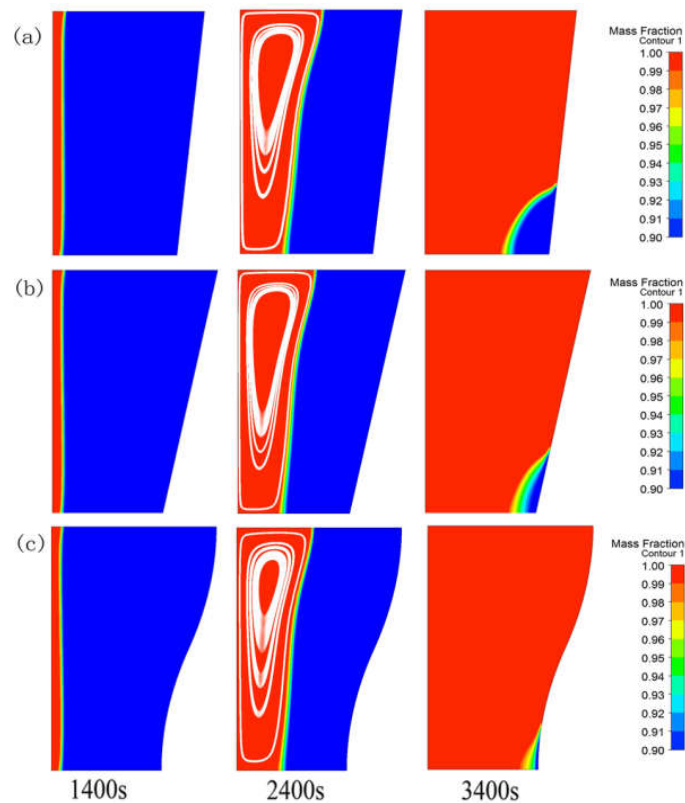


Fig. 4.13. Melting process of Method II at different times. (a) Cond.4 (b) Cond.5 (c) Cond.6.

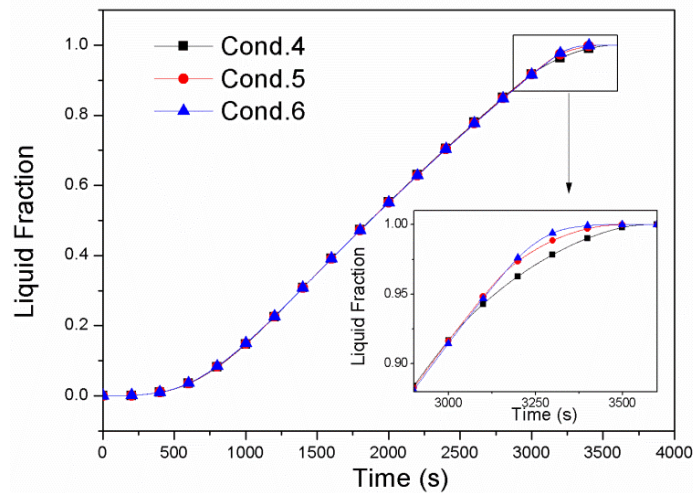


Fig. 4.14. Variation of liquid fraction with time for method II

(c) Method III

Fig. 4.15 shows the melting processes of Method III. At 1400 s, the circulations of liquid zones are separate, and the region near the bottom has the larger melting rate as a result of thermal isolation of bottom surface. After that, the streamline results demonstrate that these zones start to combine together and form a single convection region in the liquid zone. The top parts of the liquid zone protrude to the solid phase in Cond. 8 and Cond.9 at 2400 s, which is similar to the process in the uniform heating conditions. However, the two circulations of Cond.7 do not mix together completely at this moment, because the paraffin at the bottom melts much faster than that at top at beginning. Although the shapes of the interfaces of three conditions are different at 2400 s, the variations of the liquid fraction are almost the same, as shown in Fig. 4.16. Binet and Lacroix [147] found the discrete heat sources could shorten the melting time of pure PCM. However, for the composite, this method is not effective for improving the melting rate. This phenomenon may be caused by the heat loss on the cold wall, which is needed to be analyzed quantitatively.

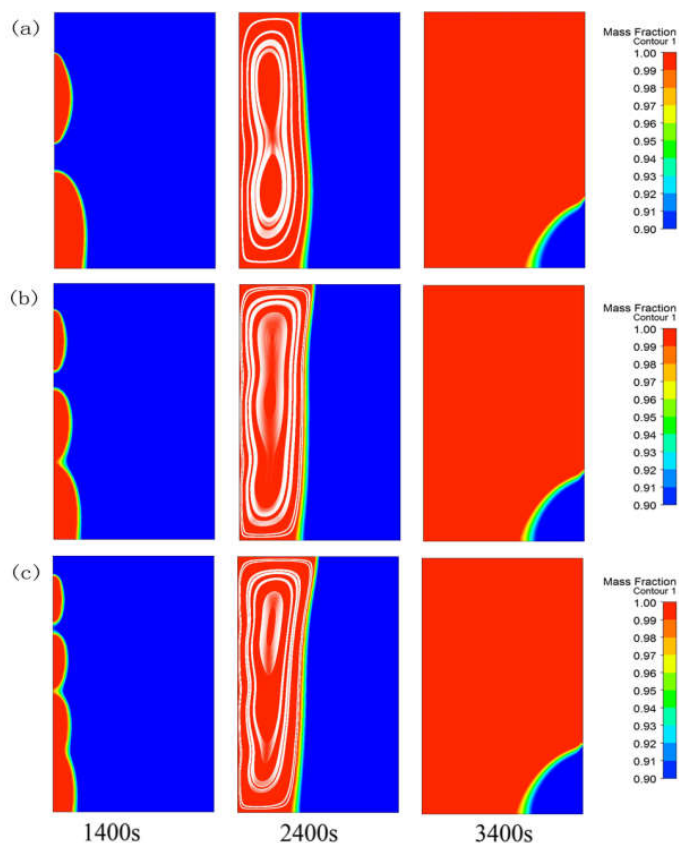


Fig. 4.15. Melting process of Method III at different times. (a) Cond.7 (b) Cond.8 (c) Cond.9

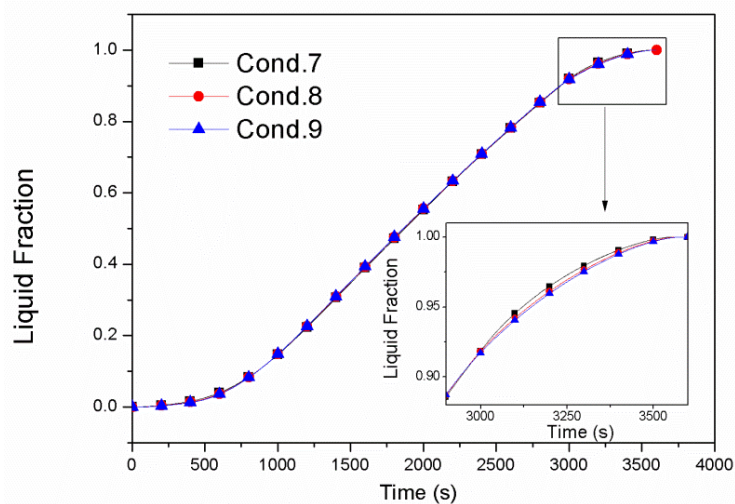


Fig. 4.16. Variation of liquid fraction with time for method III

4.4.3 Comparison among three enhancement methods

(a) Heat loss

During the melting process, the heat in the composite always releases from

the cold wall. Because the input power is constant for different conditions, the amount of heat loss could be considered as a crucial factor to analyze the melting rate of the paraffin. Based on the characteristic of the melting processes, the rate of heat loss of the cold wall will increase when liquid phase touches the cold wall, because the heat in the liquid paraffin will release from the cold wall after this time. Therefore, the moment is critical for the melting process when the liquid phase touches the cold wall firstly. Jany and Bejan [148] proposed the method to determine this moment quantitatively by using the surface average Nusselt number. And the Nu number is defined as:

$$Nu = \frac{q_w H'}{k_f (T_w - T_m)} \quad (4-15)$$

where, H' is the characteristic length and it is considered as the length of the heat source in this study. Fig. 4.17 presents the surface average Nu number of the heat source in Cond.1 (left) and its gradient (right) varies with time. The Nu number drops rapidly before 750s, because the heat conduction dominates in this period. After that, the variation of Nu number is slight, which represents that the heat convection starts to govern the melting process [128]. At last, the slope of Nu number changes again when the time passes the 'knee' point. This time is defined as t_{knee} , and it is the moment when the liquid phase arrives on the cold wall initially [148]. The value of t_{knee} could also be obtained from the horizontal coordinate value of peak point in the curve of Nu gradient. Furthermore, in order to confirm the effect of t_{knee} , the total heat loss from the cold wall during the melting process is calculated by Eq. (13):

$$Q_{loss} = \int_0^{t_{total}} q_c D_c dt \quad (4-16)$$

The quantitative results of t_{knee} and Q_{loss} of nine conditions are shown in Fig. 4.18. For t_{knee} , the values of Cond.3, 5 and 6 are large, which means that the liquid

touches the cold wall later. In this case, the amounts of the heat loss for these three conditions are less than others, which is confirmed in Fig. 4.18 (b). The contrary trends of the t_{knee} and Q_{loss} results demonstrate that the delay of the moment t_{knee} could reduce the heat loss of the cold wall. As a result, the melting rates of Cond.3, 5 and 6 are greater than others, which also explains that the solid fractions of these conditions are less than other conditions in section 4.4.2.

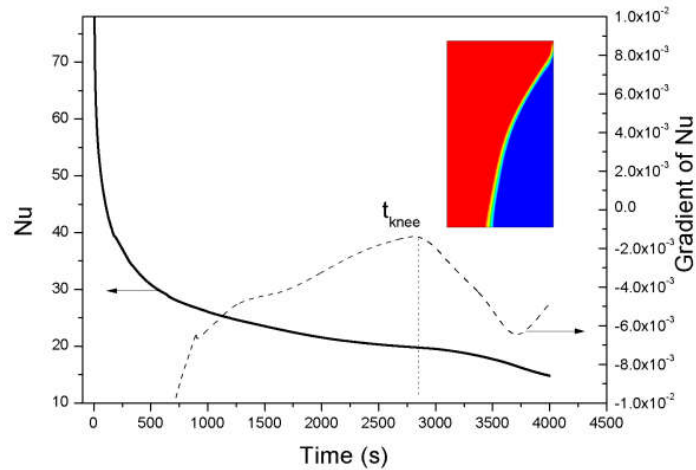


Fig. 4.17. Variation of surface average Nu number of hot wall versus time for Cond.1

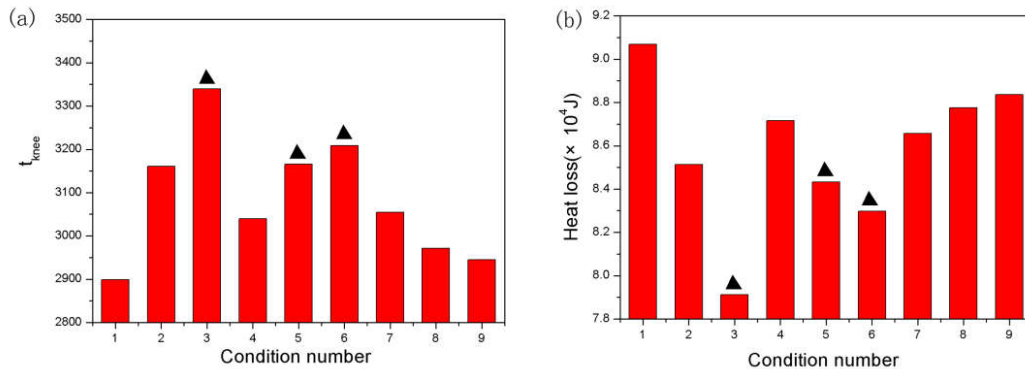


Fig. 4.18. Comparison of the heat loss among the nine conditions (a) result of t_{knee} (b) result of quantity of heat loss from the cold wall

(b) Natural convection

Except for Cond.3, the effect of natural convection is significant for other conditions. It is found that the natural convection could make the temperature distribution more uniform, which is advantageous for the energy storage [66].

Hence, it is necessary to analyze the influence of the enhancement methods on natural convection during the melting process. Grashof number is a dimensionless number which could evaluate natural convection. The express of Gr number is

$$Gr(t) = \frac{g\beta(T_w - T_u)L^3}{\nu^2} \quad (4-17)$$

In order to analyze the extent of natural convection during the whole melting process, the time average Gr number and time average velocity are defined. Their expressions are as follow:

$$Gr_{ave} = \frac{1}{t_{total} - t_l} \int_{t_l}^{t_{total}} Gr(t)dt \quad (4-18)$$

$$V_{ave} = \frac{1}{t_{total} - t_l} \int_{t_l}^{t_{total}} V(t)dt \quad (4-19)$$

where, t_l is the time when the liquid appears firstly in the container. Fig. 4.19 displays the statistical results of Gr_{ave} and V_{ave} for different conditions. For Gr_{ave} results, all the values have the same order of magnitude because the input powers are constant for these conditions. The values of Gr_{ave} in Cond.7-9 are larger than others. This is because the input heat flux is focused on discrete heat sources, which leads to a larger temperature gradient in the liquid phase. Therefore, the driving forces of natural convection in these three conditions are enhanced. However, the natural convection is also affected by the permeability of metal foam and the form of the container. Thus, the value of V_{ave} could reveal the synthesized effect of natural convection during the melting process. In Fig. 4.19 (b), it is obvious that the values of V_{ave} in Cond.5-7 are larger than others. As discussed above, the value of t_{knee} in Cond.5 and Cond.6 is large and the heat loss is less, which could contribute to the natural convection. For Cond.7, although the discrete heat source could ameliorate the natural convection, the distinct improvement of melting rate is not found in the melting process. This

phenomenon is caused by the quantity of heat loss in the cold wall, which could be observed from the result in Fig. 4.18 (b). Therefore, the enhancement extent of Method III is reduced.

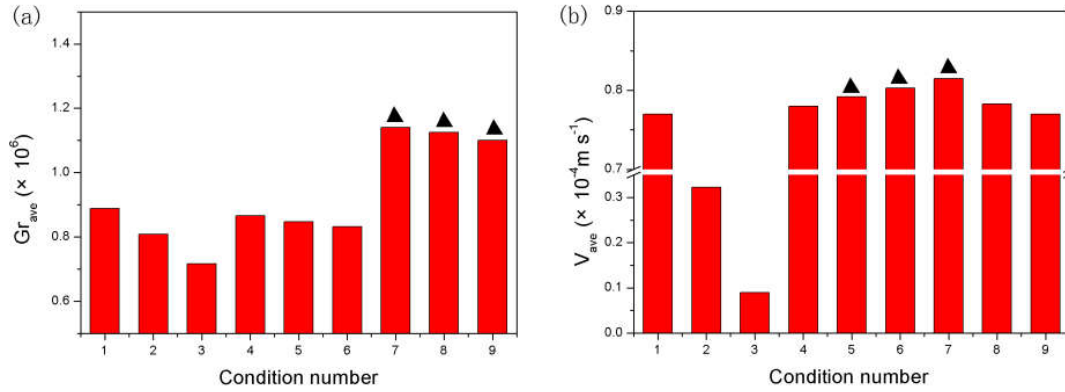


Fig. 4.19. Comparison of the natural convection among the nine conditions (a) result of Gr_{ave} (b) result of V_{ave}

4.4.4 Proposition of optimization methods

Combining the results of these conditions, Cond.3, Cond.5 and Cond.6 have the better thermal performance. For Cond.3, the effect of conduction is greatly enhanced by increasing the interfacial area density. The Cond.5 and Cond.6 prolong the t_{knee} by changing the angle and shape of cold wall to reduce the heat loss. However, these methods are not perfect and some problems still exist. For example, the temperature difference of Cond.3 is very high due to the weak convection, which maybe limits their service life. The enhancement effect of natural convection of Method III is reduced by heat loss. In this case, these enhancement methods could be combined to exert each advantage. Two discrete heat sources could be applied in Cond.6, and this condition is named Cond.10 (Fig. 4.20 (a)). The melting process of this optimization method is presented in Fig. 4.20 (b). It is observed that all the paraffin of Cond.10 become liquid at 3400 s, but there is still solid paraffin in other conditions at this moment. Thus, the thermal performance of Cond.10 is better than others.

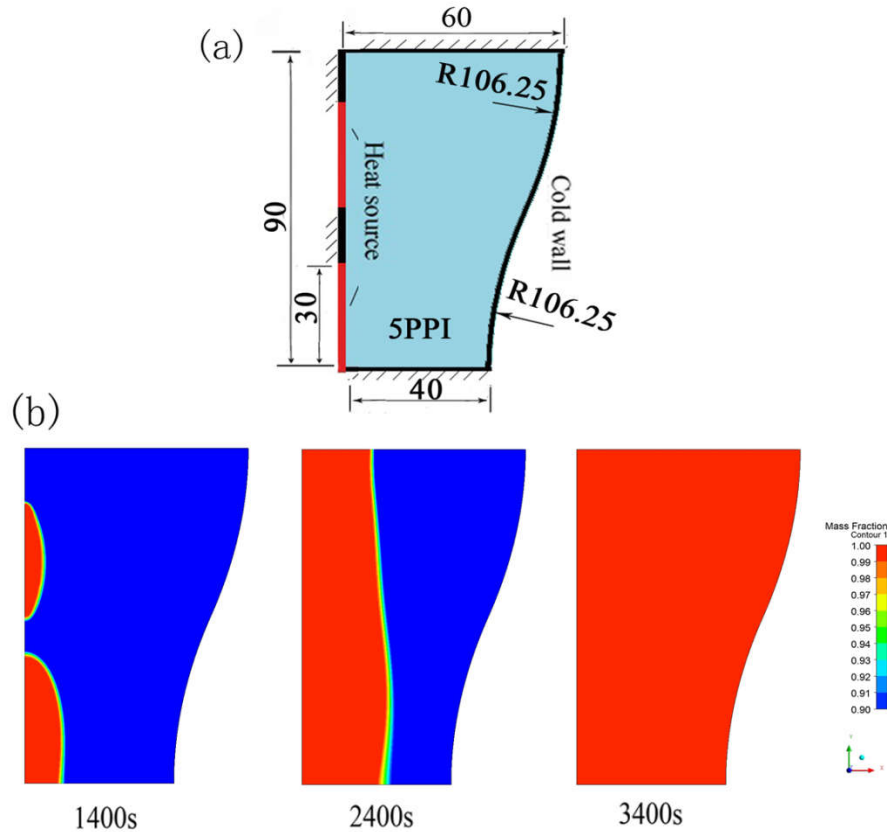


Fig. 4.20. Schematic representation (a) and melting process (b) of the optimization method (Cond.10)

4.4.5 Comprehensive evaluation of enhancement methods

In order to evaluate these enhancement methods in the application of thermal energy storage, the results of total melting time (t_{total}) and effective thermal efficiency (η_e) are compared, as shown in Fig. 4.21. The pure paraffin is regarded as a reference condition (Cond.0), which possesses the same quality of paraffin as other conditions. It is obvious that the addition of the aluminum foam could improve significantly the thermal behavior of the paraffin. For the total melting time, the values of Cond.3, 6 and 10 are shorter than other conditions. Among them, the t_{total} of Cond.10 is the shortest, which could reduce the total melting time by 45.4% comparing with pure paraffin. Besides, the effective thermal efficiencies of Cond.3 and Cond.10 are highest in all conditions, which is 10% more than that

of Cond.0. Combining these two factors, it is concluded that Cond.3 and 10 are two kinds of enhancement methods that have the best comprehensive result. As mentioned above, the substance of Cond.3 is that thermal conduction is enhanced through decreasing the pore size, while the purpose of Cond.3 is to accelerate the convective heat transfer in the composite. In consequence, the thermal performance of the aluminum foam/paraffin could be further improved through enhancing the thermal conduction or thermal convection.

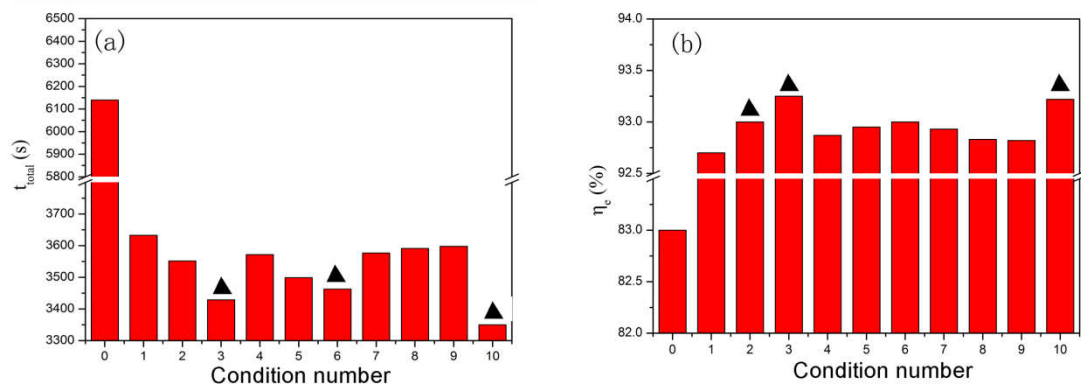


Fig. 4.21. Comprehensive evaluation of enhancement methods (a) result of t_{total}
(b) result of η_e

4.5 Conclusion

The model of HPAM/PCM composite based on finite volume element and non-equilibrium equation is established and it is validated with experimental data. The numerical results demonstrate that the convective heat transfer plays a vital role in the HPAF/PCM composite.

Combining the LPAF model and HPAF model in the same condition, the thermal behavior of the aluminum foam with the porosity (ϵ) range from 65% to 95% could be analyzed numerically. The effective thermal efficiency is defined to evaluate the thermal performance of the composite with different porosities. The optimized porosity for the composite is determined in the range from 85% to 90%, which could balance the energy storage quantity and the melting time.

According to the composite with the optimized porosity, three thermal performance enhancement methods are investigated and compared numerically. It turns out that the PPI of aluminum foam, the shape of cold wall and the distribution of heat sources could affect the thermal performance of the aluminum foam/ paraffin composite. The melting rate of paraffin embedded in aluminum foam with high PPI could be improved because the large interfacial area density could contribute the conductive heat transfer. For the aluminum foam with low PPI, changing the shape of the cold wall could reduce the heat loss and benefit the convective heat transfer. The advantage of the discrete heat sources is the higher average velocity. Combining the advantages of two methods, an optimization method is proposed. The results of comprehensive evaluation indicate that the composite heated by optimization method has the best thermal performance as well as the composite with 20 PPI. These two kinds of enhancement methods could improve the thermal efficiency up to 10% compared with pure paraffin.

Chapter 5.
**Thermal behavior of aluminum
foam/PCM composite with
modified structure**

Chapter 5 Thermal behavior of aluminum foam/PCM composite with modified structure

5.1 Introduction.....	129
5.2 Heat transfer characteristic of the composite under constant temperature	130
5.2.1 Physical model.....	130
5.2.2 Effect of the porosity	132
5.2.3 Effect of the pore size.....	135
5.3 Proposition and investigation of the composite with modified structure.....	137
5.3.1 Description of the aluminum foam with modified structure	137
5.3.2 Validation of model of the aluminum foam with graded porosity	139
5.3.3 Melting characteristic of PCM in FFGP structure	141
5.4 Optimization of the structural parameters of FFGP structure.....	142
5.4.1 Effect of the thickness of metal fin.....	143
5.4.2 Effect of the porosity gradient	145
5.4.3 Effect of the pore per inch (PPI).....	146
5.5 Preliminary study of the aluminum foam prepared by 3D printing.....	148
5.5.1 Feasible methods	148
5.5.2 Manufacturing process of the aluminum foam with 3D printing method .	149
5.5.3 Thermal behavior of the aluminum foam prepared by 3D printing.....	151
5.6 Conclusion	153

5.1 Introduction

The heat transfer process of composite is affected by both thermal conduction and convection. When the composite is heated by constant power, the temperature difference always exists in the composite, which is the driving force for the conductive and convective heat transfer [149]. However, in certain practical applications (such as waste heat recovery), the composite will be utilized under the constant temperature condition. In this case, the temperature difference in the composite continues to reduce to zero, and the heat transfer characteristic may be different with the composite heated by constant power.

The objective of this section is to study and optimize the thermal behavior of the aluminum foam/PCM composite under constant temperature condition. The first part focuses on the effects of the porosity and pore size of aluminum foam on the energy storage performance. Then, to further improve the thermal performance of composite, a modified structure is proposed by combining the metal fin and gradient metal foam. It is defined as finned metal foam with graded porosity (FFGP). The melting process and energy storage performance of PCM embedded in FFGP structure are analyzed numerically. The effect of the thickness of metal fin, porosity gradient in metal foam and pore per inch on the melting process are investigated. Comparing the results of energy storage quantity and energy storage power of different configurations, the optimized FFGP structure is obtained. Finally, the methods to prepare the FFGP structure are discussed, and it is found that 3D printing is a promising method to prepare the aluminum foam with modified structure. The aluminum foam with Kelvin structure is made, and the preliminary study for the thermal performance of this material is also conducted.

5.2 Heat transfer characteristic of the composite under constant temperature

5.2.1 Physical model

The physical models under investigation are 2D configurations. The rectangular zone with the dimension 100 mm × 300 mm represents the aluminum foam/PCM composite, as shown in Fig. 5.1. The left side represents the heat source with a constant temperature 78°C, and the other sides are adiabatic. The initial temperature is 50°C. The sodium acetate is chosen as PCM, and aluminum of AS7G is used as the metallic matrix in the present study. Their thermal properties [150, 151] are listed in Table 5.1. The modeling method and the structural parameters of the aluminum foam are according to the models of LPAF/PCM composite and HPAF/PCM composite, as mentioned in Section 3.5 and Section 4.2. The mesh of the model consists of the uniform quadrilateral cells, and the mesh independence is also examined. If the value of the 15000 cells is considered as standard data, the deviations of 3700 cells and 6600 cells are less than 4% and 2%, respectively. Thus, the grid with 6600 cells is chosen in the final calculation to ensure the mesh independence.

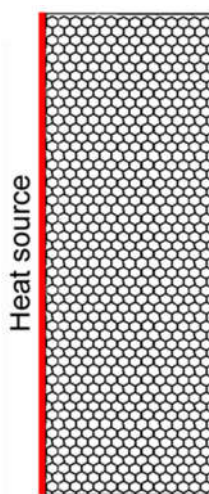


Fig. 5.1. Schematic representation of 2D model

Table 5.1 Thermal properties of materials

Property	Material	
	Sodium acetate	AS7G
Density, ρ (kg m ⁻³)	1360	2680
Specific heat of liquid phase, C_l (J kg ⁻¹ K ⁻¹)	3680	
Specific heat of solid phase, C_s (J kg ⁻¹ K ⁻¹)	2790	963
Thermal conductivity, λ (W m ⁻¹ K ⁻¹)	0.6	160
Viscosity, μ (kg m ⁻¹ s ⁻¹)	0.0037	
Thermal expansion coefficient, γ (K ⁻¹)	0.0003	
Latent heat, L (kJ kg ⁻¹)	226	
Solidus temperature, T_{m1} (°C)	57	
Liquidus temperature, T_{m2} (°C)	59	

In the evaluation of the energy storage performance of composite, two parameters are very important: energy storage quantity, E (kJ) and energy storage time, t (s). The value of E is the function of time and it represents the sum energy stored in the sample, including the energy stored in PCM and metallic material. The Eq.(5-1) – Eq.(5-3) give the expression of E . Because the heat loss from the boundary side is neglected, the temperature of the sample could reach the value of the heat source finally and the stored energy at this time is the maximum value, E_{max} . Due to the decrease of the temperature difference during the melting process, it needs a relatively long time to reach the value of E_{max} . In fact, phase transition process is the main function of PCM in thermal energy storage (TES) system, and the latent heat of PCM accounts for a large portion in E_{max} . In this condition, the value of E at the moment when the PCM totally melts is defined as the effective energy storage quantity, $E(t_{total})$. As a result, the average energy storage power, P is defined as the ratio of the $E(t_{total})$ and the total melting time of PCM, t_{total} , as shown in Eq.(5-4). From the value of P , a comprehensive evaluation of the energy storage performance of composite could be obtained.

$$E(t) = E_{PCM}(t) + E_{metal}(t) \quad (5-1)$$

$$E_{PCM}(t) = \begin{cases} m_{PCM} C_{s,PCM} (T_{PCM}(t) - T_0) & T \leq T_m \\ m_{PCM} C_{l,PCM} (T_{PCM}(t) - T_m) \\ + m_{PCM} C_{s,PCM} (T_m - T_0) + m_{PCM} L & T > T_m \end{cases} \quad (5-2)$$

$$E_{metal}(t) = m_{metal} C_{metal} (T_{metal}(t) - T_0) \quad (5-3)$$

$$P = \frac{E(t_{total})}{t_{total}} \quad (5-4)$$

Despite the heat condition, the metal foam always plays an important role in the heat transfer process in PCM. Thus, in order to better understand the thermal behavior of composite in the constant temperature condition, the effects of porosity and pore size of metal foam on the melting characteristic and energy storage performance of the composite are analyzed as following.

5.2.2 Effect of the porosity

The melting processes of these composites (10 PPI) with different porosities are depicted in Fig. 5.2. For the composite with $\varepsilon = 70\%$, the interface is always parallel to the heat source, which demonstrates that the melting process is always governed by thermal conduction. As the porosity increasing, the natural convection develops in the liquid PCM, thus the effect of convective heat transfer on the melting process becomes more pronounced. However, for the composite with high porosity, the improvement of the thermal convection could not make up its low effective thermal conductivity. Thus, the melting process of the composite is accelerated obviously as the porosity decreasing, as presented in Fig. 5.3. Although the melting time of composite is reduced greatly comparing with pure paraffin, a problem still exists in the melting process in composite. It is seen that the melting rate of the PCM decreases as time progressed, especially for the last

stage. For the composite with $\varepsilon = 90\%$, the melting rate becomes too low after the liquid fraction reaching 0.9, which may worsen the energy storage performance of the system.

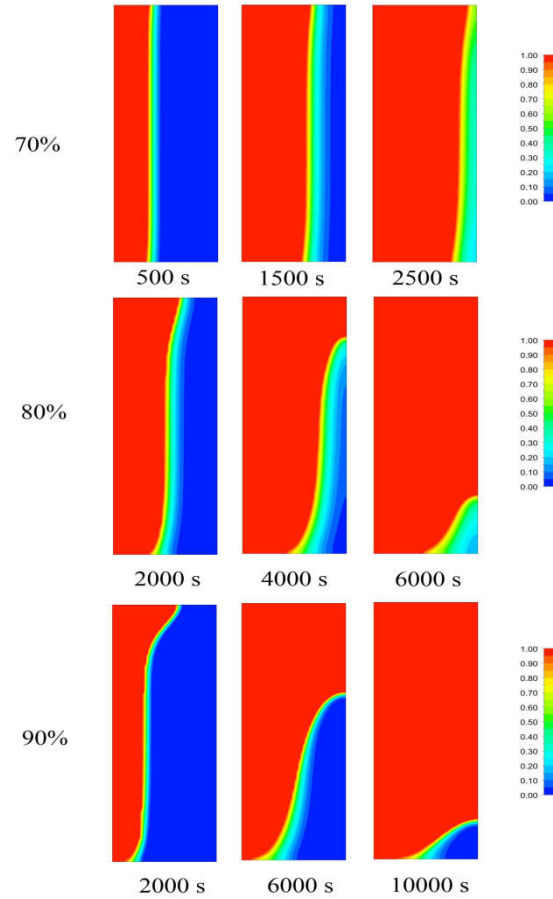


Fig. 5.2. Melting processes of composite with different porosities

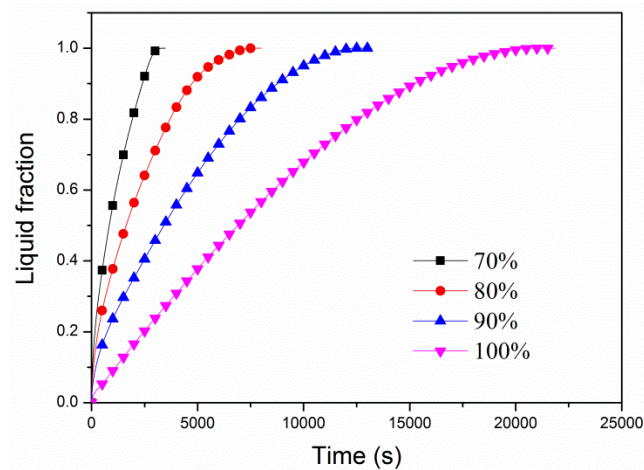


Fig. 5.3. Variations of the liquid fractions for the composites with different porosities

In order to analyze quantitatively the effect of the porosity on energy storage

performance, the energy storage quantity (E) and average energy storage power (P) are of the composites are compared. The results are presented in Fig. 5.4 and Fig. 5.5. With the elapse of time, the value of E continues to increase until reaching the maximum, E_{\max} , but it needs a relatively long time to achieve this highest value. Thus, the E_{total} is more meaningful for the study. By analyzing the results in Fig. 5.4, the increase of the porosity could improve simultaneously the E_{total} and total melting time (t_{total}). Thus, the comparison of the average energy storage power (P) could provide a comprehensive evaluation for these composites, as shown in Fig. 5.5. It is found that the average energy storage powers of the composites are much larger than that of pure paraffin. The results confirm that the addition of metal foam in PCM could enhance significantly the energy storage performance of the system. Besides, the porosity is a critical factor to the value of P . It is seen that P is reduced by nearly two-third as the porosity changing from 70% to 90%. Due to the high porosity, the composite with $\varepsilon = 90\%$ has a long melting time. Besides, as discussed above, the decrease of the melting rate at last stage could also prolong the melting process. Therefore, it is considered that if the solid paraffin in the right bottom corner melts quickly, the thermal performance of high porosity composite could be improved.

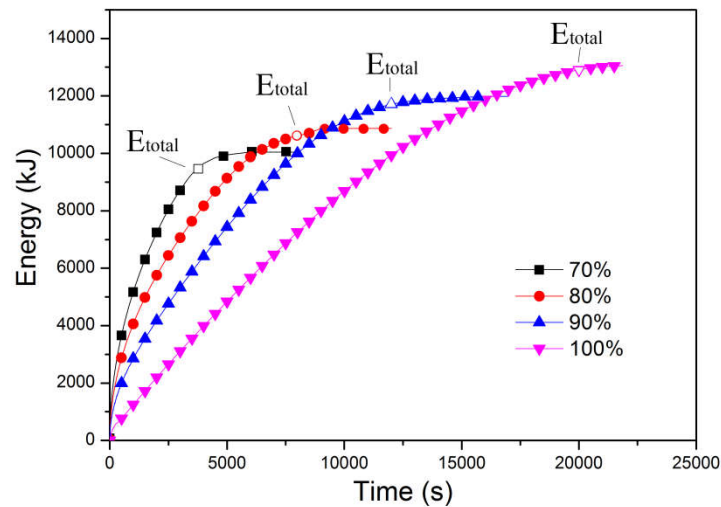


Fig. 5.4. Variation of the energy storage quantity with time for different composites

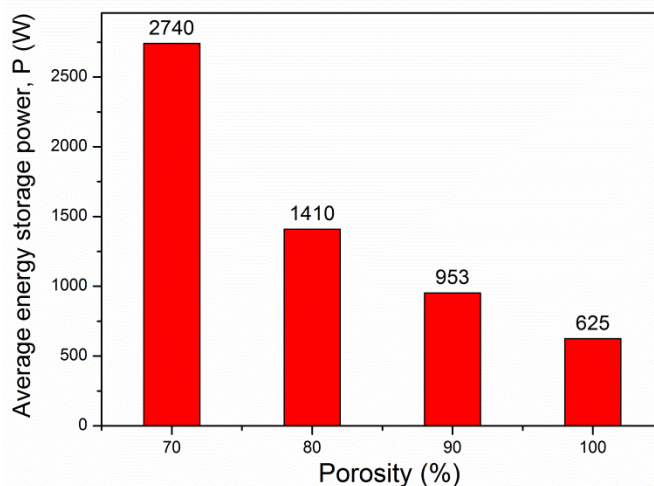


Fig. 5.5. Average energy storage powers of composites different porosities

5.2.3 Effect of the pore size

As mentioned above, the pore per inch (PPI) could affect the natural convection of PCM embedded in metal foam. Thus, the effect of PPI value on the thermal efficiency of the composite should be investigated. The melting processes of the composite with different PPIs are shown in Fig. 5.6. The porosity of the composite is constant as 90%. It is found that the heat transfer in the composite with small PPI is controlled by natural convection. Fig. 5.7 presents the variations of the liquid fractions for the composites. As PPI increasing, the melting process of the composite slows down. This phenomenon could be explained as follow. Due to the same effective thermal conductivity of these composites, the continuous decrease of the temperature difference could weaken the conductive heat transfer in the composite. In this case, the effect of the thermal convection becomes more important, which could enhance the melting process. Thus, the melting process of composite with large pore size could benefit from the convective heat transfer. Besides, it is found that the melting processes of the composite with 20 PPI and 40 PPI is similar. Based on Eq. (4-7) and Eq. (4-8), the large PPI leads to low permeability and high value of heat transfer coefficient. In this case, the natural convection in the liquid PCM is suppressed and the heat exchange between metal

ligament and PCM is enhanced. Therefore, the heat transfer in composite with high PPI follows the equilibrium equation [85] and is controlled by thermal conduction, which results in the slow melting process.

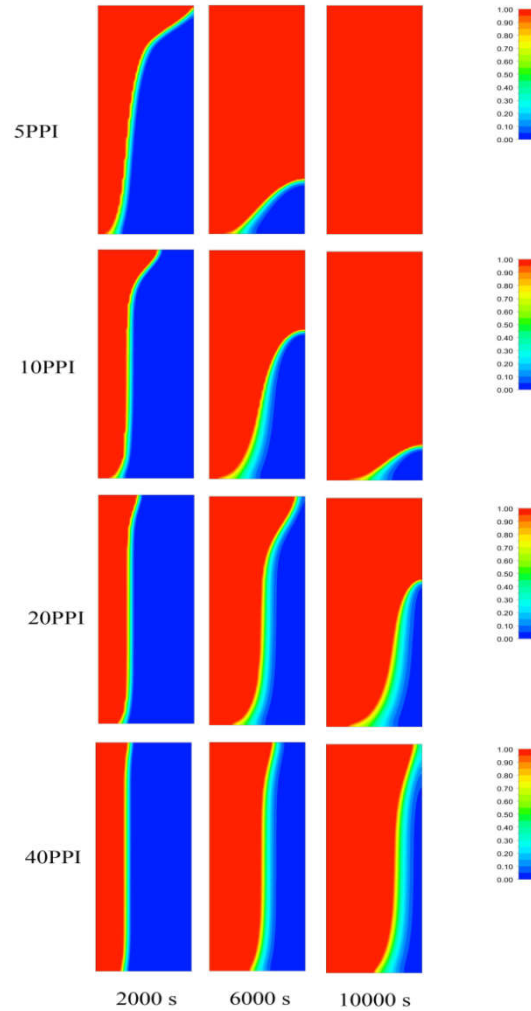


Fig. 5.6. Melting processes of composite with different PPI ($\epsilon=90\%$)

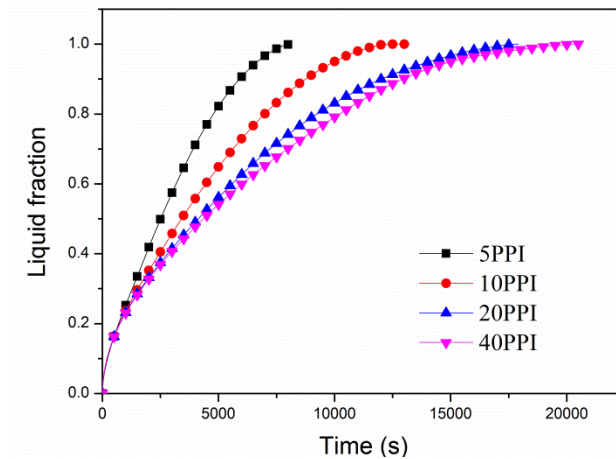


Fig. 5.7. Variations of the liquid fractions for the composites with different PPI

Fig. 5.8 shows the comparison of average storage powers of composites with different PPI. Because the E_{total} of these composites are similar, the value of P is determined greatly by total melting time. Thus, the composite with PPI =5 has the largest average energy storage power, and the thermal performance of composite could be enhanced by reducing the value of PPI.

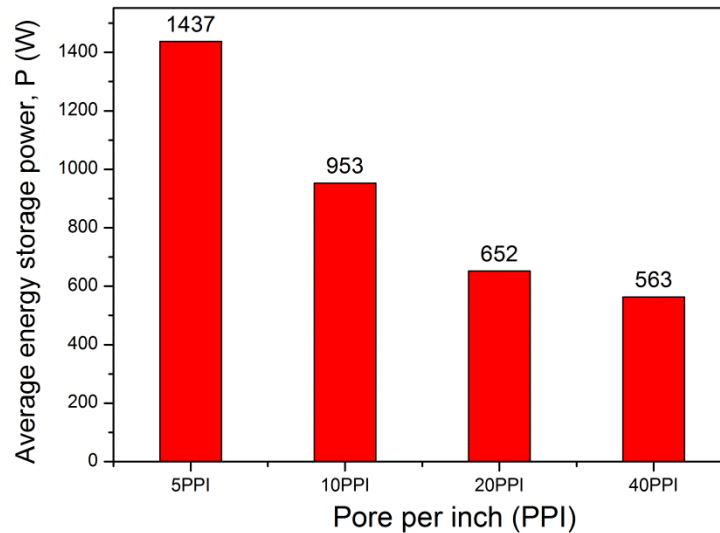


Fig. 5.8. Average energy storage powers of composites with different PPI

5.3 Proposition and investigation of the composite with modified structure

5.3.1 Description of the aluminum foam with modified structure

Although the average energy storage power of the composites with high porosity is relative low, they own the large energy storage capacity. Thus, the research works in this section focus on the improvement of the energy storage performance of composites with high porosity. As discussed above, the solid paraffin remained in the right bottom corner reduces the melting rate of PCM at last stage and deteriorates the energy storage performance of the composite. This problem is the same as the constant power condition. Considering the different

heat transfer characteristics of the composite under two heating condition, the modified methods for constant temperature condition are also different with the approaches in Section 4.4.

Recently, some researchers start to concern this problem, and they propose a new kind of structure: the gradient metal foam. Yang et.al [84] proposed the metal foam with linearly changed porosity, and the numerical results demonstrated that this structure could enhance the phase change process in PCM. Furthermore, this group also added a metal fin at the bottom of metal foam, and it is found that the transfer rate of this structure is larger than that of the metal foam without metal fin [132]. In this study, combining these two methods, aluminum foam with modified structure is proposed, which is defined as finned metal foam with graded porosity (FFGP). The FFGP structure is depicted in Fig. 5.9. Three metal foams with different porosities constitute the gradient metal foam. These three parts have the same size and they are connected with metal fin at the bottom. The PCM is filled in the gradient metal foam.

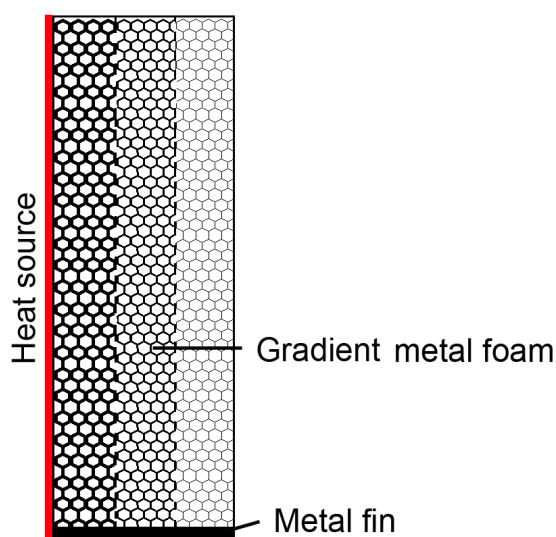


Fig. 5.9. Schematic representation of FFGP structures

5.3.2 Validation of model of the aluminum foam with graded porosity

The modeling method is according to the process in Section 4.2. The finite volume method (FVM) is employed to discretize the governing equations. For the numerical analysis of the thermal behavior of metal foam with graded porosity, the modeling methods applied in previous works include the local equation model and Lattice Boltzmann Method (LBM). To author's knowledge, the paper that uses the FVM with two equations model to study the heat transfer of the PCM embedded in metal foam with graded porosity is relatively rare. In order to valid the model, it is necessary to compare the numerical results obtained by FVM with the experiment or numerical data in other research works. Fig. 5.10 shows the variations of liquid fractions predicted by LBM [85] and FVM the melting process. It could be seen that the two curves have the same tendency and they are in accordance with each other.

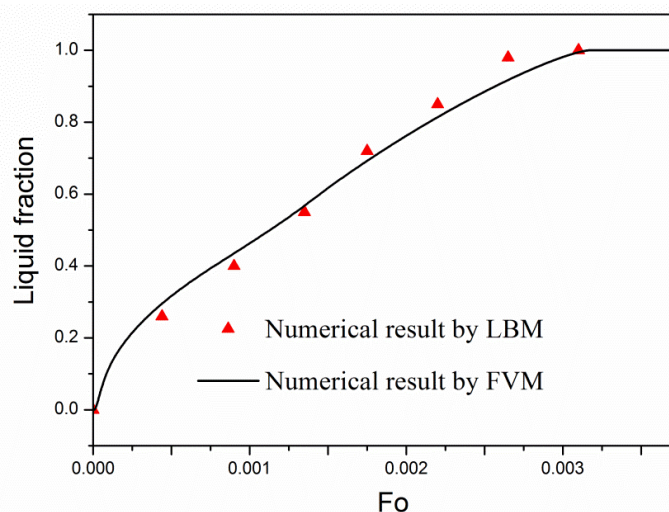


Fig. 5.10. Comparison of liquid fractions between the numerical results obtained by LBM [85] and FVM

Besides, based on the conditions in Ref.[15], the comparison of solidification process is also performed between experimental and numerical results, as shown in Fig. 5.11 and Fig. 5.12. It is observed that the liquid fraction and the evolution

of the interface obtained by two equation model agree well with the experiment results. Thus, these comparison results indicate that the model applied in this study is adequate and reliable.

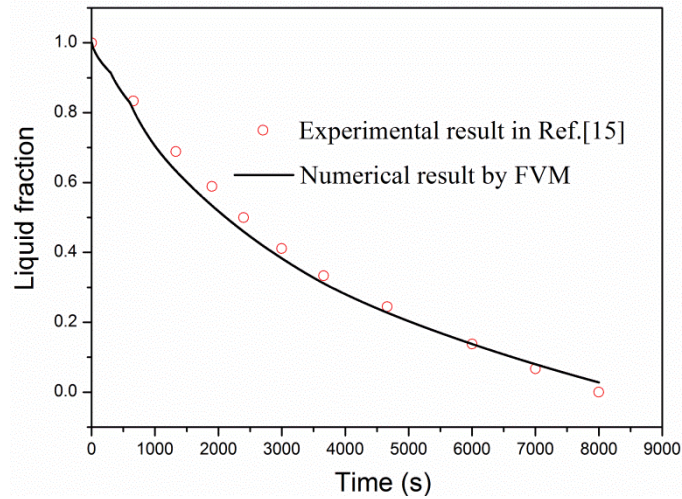


Fig. 5.11. Comparison of liquid fractions between the experimental data [15] and numerical results by FVM

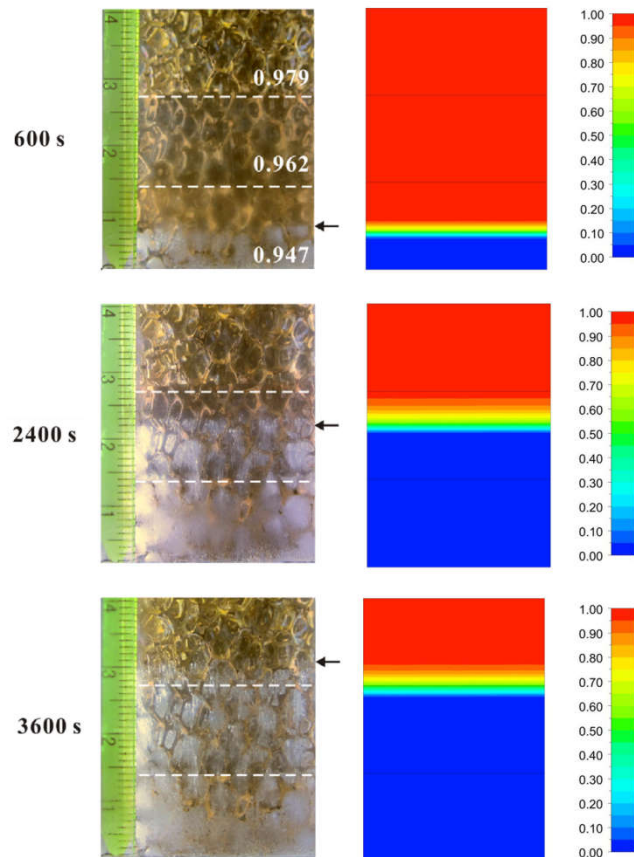


Fig. 5.12. Comparison of the interface locations between the experimental photos [15] (left) and numerical results (right)

5.3.3 Melting characteristic of PCM in FFGP structure

Fig. 5.13 presents the comparison of interface evolutions of the PCM embedded in uniform metal foams and FFGP structure. Two kinds of structures have the same metal fraction and PPI value. As discussed above, the circulation flow in uniform metal foam makes PCM in right bottom corner melt at last, as shown in Fig. 5.13(a). Because the driving force of the natural convection decreases at last stage, the PCM in this position will melt slowly. In our previous research [152], this phenomenon could reduce the energy storage performance.

The melting process of PCM saturated in FFGP structure is depicted in Fig. 5.13 (b), which is different with the uniform one. Due to the addition of the metal fin, the PCM could melt from both horizontal and vertical directions. It is observed that the evolution process of the vertical interface is similar to that of the uniform structure. For the horizontal interface, its form is smooth at beginning. As the interface rising up gradually, the shape becomes wavy and rough, as presented at 2000s and 4000s in Fig. 5.13 (b). The phenomenon indicates that the natural convection develops between the metal fin and the interface. The result of velocity vector could visualize the circulation in the liquid, as illustrated in Fig. 5.14. Except for the large circulation flow between heat source and vertical interface, some small flows exist in the liquid near the metal fin, which contributes to the heat transfer between metal fin and solid PCM. In addition, the velocity of the fluid adjacent to the vertical interface in FFGP structure is larger than that in uniform porosity structure, which demonstrates the metal foam with graded porosity could benefit the development of natural convection. Finally, comparing the amounts of solid PCM of two configurations at 6000s in Fig. 5.13, it is concluded that the FFGP structure improves significantly the melting process of

PCM.

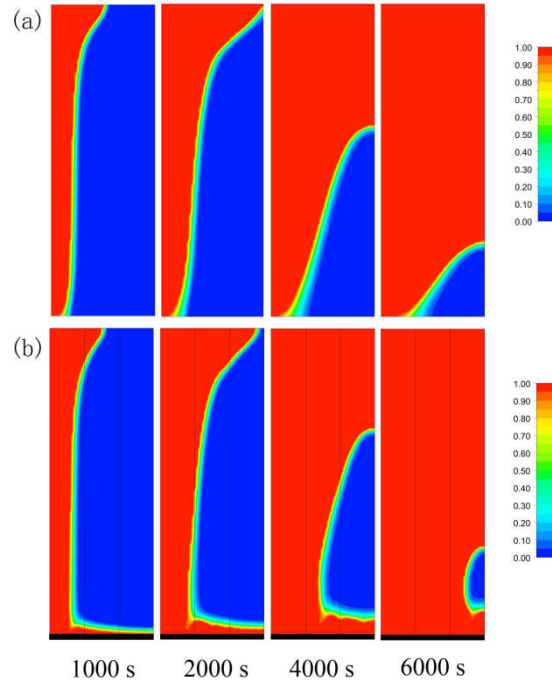


Fig. 5.13. Melting process of PCM (a) in uniform metal foam (b) in FFGP

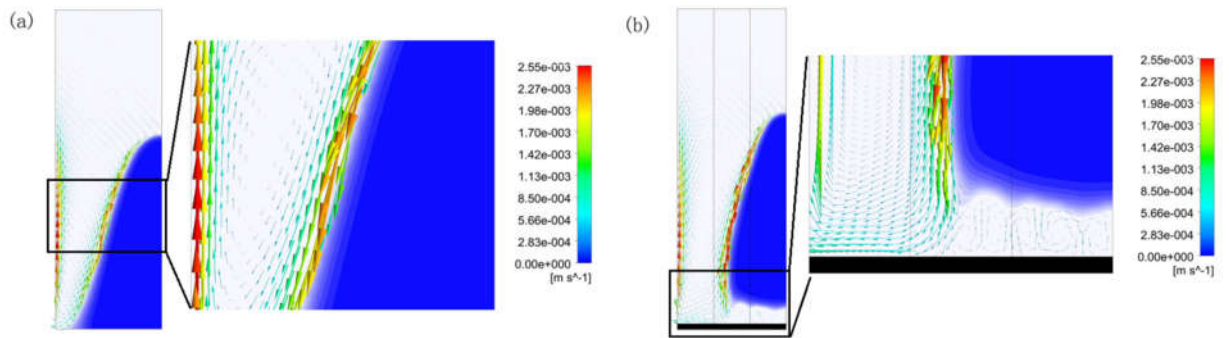


Fig. 5.14. Velocity vectors of liquid PCM (a) in uniform metal foam (b) in FFGP

5.4 Optimization of the structural parameters of FFGP structure

Comparing with the uniform metal foam, the FFGP has the relatively complicated structure. In order to obtain the optimization configuration, the effect of some critical parameters on the heat transfer should be analyzed, such as the thickness of metal fin (h), the porosity gradient (Δ), pore per inch (PPI), etc.

Therefore, ten different configurations are proposed and compared, whose detail parameters are listed in Table 5.2. All the samples have the same volumes of metal. The sample of C1 with the uniform metal foam is treated as the reference structure. For the three parts of metal foams in FFGP structure, the porosity decreases from the left part to the right part, and the porosity gradients (Δ) of the adjacent parts are constant in each configuration. The heat could transfer in the metal foams with graded porosity, and the convection of liquid phase could also occur in this structure.

Table 5.2 Structure parameters of the configurations

Configuration	Thickness of metal fin, h (mm)	Porosity gradient, Δ (%)	Porosity range (%)	Pore per inch (PPI)
C1	0	0	90	5
C2	0	2	88-90-92	5
C3	2.5	2	88.8-90.8-92.8	5
C4	5	2	89.5-91.5-93.5	5
C5	7.5	2	90.3-92.3-94.3	5
C6	10	2	91.1-93.1-95.1	5
C7	5	3	88.5-91.5-94.5	5
C8	5	5	86.5-91.5-96.5	5
C9	5	5	86.5-91.5-96.5	10
C10	5	5	86.5-91.5-96.5	20

5.4.1 Effect of the thickness of metal fin

As discussed above, the metal fin is a critical part in FFGP structure because it could enhance the melting rate of PCM, especially for the solid phase far away from the heat source. Fig. 5.16 presents the variations of the liquid fraction obtained from six different configurations (C1-C6). It is obvious that the melting processes of other modified structures are all faster than that of C1. In the initial stage, the liquid fraction of C2 without fin is the largest because the porosity near the heat source is the lowest in these six configurations. In this case, the heat could

be transferred quickly from the heat source to the interior of the sample due to the large thermal conductivity. However, as time progressed, this advantage becomes weak and the curve of liquid fraction approaches guardedly the result of C1. This is because all the structure has the same volume of aluminum, the C2 with the graded porosity leads to a relatively high porosity in the right side. Therefore, the solid phase in the right bottom corner melts slowly, like C1. After adding the metal fin in the metal foam with graded porosity, the FFGP structure is formed and the melting order is also modified. It can be seen that the results of C3-C6 is better than that of C2 after 4000 s, and the total melting time is reduced significantly by using FFGP structure. Upon comparing the results of C3-C6, the melting processes of C4 and C5 finish earliest of all FFGP structures.

In order to obtain the comprehensive evaluation of these configurations, the energy storage quantity, E (kJ) and energy storage power, P (W) of C1-C6 are calculated and compared. In Fig. 5.16 (a), it is observed that the energy stored in the samples increases with the melting process. At the same moment, the FFGP structures could always store more energy than the uniform structure. Fig. 5.16 (b) shows the values of P of C1-C6. It is noted that the FFGP structures could improve significantly the energy storage power. From C3 to C6, the value of P increasing firstly then decreases. This is because the average porosity of metal foam is reduced with the increase of the thickness of metal fin. In this condition, the nature convection in the PCM embedded in metal foam is enhanced while the thermal conduction is deteriorated. Besides, due to the existent of the circulation on the surface of metal fin, the heat transfer is enhanced at the bottom part as the thickness of metal fin increasing. Under the effect of these three factors, the energy storage power of C4 possesses the highest value, which is 23.7% up on that of C1. After that, the heat transfer process in the metal foam is deteriorated, leading to the decrease of power. As a result, it is concluded that the FFGP

structures have the advantage in the enhancement of the melting process, and the configuration C4 with metal fin of 0.5mm has the best thermal performance.

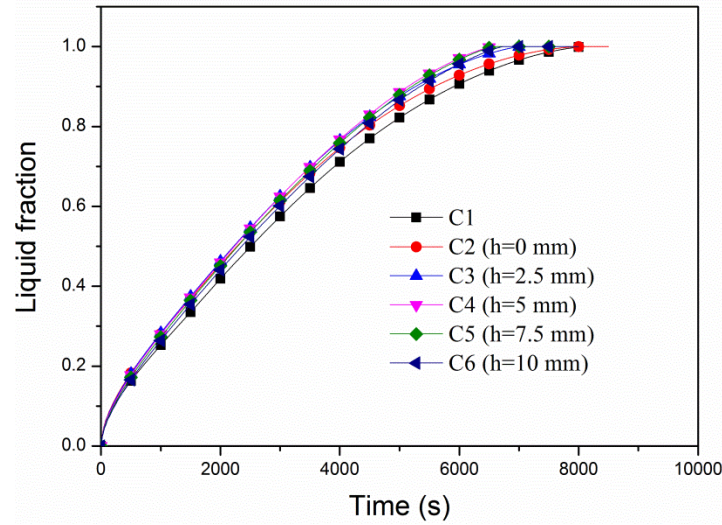


Fig. 5.15. Liquid fractions of PCM embedded in the uniform metal foam and the FFGP structures with different thicknesses of metal fin

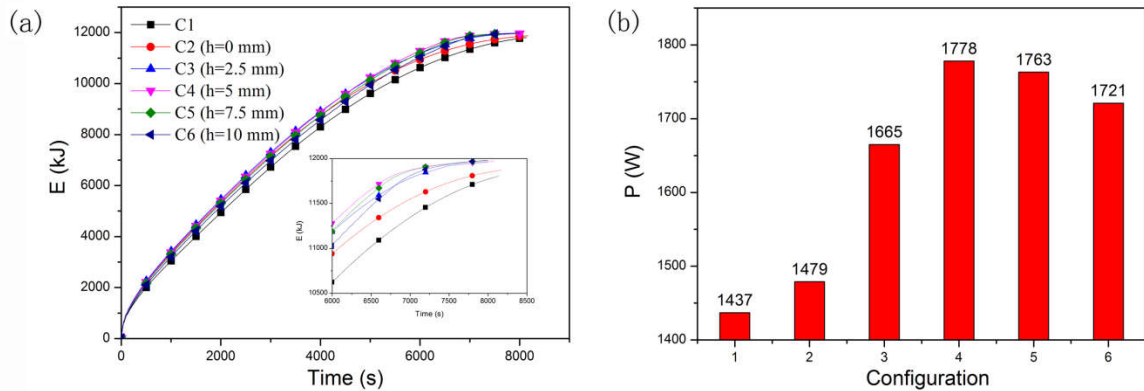


Fig. 5.16. Performance evaluation of the uniform metal foam and the FFGP structures with different thicknesses of metal fin (a) value of E (b) value of P

5.4.2 Effect of the porosity gradient

The metal foam with graded porosity also plays an important role in the improvement of the heat transfer in PCM. In this section, the effect of the porosity gradient in metal foam is investigated. The porosity gradient is constant for each configuration and the values of porosity decrease along the horizontal axis. With the same thickness of metal fin, three kinds of metal foams with different porosity

gradients ($\Delta=2\%$, 3% , 5%) are adopted in FFGP structure. And the detail parameters of structure are listed in Table 5.2 with the configuration numbers of C4, C7 and C8. Fig. 5.17 (a) shows the comparison results of E of three samples. It is observed that the energy stored in the system increases with the increase of Δ value before 5000 s. The reason can be explained by the different thermal properties of metal foams with varied porosities. For the structure of C8, the metal foam with lower porosity adjacent the heat source owns the large thermal conductivity and large interior surface area, which could contribute to the heat conduction. However, the porosity of metal foam far away from heat source is higher, leading to the decrease of melting rate. Therefore, the E values of three samples become similar after 5000 s. With the help of the P results, the optimized porosity gradient of 3% is obtained, as showed in Fig. 5.17 (b). It is seen that the configuration C7 owns the largest P value of 1796 W, which improves the thermal efficiency by 25% comparing with C1.

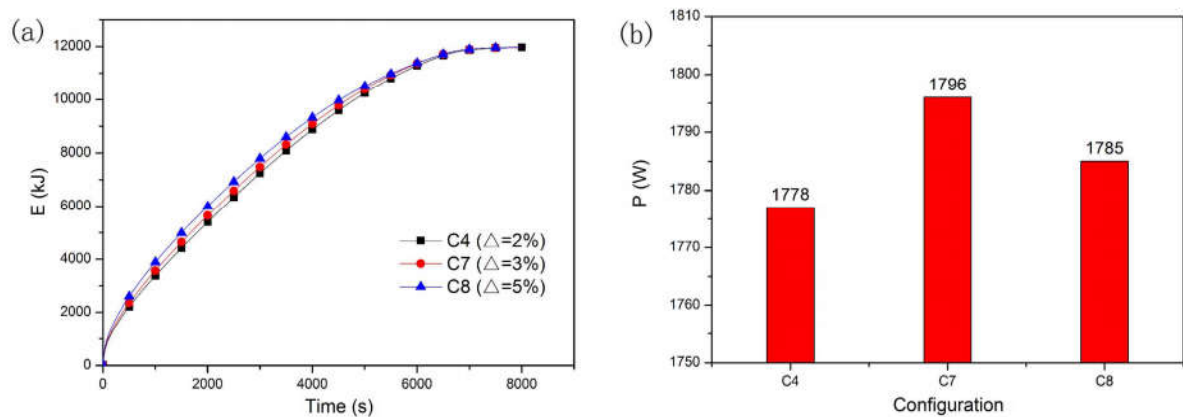


Fig. 5.17. Performance evaluation of the FFGP structures with different porosity gradients (a) value of E (b) value of P

5.4.3 Effect of the pore per inch (PPI)

In this section, the FFGP structures with different PPI are compared. Fig. 5.18 presents the average velocity in the liquid phase during the melting process. It is seen that the velocity decreases greatly with the increase of PPI, which

deteriorates the thermal convection in the liquid PCM. The variation of the E and P in Fig. 5.19 also demonstrates the metal foam with small PPI could store energy more quickly. Because the thermal convection is more efficient for the heat transfer in FFGP structures, the metal foam with small PPI should be chosen in the FFGP structures.

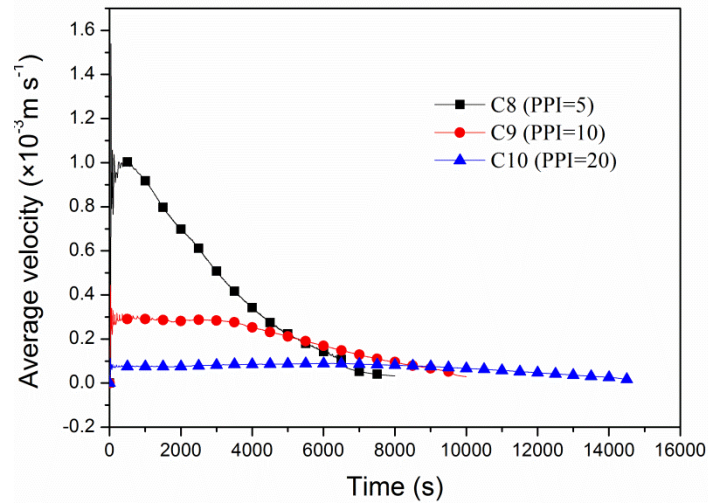


Fig. 5.18. Average velocity of liquid PCM in the FFGP structures with different PPI

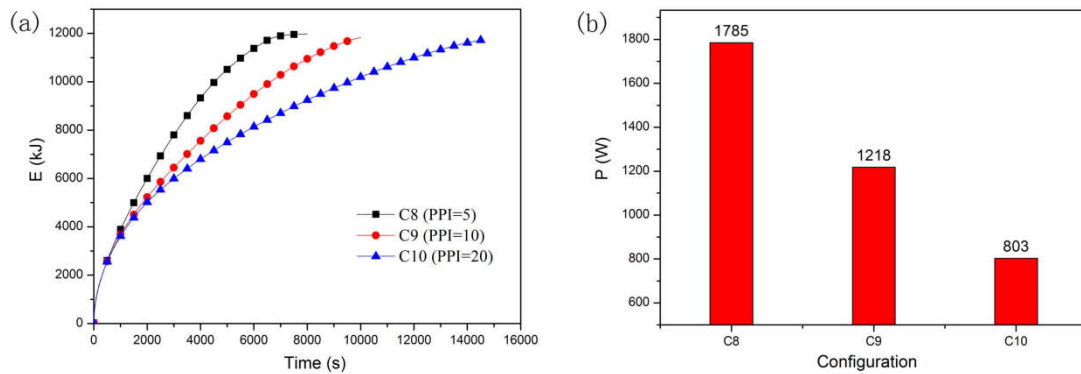


Fig. 5.19. Performance evaluation of the FFGP structures with different PPI (a) value of E (b) value of P

5.5 Preliminary study of the aluminum foam prepared by 3D printing

5.5.1 Feasible methods

In previous section, it is found that the metal foam with graded porosity is a kind of promising material, because this modified structure could accelerate the heat transfer in composite with high porosity. However, the preparation of the high porosity metal foam mainly based on the investment casting method or electro-deposition method, which adopts the polymer foam as preform. Thus, the commercial products of metal foam are almost uniform structure. In order to fabricate the gradient metal foam, the researchers proposed several methods, which are summarized as following

(a) Compressed preform method

This method is proposed by Brothers and Dunand [83], and it could prepare the open cell metal foam with controlled, continuous gradient porosity. The principle of the method is using the gradient-compressed elastomeric foam as the preform. According to the process of investment casting method, the metal foam with graded porosity could be shaped directly after infiltration process.

(b) Sintering method

The sintering method used the several single layer metal foams with different porosity, and these metal foams were sintered together in a high temperature furnace to form the gradient metal foam. Due to the simple process, this method is applied by many researchers [81, 153, 154].

(c) Adhesion method

In this method, the separate metal foams are bonded together with an organic adhesive. The contact condition between different metal foams is a problem for this method due to the existence of adhesive material. Feng et al. [82] considered the difference between two contact conditions: high thermal conductivity adhesive and natural contact is little for the solidification rate. Thus, it is considered that the effect of this method may be limited to the enhancement of heat exchange between two different metal foams.

5.5.2 Manufacturing process of the aluminum foam with 3D printing method

Recently, the additive manufacturing (AM) technology becomes more and more popular and available, which could prepare the material with complex structure. Based on the different kinds of the matrix materials, the AM technology includes several various methods [155, 156], such as Selective Laser Sintering (SLS), Selective Laser Melting (SLM), Stereolithography (SLA), and 3D Printing (3DP). Among these methods, SLS and SLM are suitable for the preparation of the gradient metal foam [157-159]. However, Maeda and Child found [160] that the product made by SLS is not full density, and pores exist in the material. Thus, it is considered that aluminum foam with this kind of structure may be not suitable to be used as the heat exchanger material.

In this study, a method is proposed by combining the 3D printing with infiltration casting. The manufacturing process is illustrated in Fig. 5.20. Firstly, the mold with interconnected cells is designed by CAD software. Then, it should be converted to a special format for the 3D printing machine (ProJet[®] 460 Plus). The power used in 3D printer is plaster, and the product is prepared layer by layer through binder jetting on powder bed. After that, the plaster powder remained in

the pores should be removed to obtain the final mold with open cells. Several molds could be stacked up to make the template with large dimension. Finally, the molten aluminum is filled in the mold according to the infiltration casting method. After removing the plaster, the final aluminum foam could be obtained.

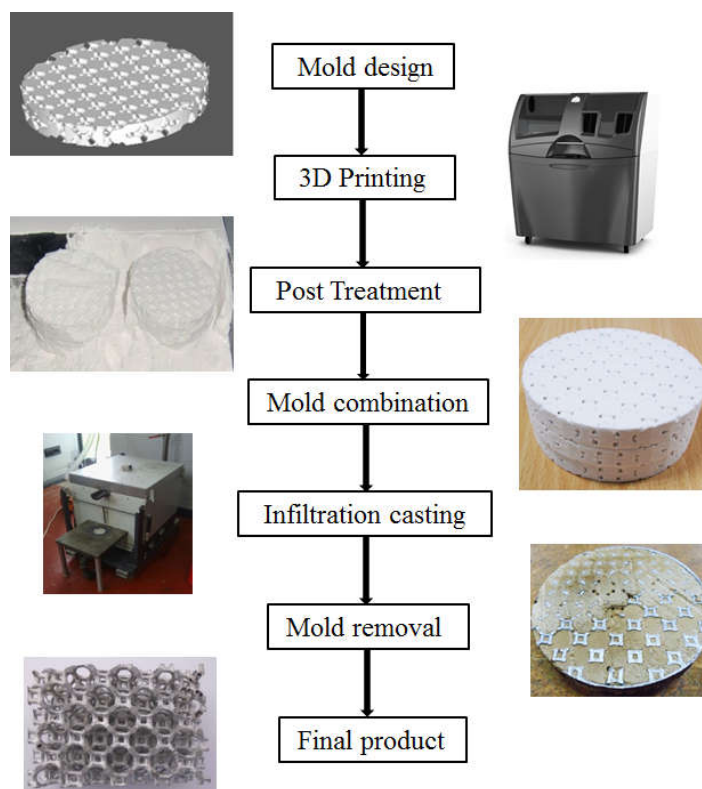


Fig. 5.20. Manufacturing process of aluminum foam with modified structure

The main advantage of this method is that the structure of aluminum foam could be controlled accurately, and the porosity and pore size are unrestricted by preform. Moreover, the matrix of the aluminum is continuous due to casting shaping method. In the process of mold combination, if we use several plaster molds with different structures, the combined mold could own the gradient structure. Thus, it is considered that the gradient aluminum foam could be prepared by this method, which should be studied in our further research.

In this study, the aluminum foam based on tetrakaidecahedron geometry is designed and prepared, because this kind of structure has the good filling ability

by molten aluminum and it is the representative structure for the traditional aluminum foam. The aluminum foam is made of many uniform and repetitive tetrakaidecahedron cells, as shown in Fig. 5.20. This kind of aluminum foam owns the relatively large pore size, thus its thermal behavior may be different with the traditional ones, which is worthy to be investigated.

5.5.3 Thermal behavior of the aluminum foam prepared by 3D printing

In order to study the thermal performance of the aluminum foam prepared by 3D printing, the melting process of paraffin is embedded in the porous structure is observed and the results are illustrated in Fig. 5.21. The porosity of aluminum foam is 88% and the pore size is 9 mm. Three thermocouples are applied in the center of the composite to measure the temperature variation. From the result of temperature distribution, it is obvious that the temperature of aluminum foam is higher than other parts, indicating that the heat is transferred from the aluminum to paraffin. In this condition, the paraffin in the whole region could be heated uniformly. Besides, due to the large pore size, the circulation flow in the composite may be less restricted during melting process. The temperature variation of three detected points is presented in Fig. 5.22. It is seen that the curve is smooth at beginning, while the temperature fluctuation occurs after the paraffin reaching 50°C. This phenomenon is not found in the composite with traditional foam, but it could be observed in the melting process of pure paraffin. Thus, it is considered that the effect of convective heat transfer on the enhancement of the melting process is more pronounced in this kind of composite. According to our previous research, this characteristic maybe becomes the advantage for the aluminum foam prepared by 3D printing.

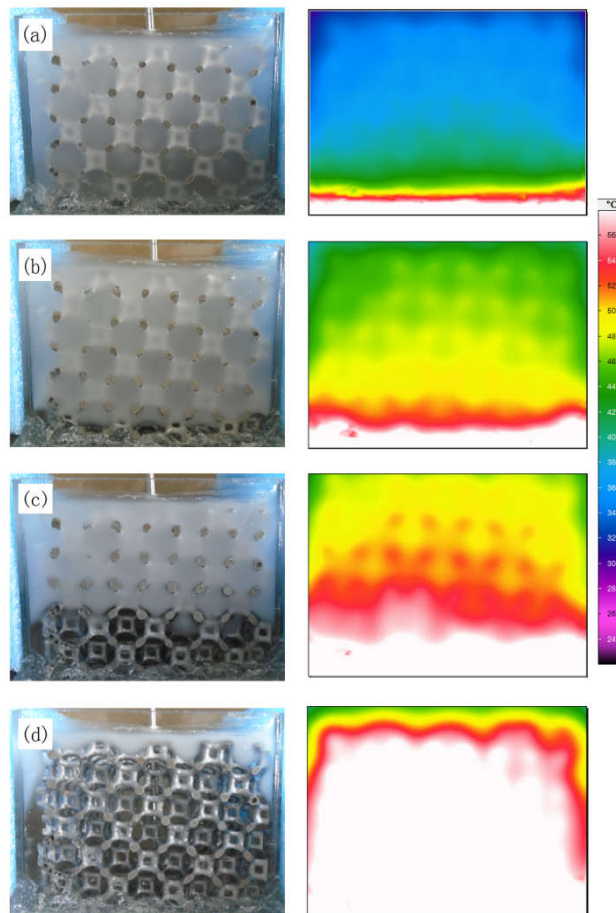


Fig. 5.21. Melting process and temperature distribution of the paraffin embedded in aluminum foam with Kelvin structure (a) 600 s (b) 1200 s (c) 1800 s (d) 2400 s

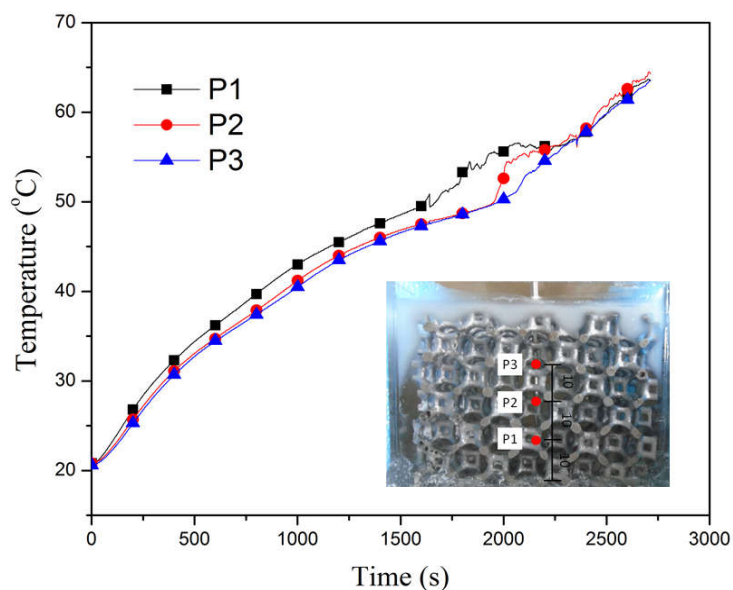


Fig. 5.22. Temperature variation of three detected points for paraffin embedded in aluminum foam with Kelvin structure

5.6 Conclusion

The thermal behavior of the aluminum foam/PCM composite under constant temperature condition is investigated numerically. The average energy storage power (P) is defined as the evaluation indicator to study the effects of porosity and pore size on the energy storage performance. The results show that the thermal performance of the composite becomes worse as the porosity increasing. For a fixed porosity, the large pore size could accelerate the convective heat transfer in the composite, thus it could improve the average energy storage power.

The finned metal foam with graded porosity (FFGP) is proposed and studied. The FFGP structure could modify the melting process of PCM and enhance the heat transfer at the bottom of the sample. Due to the metal fin and gradient metal foam, the melting rate of PCM in FFGP structure is greater than that of uniform metal foam, especially at the last stage. As the metal fin in FFGP thickening, the enhancement effect for the melting process of PCM increases first and then decrease. The same tendency could also be obtained when the porosity gradient in metal foam increases. Comparing with different configurations, the optimized structure of FFGP is obtained whose the thickness of fin is 5 mm and the porosity gradient is 3%. The value of P of the optimized structure is 25% more than that of uniform foam.

The 3D printing is applied in the manufacturing process of aluminum foam combining with casting method. The aluminum foam with tetrakaidecahedron geometry prepared by this method owns the uniform and repetitive structure. Due to the large pore size, the effect of convective heat transfer on the melting process is enhanced, which may be a potential advantage for this kind of aluminum foam.

Conclusions and perspectives

Conclusions

The utilization of open-cell aluminum foam is a promising and effective method to enhance the heat transfer in PCM. Based on the previous research works, this thesis aims at studying the heat transfer characteristic in the aluminum foam/PCM composite and further improving the energy storage performance of the composite by optimizing the structure of aluminum foam.

As the skeleton material, the aluminum foam plays a critical role in the composite due to its high thermal conductivity and porous structure. The manufacturing methods of aluminum foam could determine the structure characteristics and further influence the thermal performance of the composite.

For the aluminum foam prepared by infiltration casting method, bubbles and shrinkage are the causes of the defects. The defects in the surface and bottom of the aluminum foam are due to gas entrapment. The shrinkage will occur when the volume of molten aluminum remained on the preform top is not enough. For injection process, adjusting injection angle could reduce the turbulent extent and results in fewer bubbles trapped in the molten aluminum. The small particle and low negative pressure contribute to reduce the bubbles in the porous zone during infiltration process. Through controlling the infiltration length, the appearance of the shrinkage could be avoided.

The effective thermal conductivity of the LPAM is much higher than that of pure paraffin. The addition of LPAM could remarkably enhance the heat transfer of the paraffin and make the temperature distribution of the composite more uniform. Both thermal conduction and thermal convection contribute to the melting process of the composite. As the increase of porosity, the natural convection is enhanced while the conductive heat transfer becomes weak. For the modeling methods of the

LPAM/PCM composite, the equilibrium model could satisfy the simulation of the composite with $\varepsilon = 67\%$. As the porosity increasing, the non-equilibrium model owns the advantages in reflecting the natural convection and temperature stratification.

Combining of LPAM/PCM model and HPAM/PCM model, the heat transport characteristics and the energy storage efficiencies of the composites with the porosities range from 65% to 95% could be obtained. The optimized porosity for the composite is determined in the range from 85% to 90%. For the composite with the optimized porosity, modifying the structure of aluminum foam could further improve the energy storage performance of the composite, including changing PPI and shape of cold wall. Combining the advantages of the enhancement methods, an optimization method is also proposed. Composite heated by optimization method has the best thermal performance as well as the composite with 20 PPI, which improves the thermal efficiency up to 10% compared with pure paraffin.

In the constant temperature condition, thermal performance of the composite becomes worse as the porosity increasing. For a fixed porosity, the large pore size could accelerate the convective heat transfer in the composite. The FFGP structure could modify the melting process of PCM and enhance the heat transfer at the bottom of the sample. The optimized structure of FFGP is obtained whose the thickness of fin is 5 mm and the porosity gradient is 3%. The value of P of the optimized structure is 25% more than that of uniform foam. The aluminum foam prepared by combination of 3D printing and casting method owns the uniform and repetitive structure, and the convective heat transfer of the PCM in this kind of aluminum foam is enhanced.

Perspectives

The previous research always focuses the study heat transfer characterizes of aluminum foam composite. This thesis focuses on improving the energy storage performance of the composite through changing the structural parameters of aluminum foam. For the future research, some aspects are needed to be studied.

1. The preparation of aluminum foam with graded porosity

With the help of 3D printing, the mold with different porosities could be obtained. Combining these molds, the aluminum foam with graded porosity could be prepared by casting method. Besides, its thermal performance also needs further investigation.

2. The effect of different kinds of PCM on the energy storage performance.

According to various conditions, the different kinds of PCM should be applied. Thus, in order to optimize the performance of the composite, the melting characteristics of some common PCMs needs to be analyzed experimentally.

3. The energy release process

The energy release process is an important aspect for energy storage system, and it may be improved by aluminum foam. If we want to control this process, some parameters of the composite need to be modified, such as container shape, the material of cold wall or structure of aluminum foam.

Résumé en français

Résumé en français

1. Introduction	161
2. Analyse numérique des défauts de fabrication	163
2.1 Principe d'élaboration	163
2.2 Modélisation sur procédé de fabrication	163
2.3 Analyse numérique des causes des défauts	165
2.4 Prévention pour éviter les défauts	168
3. Etude de la performance thermique du composite MAFP/MCP	169
3.1 Procédé de fusion de la paraffine	169
3.2 Procédé de fusion du composite mousse d'aluminium/paraffine	170
3.3 Effet de la porosité sur le transfert de chaleur dans le composite.....	172
3.4 Modélisation de transfert de chaleur composite MAFP/MCP.....	173
4. Analyse numérique des performances thermiques du composite MAHP/MCP ...	176
4.1 Modèle physique	176
4.2 Détermination de la porosité optimisée.....	177
4.3 Méthodes d'amélioration de l'efficacité thermique efficace du composite	179
5. Comportement thermique de composite à structure modifiée en température constante.....	181
5.1 Modèle physique	181
5.2 Optimisation des paramètres de la structure modifiée.....	183
5.3 Etude préliminaire de la mousse d'aluminium élaborée par impression 3D...	185
6. Conclusion.....	186

1. Introduction

Le matériau à changement de phase (MCP) peut absorber ou libérer l'énergie thermique pendant leur changement de phase liquide/solide [39]. Récemment, le MCP organique attire l'attention de nombreux chercheurs grâce à sa stabilité chimique et sa faible densité [47]. Pourtant, le MCP organique souffre toujours de la faible conductivité thermique ($< 2 \text{ W m}^{-1} \text{ K}^{-1}$), ce qui limite principalement ses applications réelles. Afin d'améliorer le comportement thermique du MCP, diverses technologies sont étudiées en utilisant des méthodes expérimentales et numériques, comme l'addition d'ailettes métalliques [45], la dispersion des particules à haute conductivité [60] et l'utilisation de la mousse métallique [152].

Parmi ces méthodes, une des méthodes est d'introduire le MCP dans une mousse métallique, ce qui compose un nouveau composite bi phase Mousse métallique/MCP. Selon les études du transfert de chaleur dans la mousse métallique composite, le flux de chaleur est transféré à toute la région du composite grâce aux parois de la mousse métallique [90], chaque cellule remplie de MCP peut être donc chauffée rapidement. Dans ce cas, la conduction thermique du composite est largement augmentée. D'ailleurs, la convection naturelle du MCP fondu existe également dans le composite à cause de la structure poreuse de la mousse métallique, pouvant accélérer le transfert de chaleur et uniformiser la température dans la région liquide [74, 161].

Le transfert de chaleur du composite peut être influencé par de nombreux facteurs, tels que la porosité, la taille des pores, la matrice métallique et la température. Le comportement thermique de ce type de composite est étudié depuis plus dix ans. Néanmoins, la plupart des chercheurs se concentrent sur la méthode de la modélisation [162, 163] ou l'analyse du transfert de chaleur. Bien que ces travaux concluent que la performance thermique du composite est

meilleure que celui du MCP pur, les recherches sur le comportement de stockage d'énergie thermique sont très rarement étudiés et la performance thermique n'a pas pu être analysée de façon approfondie.

Afin d'améliorer le comportement thermique du composite, de nombreuses méthodes ont été proposées et étudiées dans cette thèse. Par exemple, l'addition d'ailette métallique dans le composite, le changement de forme du composite, et l'utilisation de la source de chaleur discrète... etc. Un nouveau type de structure: la mousse métallique à porosité variable a permis également d'améliorer la performance du système de stockage d'énergie. Ce nouveau type de mousse semble très prometteur dans leur future utilisation.

L'objectif de cette thèse est d'étudier expérimentalement et numériquement le comportement thermique des mousses d'aluminium et des matériaux à changement de phase (MCP) composite afin de connaître le phénomène de stockage d'énergie thermique, et d'améliorer sa performance thermique dans ces matériaux. Le procédé de fabrication de la mousse d'aluminium à cellules ouvertes est d'abord analysé numériquement dans le but de réduire les défauts formés durant la fabrication. Les caractéristiques de transfert de chaleur du MCP dans les mousses d'aluminium à différentes porosités sont ensuite étudiées en analysant les processus de fusion et la variation de températures dans ces composites. Deux modèles numériques pour la Mousse d'Aluminium à Faible Porosité (MAFP, $50 < \varepsilon < 85\%$) et à Haute Porosité (MAHP, $\varepsilon > 85\%$) sont établis afin d'évaluer la performance de stockage d'énergie de ces composites. Certains procédés sont également proposés et comparés pour améliorer encore la performance de stockage d'énergie des composites.

2. Analyse numérique des défauts de fabrication

2.1 Principe d'élaboration

Le procédé d'infiltration à pression négative a été utilisé pour la fabrication des mousses métalliques, cette technique se compose de trois étapes: Versement, Infiltration et Solidification. La Fig. 6.1 montre le principe d'élaboration de mousse pure. Dans le processus de versement, l'aluminium fondu (700 °C) est versé dans le moule qui est rempli de sel d'un diamètre prédéfini entre 0,2 à 2 mm, que nous appelons « Préforme ». A cause de la viscosité de l'aluminium fondu et la tension superficielle de préforme, l'aluminium fondu remplit difficilement la préforme par gravité. La pression négative doit être appliquée tout de suite pour aspirer l'aluminium fondu rentrant dans la préforme (Infiltration). L'étape finale est la solidification, le moule avec son échantillon (mélange de sel et aluminium) est refroidi à température ambiante. Après démoulage, l'échantillon est lavé à l'eau pour évacuer la préforme (sel), et un échantillon de mousse d'aluminium est ainsi fabriqué.

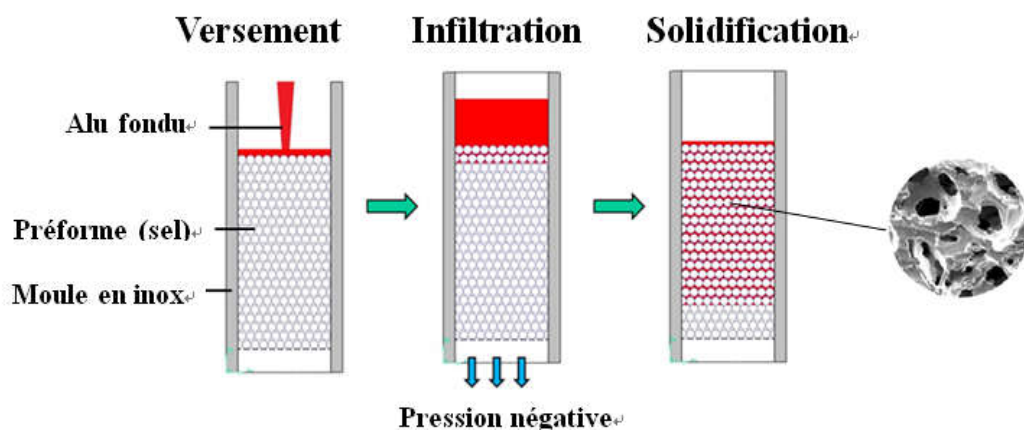


Fig. 6.1. Principe d'élaboration du mousse d'aluminium à pore ouvert

2.2 Modélisation sur procédé de fabrication

Afin de connaître la cause des défauts de fabrication dans les échantillons, un

modèle numérique en 3D est créé pour analyser chaque étape du processus de fabrication. La Fig. 6.2 montre la dimension du moule (la partie noire) et la préforme (la partie verte). La hauteur (H) et le diamètre (D) du moule sont de 240 mm et de 100 mm. Pour la préforme, la hauteur (h) est de 160 mm et le diamètre (d) est de 80 mm. L'alliage d'aluminium choisi pour cette étude est AS7G et le moule est en inox.

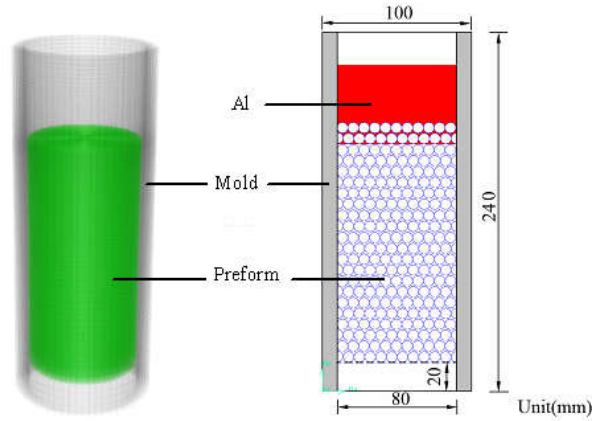


Fig. 6.2. Dimension du modèle numérique

Pour la simulation numérique du procédé de fabrication, l'aluminium fondu est considéré comme le liquide incompressible. Les équations de conservation appliquées dans la simulation est comme suit :

L'équation de continuité :

$$\frac{\partial \rho}{\partial t} + \frac{\partial(\rho u)}{\partial x} + \frac{\partial(\rho v)}{\partial y} + \frac{\partial(\rho w)}{\partial z} = 0 \quad (1)$$

L'équation de conservation de la quantité de mouvement :

$$\rho \left(\frac{\partial u}{\partial t} + u \frac{\partial u}{\partial x} + v \frac{\partial u}{\partial y} + w \frac{\partial u}{\partial z} \right) = \mu \left(\frac{\partial^2 u}{\partial x^2} + \frac{\partial^2 u}{\partial y^2} + \frac{\partial^2 u}{\partial z^2} \right) - \frac{\partial p}{\partial x} - \frac{\mu}{K_s K_r} u + \frac{1}{2} C_f \rho |u| \quad (2)$$

$$\rho \left(\frac{\partial v}{\partial t} + u \frac{\partial v}{\partial x} + v \frac{\partial v}{\partial y} + w \frac{\partial v}{\partial z} \right) = \mu \left(\frac{\partial^2 v}{\partial x^2} + \frac{\partial^2 v}{\partial y^2} + \frac{\partial^2 v}{\partial z^2} \right) - \frac{\partial p}{\partial y} - \frac{\mu}{K_s K_r} v + \frac{1}{2} C_f \rho |v| \quad (3)$$

$$\rho \left(\frac{\partial w}{\partial t} + u \frac{\partial w}{\partial x} + v \frac{\partial w}{\partial y} + w \frac{\partial w}{\partial z} \right) = \mu \left(\frac{\partial^2 w}{\partial x^2} + \frac{\partial^2 w}{\partial y^2} + \frac{\partial^2 w}{\partial z^2} \right) - \frac{\partial p}{\partial z} - \frac{\mu}{K_s K_r} w + \frac{1}{2} C_f \rho |w| \quad (4)$$

L'équation de conservation d'énergie:

$$\frac{\partial T}{\partial t} [(1-\varepsilon)\rho_s c_s + \varepsilon\rho_f c_f] + \rho_f c_f \left(u \frac{\partial T}{\partial x} + v \frac{\partial T}{\partial y} + w \frac{\partial T}{\partial z} \right) = k_{eff} \left(\frac{\partial^2 T}{\partial x^2} + \frac{\partial^2 T}{\partial y^2} + \frac{\partial^2 T}{\partial z^2} \right) + \varepsilon\rho_f L \frac{\partial \beta}{\partial t} \quad (5)$$

Où ε est porosité; ρ_s et ρ_f sont des densités de matrice solide et de matériau fluide; c_s et c_f sont des chaleurs spécifiques de matrice solide et de matériau fluide; L est la chaleur latente; β est la fraction volumique d'aluminium fondu (liquide); k_{eff} est la conductivité thermique totale.

2.3 Analyse numérique des causes des défauts

(a) Versement

La Fig. 6.3 (a) montre le procédé de versement de l'aluminium fondu. On constate que l'aluminium fondu est versé au centre du moule, puis la surface du liquide monte progressivement. A ce moment, seule une petite partie d'aluminium pénètre dans la préforme sous l'effet de la gravité. Il est évident que certaines bulles se mélangent dans l'aluminium fondu comme ce que nous observons dans la Fig. 6.3 (b). En raison de la différence de température entre la préforme et l'aluminium fondu, la viscosité du liquide augmentera lorsque le liquide est en contact avec la préforme. Dans ce cas, certaines bulles sont piégées dans le liquide. D'ailleurs, sur la vue de dessus du moule, la plupart des bulles se répartissent dans la surface intérieure du moule. Ces bulles deviendront des défauts après le refroidissement de l'échantillon, comme le montre la Fig. 6.4.

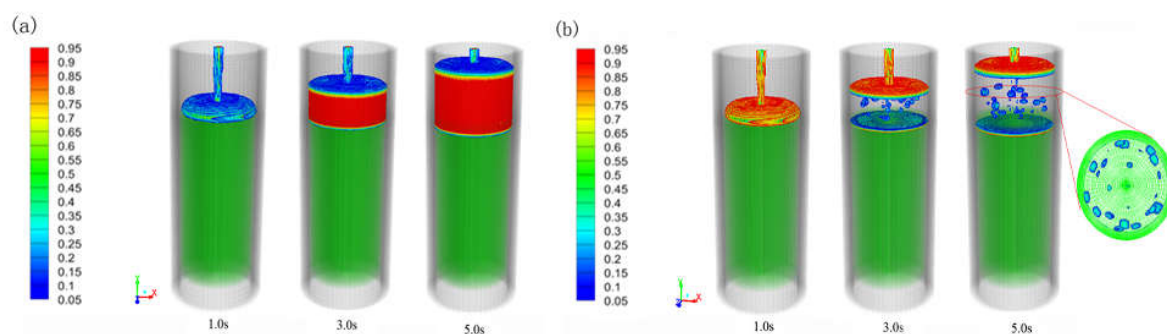


Fig. 6.3. Procédé de versement (a) distribution de liquide en aluminium, (b) distribution d'air



Fig. 6.4. Défauts formés lors du processus de versement de l'aluminium fondu

(b) Infiltration

Après le processus de versement, la viscosité de l'aluminium fondu augmente, la pression négative doit être appliquée tout de suite pour aider la pénétration de l'aluminium fondu dans la préforme. Nous pouvons observer dans la Fig. 6.5 (a), l'aluminium fondu est aspiré progressivement dans les préformes à l'aide de la pression négative. Il est clair que certaines bulles entrent, encore une fois, dans la préforme avec le liquide d'alu, tel qu'il est présenté dans la Fig. 6.5 (b). Cependant, si la distance d'infiltration et la pression négative n'ont pas été contrôlées de façon exacte, les bulles resteront dans l'échantillon et deviendront des défauts après la solidification, comme le montre la Fig. 6.6.

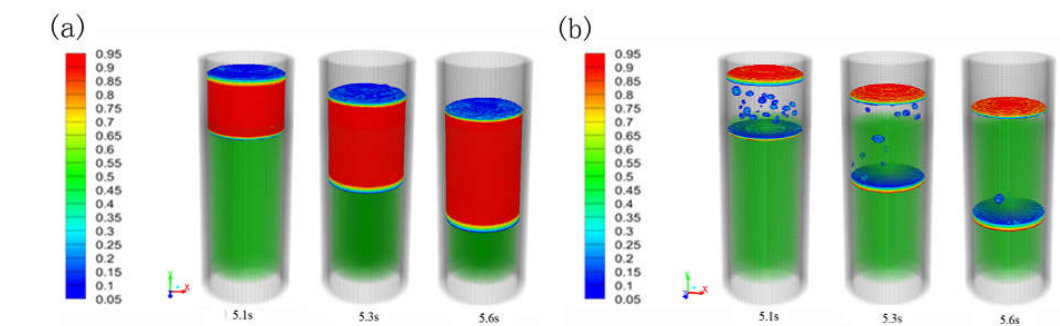


Fig. 6.5. Procédé d'infiltration (a) distribution de l'alu fondu (b) distribution d'air

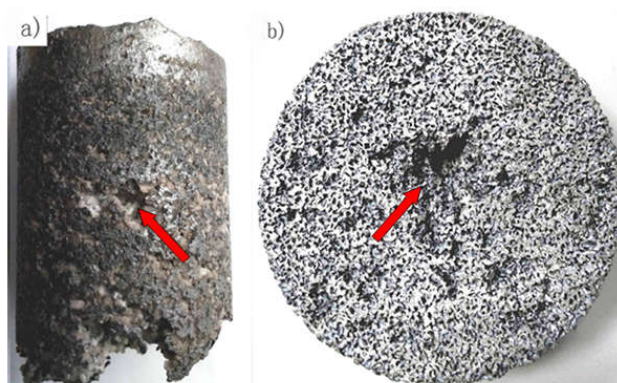


Fig. 6.6. Bulles dans une mousse d'aluminium

(c) Solidification

A l'aide de la méthode numérique, nous pouvons obtenir la séquence de solidification. La Fig. 6.7 montre que le fond du métal se solidifie en premier lieu car la température à cet endroit est plus basse que les autres parties. En outre, lors de la solidification en température ambiante, la chaleur s'échappe de la surface du moule par convection et rayonnement. Pour ces raisons, la solidification commence de l'extérieur à l'intérieur, et simultanément la partie en bas du moule. Dans ce cas, la partie supérieure de l'échantillon se solidifie à la fin. Lorsque la distance d'infiltration est importante et le volume d'alu fondu n'est pas suffisant pour toute la préforme, le défaut se trouve souvent au centre de la partie supérieure de l'échantillon, comme le montre la Fig. 6.8.

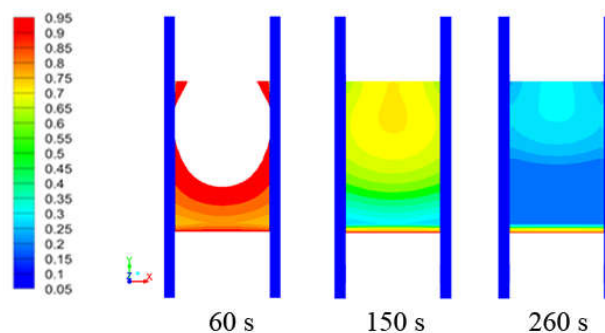


Fig. 6.7. Séquence de solidification de la mousse d'aluminium

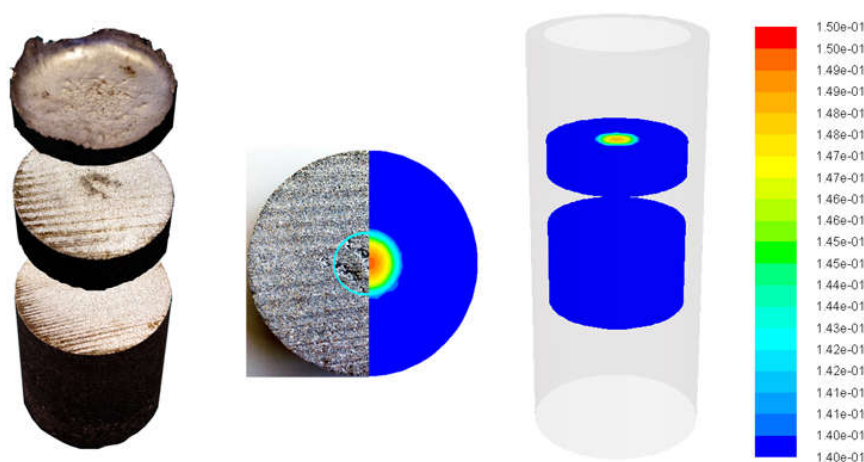


Fig. 6.8. Emplacement de retrait dans l'échantillon réel et modèle numérique

2.4 Prévention pour éviter les défauts

Les défauts de fabrication sont dus essentiellement les bulles d'air entrant dans l'échantillon au cours de fabrication. Pour éviter ce problème, nous proposons de réduire la vitesse de versement (réduire l'intensité de la turbulence). Dans l'industrie de la fonderie, l'augmentation du diamètre de jet de coulée et la modification de l'angle de coulée pourraient être les deux solutions potentielles d'amélioration, permettant de réduire les bulles indésirables. Pour éviter le retrait au centre, il est nécessaire de laisser l'aluminium suffisant au sommet de la préforme comme la masselotte. Donc, la longueur d'infiltration doit être bien contrôlée.

3. Etude de la performance thermique du composite MAFP/MCP

3.1 Procédé de fusion de la paraffine

Dans cette étude, la paraffine est utilisée comme le matériau de changement de phase (MCP). Une fois la mousse d'aluminium fabriquée, la paraffine est introduite dans la mousse d'aluminium, remplissant les pores de la mousse, un composite mousse d'aluminium/paraffine est ainsi fabriqué. Nous commençons notre analyse par le transfert de chaleur (température) sur la paraffine pure.

La Fig. 6.9 présente la distribution de température de paraffine pure pendant le processus de fusion (la source de chaleur est en bas), où la partie blanche représente la phase liquide et la partie rouge est l'interface solide-liquide de la paraffine pure. Dans la Fig. 6.9 (a), au début de chauffage, l'interface est parallèle à la surface inférieure, indiquant que la conduction thermique est le mode thermique dominant dans le liquide. Quand la fraction volumique de liquide augmente au fur et à mesure, la circulation de la convection de Bénard provoquées par la force de flottaison se développe dans la phase liquide, ce qui est confirmé par la forme ondulée de l'interface solide-liquide de la Fig. 6.9 (b). Après ce stade, le transfert de chaleur dans la paraffine pure est dominé par convection thermique, l'interface liquide/solide n'est plus linéaire (Fig. 6.9 (c) et (d)).

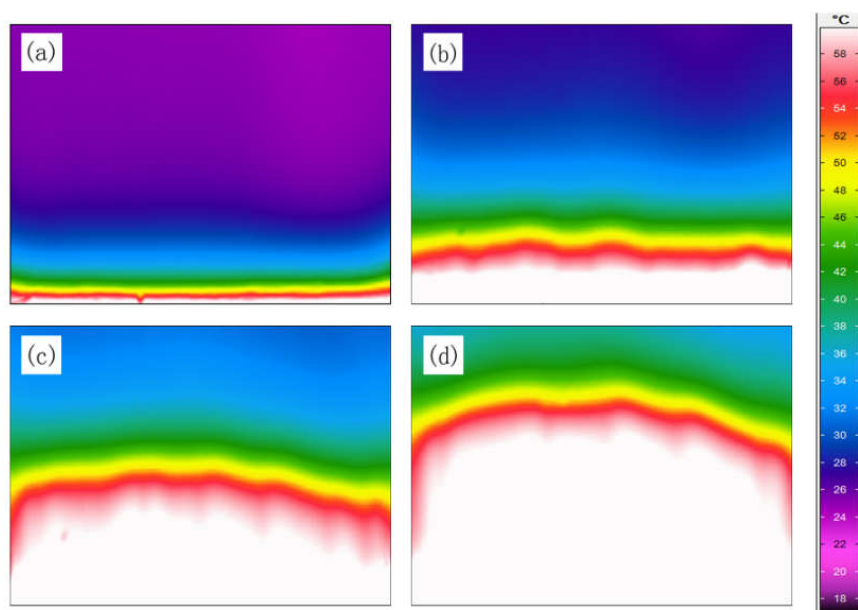


Fig. 6.9. Distribution de température de paraffine pure (a) 800 s (b) 1800 s (c) 2600 s (d) 3300 s

3.2 Procédé de fusion du composite mousse d'aluminium/paraffine

En utilisant la mousse d'aluminium dans la paraffine, la paraffine est divisée en cellules par des ligaments métalliques, comme ce qu'on peut voir dans la Fig. 6.10 (a). Grâce à la conductivité thermique élevée de l'aluminium, la mousse d'aluminium est d'abord chauffée et le flux de chaleur est transféré vers la structure des ligaments métalliques, comme le montre la Fig. 6.10 (b) - (d). Dans ce cas, la paraffine dans les unités cellulaires peut être chauffée par la mousse métallique et la paraffine éloignée de la source de chaleur peut être chauffée plus rapidement.

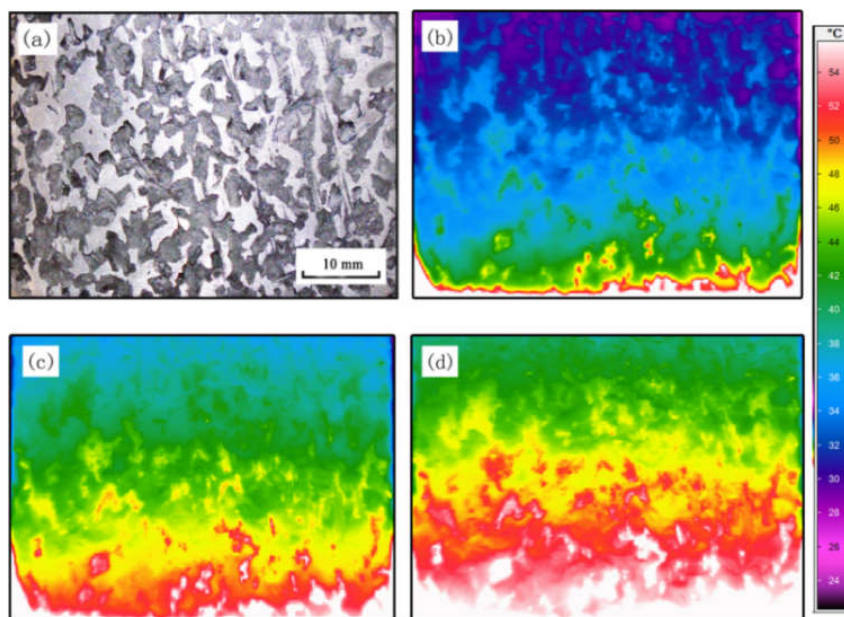


Fig. 6.10. (a) Morphologie du composite. Distribution des températures du composite (b) à 500 s (c) à 750 s (d) à 1000 s

Une comparaison des variations de température pour le composite et la paraffine pure est présentée dans la Fig. 6.11 (P1, P2 et P3 sont les 3 points de mesure de température, P1 est plus proche de la source de chaleur, P3 est plus loin de la source de chaleur). Pour le composite, les températures des trois points atteignent $70\text{ }^{\circ}\text{C}$ à environ 2500 s qui est plus court que celle de la paraffine pure ($>4000\text{ s}$). Ce phénomène peut être expliqué par le fait que par rapport à paraffine pure, le volume de la paraffine dans le composite est moins important et que le composite possède une capacité de conduction thermique plus importante. En conclusion, l'addition de la mousse d'aluminium peut améliorer le transfert de chaleur dans MCP, mais l'existence de la mousse métallique réduit la quantité de paraffine, influençant éventuellement la chaleur latente stockée dans le système. Pour trouver un compromis entre ces deux facteurs, la porosité de la mousse d'aluminium joue un rôle essentiel sur l'efficacité du stockage de l'énergie, et elle sera étudiée dans la partie suivante.

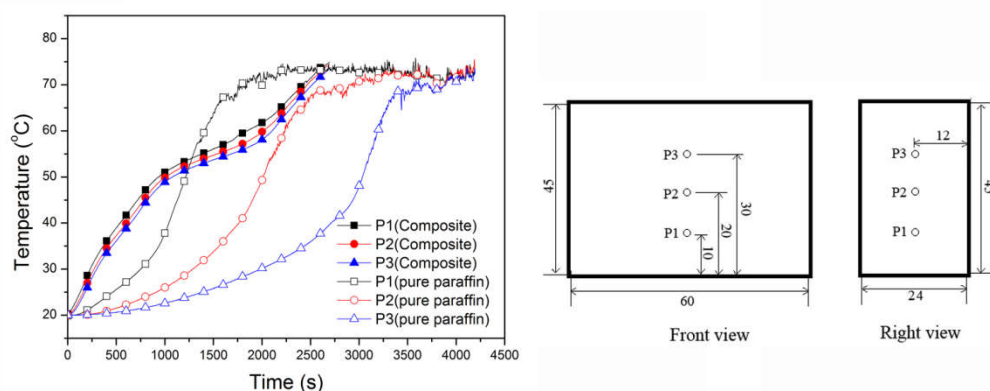


Fig. 6.11. Comparaison des variations de température pour le composite et la paraffine pure

3.3 Effet de la porosité sur le transfert de chaleur dans le composite

Afin d'analyser quantitativement l'effet de la porosité (ϵ) sur le transfert de la chaleur, les variations de température sur les 3 points (P1, P2 et P3) dans des composites sont mesurées expérimentalement et présentées dans la Fig. 6.12. Il est à constater que la différence de température entre ces 3 points augmente lorsque la porosité augmente. La conductivité thermique (k_{eff}) du composite peut accélérer le processus de transfert de chaleur et homogénéiser la température dans l'échantillon. D'ailleurs, la zone pâteuse du composite à $\epsilon = 67\%$ est évidente, alors que cette zone tend à être moins claire pour le composite à $\epsilon = 84\%$. Ce phénomène peut s'expliquer par le changement du mode de transfert de chaleur : la perméabilité de la mousse d'aluminium à $\epsilon = 67\%$ est faible, ce qui limite la convection naturelle dans la paraffine liquide. Dans ce cas, la paraffine est limitée dans les pores de la mousse d'aluminium et le transfert de chaleur est gouverné par la conduction thermique. En revanche, la mousse d'aluminium à $\epsilon = 84\%$ possède une grande perméabilité et le mouvement de la paraffine liquide dans la mousse d'aluminium entre les cellules est plus facile. La convection naturelle de la phase liquide se développera dans le composite, la variation de la température est donc

faible et uniforme [134]. Par conséquent, le transfert de chaleur dans le composite à $\varepsilon = 84\%$ est influencé par la conduction thermique et la convection thermique.

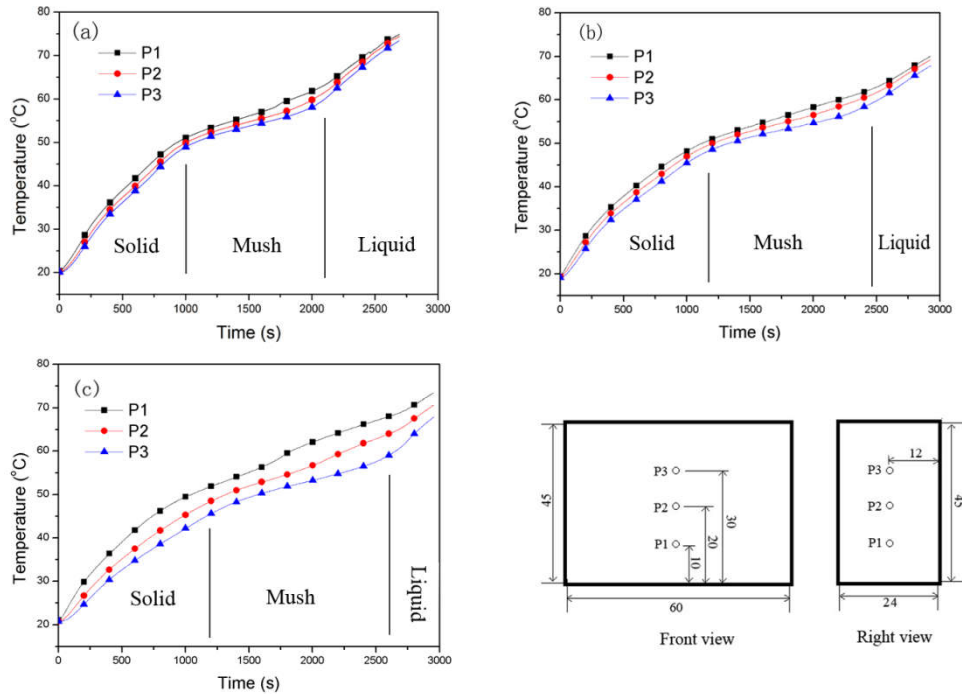


Fig. 6.12. Variations de température des composites à différentes porosités (a) 67% (b) 75% (c) 84%

3.4 Modélisation de transfert de chaleur composite MAFP/MCP

MAFP : Mousse d'Aluminium à Faible Porosité 50-85%, MCP : Matériau à changement de phase.

(a) Equations principales

Les équations principales du modèle sont basées sur les équations de continuité, de quantité de mouvement et de conservation de l'énergie, les expressions sont décrites comme suit :

L'équation de continuité :

$$\frac{\partial \rho_p}{\partial t} + \nabla \cdot (\rho_p \mathbf{U}) = 0 \quad (6)$$

L'équation de conservation de la quantité de mouvement :

$$\frac{\rho_p}{\varepsilon} \frac{\partial \mathbf{U}}{\partial t} + \frac{\rho_p}{\varepsilon^2} (\mathbf{U} \cdot \nabla) \mathbf{U} = \frac{\mu}{\varepsilon} \nabla^2 \mathbf{U} - \nabla P - \left(\frac{\mu}{K} \mathbf{U} + \frac{C_i \rho_p \mathbf{U} |\mathbf{U}|}{2} \right) + \rho_p g \gamma (T - T_0) + S \quad (7)$$

L'équation de conservation d'énergie :

$$(\varepsilon \rho_p c_p + (1 - \varepsilon) \rho_s c_s) \frac{\partial T}{\partial t} + \rho_p c_p (\mathbf{U} \cdot \nabla T) = k_{eff} \nabla^2 T - \varepsilon \rho_p L \frac{\partial \beta}{\partial t} \quad (8)$$

L'équation (8) est appelé « Modèle d'équilibre » dans certaines publications. Pour cette méthode, la mousse métallique et le MCP sont considérés comme un ensemble. Le modèle d'équilibre est relativement simple à utiliser et peut réduire le temps de calcul. Récemment, un autre modèle est développé, nommé « Modèle de non-équilibre ». Ce modèle consiste en deux équations d'énergie séparées pour le MCP et la mousse métallique, comme décrit dans l'équation (9) et (10). Le modèle de non-équilibre est souvent utilisé dans la recherche de la convection naturelle du composite.

Equation de l'énergie pour le MCP :

$$\varepsilon \rho_p c_p \frac{\partial T_p}{\partial t} + \varepsilon \rho_p c_p (\mathbf{U} \cdot \nabla) T_p = k_{pe} \nabla^2 T_p + hA(T_s - T_p) - \varepsilon \rho_p L \frac{\partial \beta}{\partial t} \quad (9)$$

Equation de l'énergie pour la mousse métallique :

$$(1 - \varepsilon) \rho_s c_s \frac{\partial T_s}{\partial t} = k_{se} \nabla^2 T_s + hA(T_p - T_s) \quad (10)$$

Les paramètres h, K et A sont déterminés de façon empirique, avec les formules de corrélation dans le Table 7.1. Les expressions de K et A sont déduites selon la structure de MAFP. Ainsi, ces équations sont choisies dans cette étude.

Table 7.1 Corrélations des paramètres de mousse d'aluminium à faible porosité

Paramètre	Corrélation	No.	Ref.
Perméabilité, K	$K = \frac{\varepsilon r^2}{\pi} \left[\frac{\varepsilon - \varepsilon_0}{3(1 - \varepsilon_0)} \right]^{3/2}$	(11)	[137]
Coefficient de transfert thermique, h	$h = \frac{k_p}{d_f} \left[\left(1 + \frac{4(1 - \varepsilon)}{\varepsilon}\right) + 0.5(1 - \varepsilon)^{0.5} \text{Re}^{0.6} \text{Pr}^{1/3} \right]$	(12)	[138]
Densité de l'aire interfaciale, A	$A = \frac{281}{d_p} \left[(1 - \varepsilon)^{1/2} - (1 - \varepsilon) \right] (1 - \varepsilon)^{0.4}$	(13)	[139]

(b) Comparaison du modèle d'équilibre et du modèle de non-équilibre

La comparaison de variations de la température expérimentales et numériques est présentée dans la Fig. 6.13 et les erreurs moyennes sont listées dans le Table 6.2. Nous pouvons constater que les deux modèles concordent bien avec l'expérience pour le composite à $\varepsilon = 67\%$ et que l'erreur moyenne du modèle d'équilibre est plus faible que celle du modèle de non-équilibre. Comme ce qu'on a déjà discuté ci-dessus, le processus de transfert de chaleur du composite à $\varepsilon = 67\%$ est dominé par la conduction thermique, dans ce cas, le modèle de non-équilibre qui est développé pour la convection naturelle ne montre pas son avantage. Donc, le modèle d'équilibre peut satisfaire la simulation du composite à faible porosité $\varepsilon = 67\%$. Pour le composite à haute porosité $\varepsilon = 84\%$, les résultats de deux types de modèles ont la même tendance comme les résultats expérimentales. Les écarts entre les résultats numériques et expérimentaux sont dus à la négligence du rayonnement thermique, taux de remplissage de paraffine et de la transition cristalline en paraffine. L'erreur moyenne du modèle de non-équilibre est plus petite que celle du modèle d'équilibre, car la convection naturelle est prise en compte dans le calcul. De plus, le modèle de non-équilibre peut refléter la séparation de la température dans le composite, comme le montre la Fig. 6.13(d). En conséquence, le modèle de non-équilibre est plus approprié au composite à $\varepsilon = 84\%$.

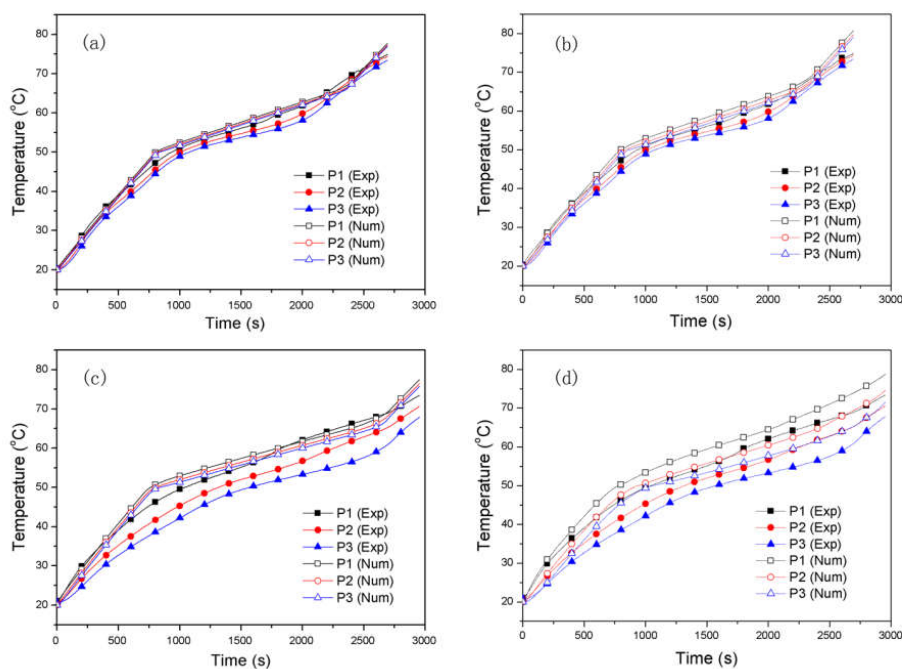


Fig. 6.13. Comparaison des variations de température entre les résultats numériques et expérimentales (a) modèle d'équilibre avec $\varepsilon=67\%$ (b) modèle de non équilibré avec $\varepsilon=67\%$ (c) modèle d'équilibre avec $\varepsilon=84\%$ (d) modèle de non équilibré avec $\varepsilon=84\%$

Table 6.2 Erreurs moyennes entre les résultats expérimentales et numériques

Model	$\varepsilon=67\%$	$\varepsilon=84\%$
Modèle d'équilibre	3,4%	8,6%
Modèle de non équilibré	4,1%	7,5%

4. Analyse numérique des performances thermiques du composite MAHP/MCP

(MAHP : Mousse d'Aluminium à Haute Porosité, $\varepsilon > 85\%$)

4.1 Modèle physique

Le diagramme schématique du modèle 2D est illustré dans la Fig. 6.14. Les équations gouvernantes sont basées sur la partie 3.4, et l'équation d'énergie utilisée est le modèle de non-équilibre. Les dimensions du modèle en 2D sont de 50mm×90mm. La surface gauche est la source de chaleur et la surface droite est la

paroi froide. Les autres surfaces sont isolées. La mousse métallique utilisée dans cette étude est élaborée par l'alliage d'aluminium AS7G et la paraffine est choisie comme MCP, dont les propriétés thermiques sont disponibles dans Ref. [79]. Pour obtenir des résultats précis, certains paramètres liés à la structure de la MAHP sont listés dans le Table 7.3.

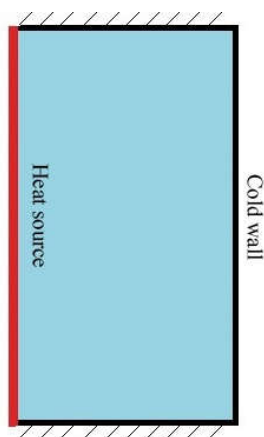


Fig. 6.14. Diagramme schématique du modèle 2D

Table 7.3 Corrélations des paramètres de mousse d'aluminium à haute porosité

Paramètre	Corrélation	No.	Ref.
Perméabilité, K et coefficient d'inertie, C_i	$\frac{K}{d_p^2} = 0.00073(1 - \varepsilon)^{-0.224} \left(\frac{d_f}{d_p}\right)^{-1.11}$	(14)	[31]
	$C_i = 0.00212(1 - \varepsilon)^{-0.132} \left(\frac{d_f}{d_p}\right)^{-1.63}$		
Coefficient de transfert thermique, h	$h = \frac{k_f}{d} \left[\left(1 + \frac{4(1-\varepsilon)}{\varepsilon}\right) + 0.5(1-\varepsilon)^{0.5} \text{Re}^{0.6} \text{Pr}^{1/3} \right]$	(15)	[138]
Densité de l'aire interfaciale,, A	$A_{ppi10} = 349.15 \ln(1 - \varepsilon) + 1667.99$	(16)	[145]
	$A_{ppi20} = 442.2 \ln(1 - \varepsilon) + 2378.62$		
	$A_{ppi40} = 694.57 \ln(1 - \varepsilon) + 3579.99$		

4.2 Détermination de la porosité optimisée

Bien que le composite à faible porosité ait un processus rapide de fusion, la

fraction basse de MCP peut réduire la quantité totale d'énergie stockée dans le composite. Pour obtenir la porosité optimisée, l'efficacité du stockage d'énergie peut être un facteur d'évaluation. Ainsi, l'efficacité thermique (η) du système est définie comme le rapport de l'énergie stockée dans le composite et de la quantité d'énergie d'entrée dans le système:

$$\eta = \frac{m_p L_f + \sum_{i=1}^M \sum_{j=1}^N \Delta m_p c_p [(T_p)_{ij} - T_0] + \sum_{i=1}^M \sum_{j=1}^N \Delta m_{al} c_{al} [(T_{al})_{ij} - T_0]}{q S_h t} \times 100\% \quad (17)$$

Le but de l'utilisation du MCP est de stocker la chaleur latente dans le matériau pendant le processus de changement de phase liquide/solide. Ainsi, nous avons défini la valeur de η au moment où la paraffine fond entièrement comme l'efficacité thermique efficace (η_e) du système. Dans ce cas, on peut établir selon ce calcul une courbe entre η_e et la porosité ε (Fig. 6.15). Nous pouvons constater sur cette courbe que la valeur de η_e atteint le maximum lorsque la porosité se trouve dans une plage de 85% à 90%. Par contre, une chute libre de la valeur de η_e a été observée après 90% de porosité. Ainsi, la porosité optimisée peut être déterminée dans le domaine au-delà de 85% de porosité, ce qui optimise la quantité de stockage d'énergie et le temps de fusion. Le composite à la porosité optimisée peut posséder la plus grande efficacité thermique.

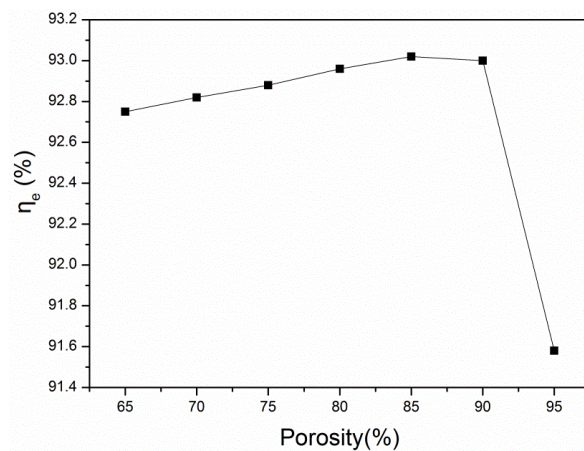


Fig. 6.15. Efficacité thermique efficace (η_e) en fonction de la porosité

4.3 Méthodes d'amélioration de l'efficacité thermique efficace du composite

Afin d'améliorer la vitesse de fusion de la paraffine, nous proposons trois méthodes d'amélioration, comme illustré sur la Fig. 6.16. La source de chaleur se trouve à gauche de chaque échantillon. La méthode I (Fig. 6.16 a) est de changer la valeur des « pores par pouce » (PPI). La méthode II (Fig. 6.16 b) est de changer la forme de la paroi froide. La méthode III (Fig. 6.16 c) est d'utiliser les sources de chaleur discrètes.

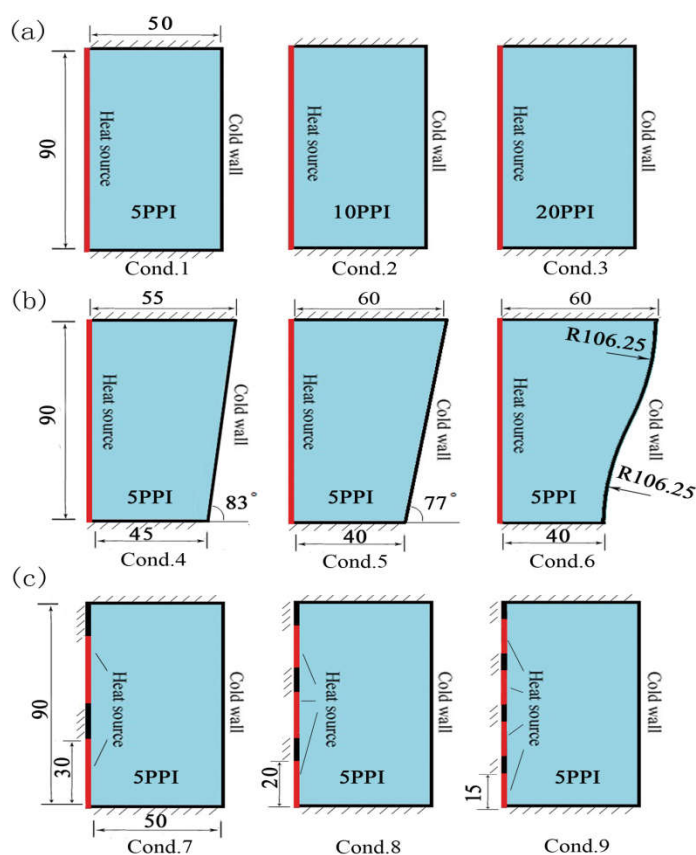


Fig. 6.16. Représentation schématique de trois méthodes d'amélioration (a) Méthode I (b) Méthode II (c) Méthode III.

Afin d'évaluer ces méthodes d'amélioration dans l'application du stockage d'énergie thermique, les résultats du temps total de fusion (t_{total}) et de l'efficacité thermique efficace (η_e) sont comparés, comme le montre la Fig. 6.17. La paraffine

pure est considérée comme une condition de référence (Cond.0), qui possède la même qualité de paraffine que les autres conditions. Cond.10 (Fig. 6.18) est la combinaison de Cond.6 et Cond.7. Il est évident que l'addition de la mousse d'aluminium peut améliorer le comportement thermique de la paraffine. Pour le temps total de fusion, les valeurs de Cond.3, 6 et 10 sont plus courtes que d'autres conditions. Parmi eux, le t_{total} de Cond.10 est le plus court, ce qui réduit le temps de fusion totale de 45,4% par rapport à la paraffine pure. D'ailleurs, les efficacités thermiques efficaces de Cond.3 et Cond.10 sont les plus élevées parmi toutes les conditions, soit 10% de plus que celle de Cond.0. En combinant ces deux facteurs, il est conclu que Cond.3 de la méthode I et Cond.10 sont les deux méthodes d'amélioration qui ont le meilleur résultat.

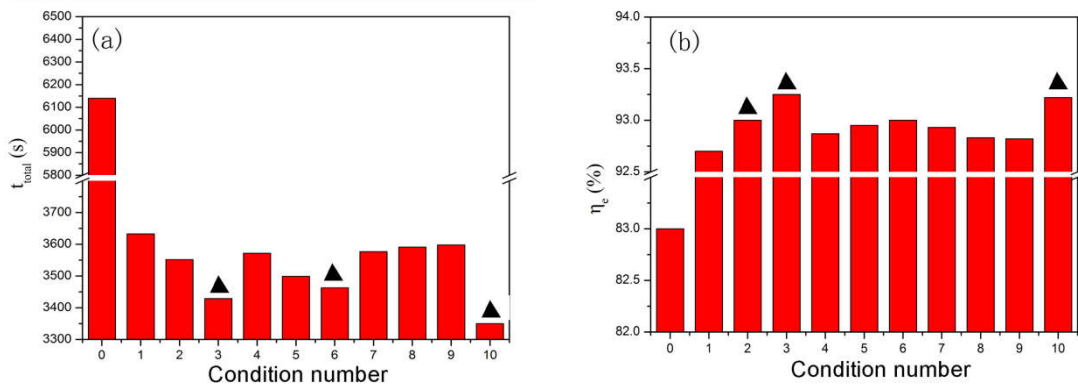


Fig. 6.17. Evaluation complète des méthodes d'amélioration (a) résultat du t_{total} (b) résultat de η_e

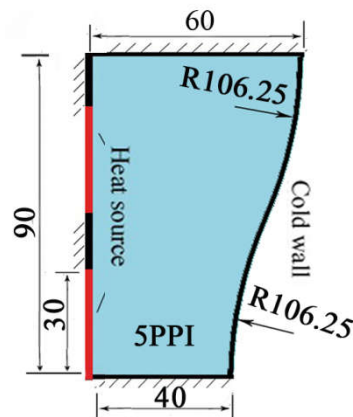


Fig. 6.18. Représentation schématique de Cond.10

5. Comportement thermique de composite à structure modifiée en température constante

Ce chapitre est consacré à la modélisation numérique de structure modifiée d'une mousse métallique (gradient de pore) et de changement de la configuration (avec ailette métallique). A la fin, une étude préliminaire portée sur la mousse fabriquée à partir de l'impression 3D permet d'optimiser la performance thermique d'une mousse métallique à pore régulier.

5.1 Modèle physique

Les modèles physiques étudiés sont des configurations en 2D. La mousse métallique uniforme est considérée comme une référence, comme le montre la Fig. 6.19 (a), et la structure modifiée avec un gradient de porosité est présentée dans la Fig. 6.19 (b). Les dimensions sont de 100mm×300mm. Le côté gauche représente la source de chaleur avec une température constante de 78°C et les autres côtés sont isolés. Trois mousses métalliques à porosités différentes sont choisies pour constituer une seule mousse métallique à gradient. La taille de pores est identique (5PPI) mais la porosité est différente. Une ailette métallique est mise en bas de l'échantillon. L'acétate de sodium est choisi comme MCP et est rempli dans la mousse métallique à gradient de pores, l'aluminium AS7G est utilisé comme matrice métallique.

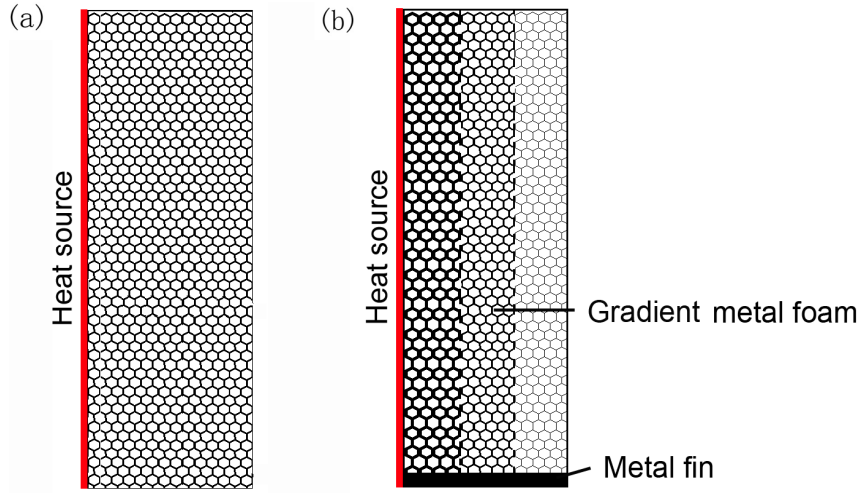


Fig. 6.19 Représentation schématique de structures en mousse métallique (a) structure uniforme (b) structure modifiée

Pour étudier la performance thermique de la structure modifiée, deux paramètres sont utilisés dans notre analyse: la quantité de stockage d'énergie E (kJ) et la puissance de stockage d'énergie P (W). La valeur E est la fonction du temps de chauffage et représente la somme totale de l'énergie de stockage dans l'échantillon. Les équations (18) - (21) donnent l'expression de ce calcul sur E . En fait, le processus de transition de phase est la principale fonction de MCP dans le composite. Donc, au moment où le MCP fond totalement, la valeur d' E est définie comme la quantité effective de stockage d'énergie $E(t_{total})$. La puissance de stockage d'énergie P est définie comme le rapport d' $E(t_{total})$ et du temps total de fusion de MCP (t_{total}), comme montré dans Eq.(22). A partir de la valeur de P , une évaluation complète de performance thermique de composites pourrait être obtenue.

$$E(t) = E_{PCM}(t) + E_{foam}(t) + E_{fin}(t) \quad (18)$$

$$E_{PCM}(t) = \begin{cases} m_{PCM} C_{s,PCM} (T_{PCM}(t) - T_0) & T \leq T_m \\ m_{PCM} C_{l,PCM} (T_{PCM}(t) - T_m) \\ + m_{PCM} C_{s,PCM} (T_m - T_0) + m_{PCM} L & T > T_m \end{cases} \quad (19)$$

$$E_{foam}(t) = m_{foam} C_{al} (T_{foam}(t) - T_0) \quad (20)$$

$$E_{fin}(t) = m_{fin} C_{al} (T_{fin}(t) - T_0) \quad (21)$$

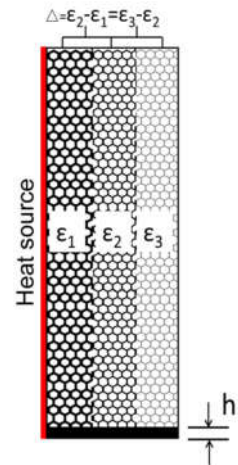
$$P = \frac{E(t_{total})}{t_{total}} \quad (22)$$

5.2 Optimisation des paramètres de la structure modifiée

En comparant avec la mousse métallique uniforme, la structure modifiée est relativement complexe. Pour obtenir la configuration optimisée, l'effet de certains paramètres critiques sur le transfert de chaleur est analysé, tels que l'épaisseur de l'ailette métallique (h) et le gradient de porosité (Δ). Huit configurations différentes sont proposées et comparées, dont le détail des paramètres est listé dans Table 7.4. Tous les échantillons ont le même volume de métal (10%). L'échantillon C1 avec la mousse métallique uniforme est une référence.

Table 7.4 Paramètres de structure des configurations

Configuration	Epaisseur de l'ailette, h (mm)	Gradient de porosité, Δ (%)	Distribution de porosité, ε_1 - ε_2 - ε_3 (%)
C1	0	0	90
C2	0	2	88-90-92
C3	2,5	2	88,8-90,8-92,8
C4	5	2	89,5-91,5-93,5
C5	7,5	2	90,3-92,3-94,3
C6	10	2	91,1-93,1-95,1
C7	5	3	88,5-91,5-94,5
C8	5	5	86,5-91,5-96,5



(a) Effet de l'épaisseur de l'ailette métallique

Les résultats de la quantité de stockage d'énergie E (kJ) et la puissance de stockage d'énergie P (W) de C1-C6 sont calculées et comparées dans la Fig. 6.20 (a). Nous pouvons constater que l'énergie stockée dans les échantillons augmente avec

le processus de fusion. Dans le même temps, les structures modifiées peuvent toujours conserver plus d'énergie que la structure uniforme. La Fig. 6.20 (b) montre les valeurs de P de C1-C6. Il est à noter que les structures modifiées peuvent améliorer sensiblement la puissance de stockage d'énergie. De C3 à C6, la valeur de P augmente d'abord puis diminue, car le volume de la mousse métallique est réduit avec l'augmentation de l'épaisseur des ailettes métalliques. Dans ce cas, la convection naturelle dans la mousse métallique est accélérée tandis que la conduction thermique est réduite. D'ailleurs, le transfert de chaleur est accéléré sur la partie proche d'ailette lorsque l'épaisseur de l'ailette métallique augmente. Sous l'effet de ces trois facteurs, C4 possède la valeur de la puissance de stockage d'énergie la plus élevée, soit 23,7% de plus que celle de C1.

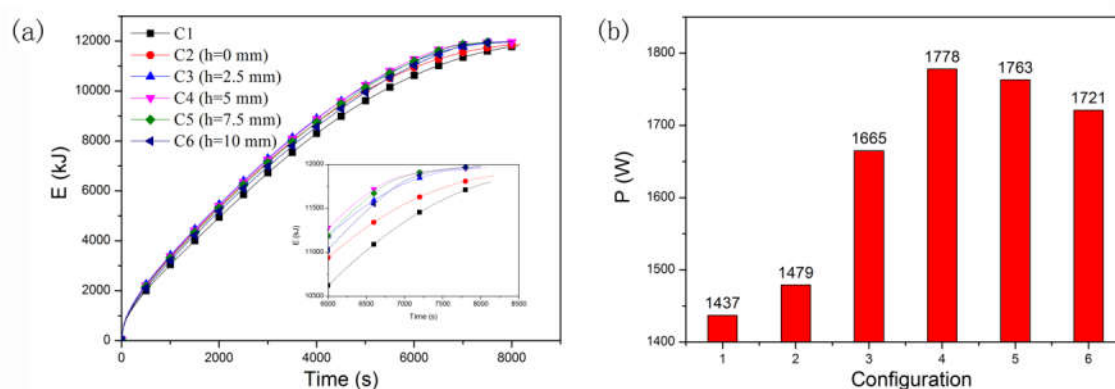


Fig. 6.20 Evaluation de la performance de la mousse métallique uniforme (C1) et les structures modifiées (C2-C6) avec différente valeur h (a) valeur d'E (b) valeur de P

(b) Effet du gradient de porosité

La Fig. 6.21 (a) montre les résultats d'E des trois échantillons : C4, C7 et C8. Nous pouvons voir que l'énergie stockée dans le système augmente en fonction du temps et plus le gradient de porosité Δ est important, plus la valeur E augmente légèrement. Après 5000s, ces valeurs E des trois échantillons deviennent identiques. A l'aide des résultats de P (Fig. 6.21(b)), il est clair qu'un gradient de porosité optimisé est de 3%, la configuration C7 possède la plus grande valeur P, soit 1796W, ce qui améliore l'efficacité thermique de 25% par rapport à une

mousse uniforme C1 (1437W).

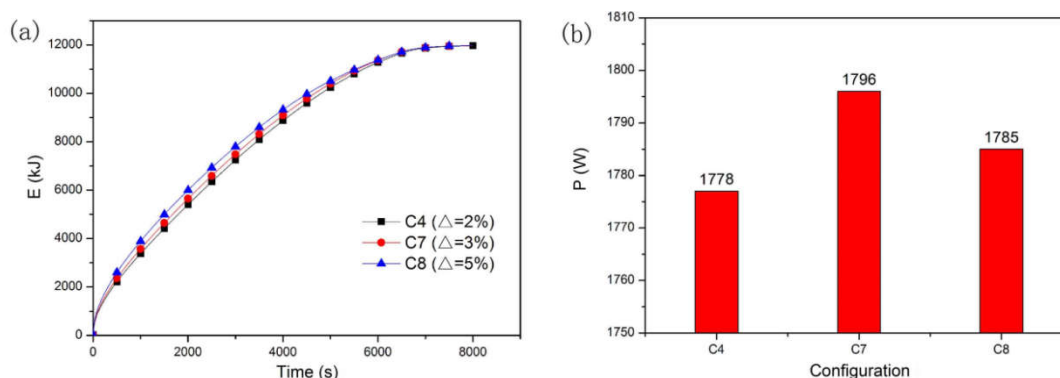


Fig. 6.21. Evaluation de la performance des structures modifiées avec valeur différente de Δ (a) valeur de E (b) valeur de P

5.3 Etude préliminaire de la mousse d'aluminium élaborée par impression 3D

Pour pouvoir fabriquer une mousse métallique avec les pores contrôlables et réguliers, une méthode est proposée en associant l'impression 3D avec la méthode de moulage (Fig. 6.22) grâce à la collaboration de Dr. J.Gardan de l'EPF. Afin d'étudier la performance thermique de la paraffine dans la mousse d'aluminium élaborée par impression 3D, la variation de température des trois points choisis est mesurée expérimentalement. Les résultats d'une mousse imprimée selon le modèle Kelvin sont présentés dans la Fig. 6.23. Le principe de mesure expérimentale est le même que la partie 3.2. Nous pouvons constater que la courbe est lisse et régulière jusqu'à 50°C , et que la température fluctue lorsque la paraffine atteint à 50°C . Nous n'avons pas observé ce phénomène dans les composites précédents, mais il a été observé dans la paraffine pure. Ainsi, nous pouvons déduire que le transfert de chaleur par convection dans ce type de composite est plus prononcé.

Cette partie de recherche reste à développer par deux thèses suivantes.

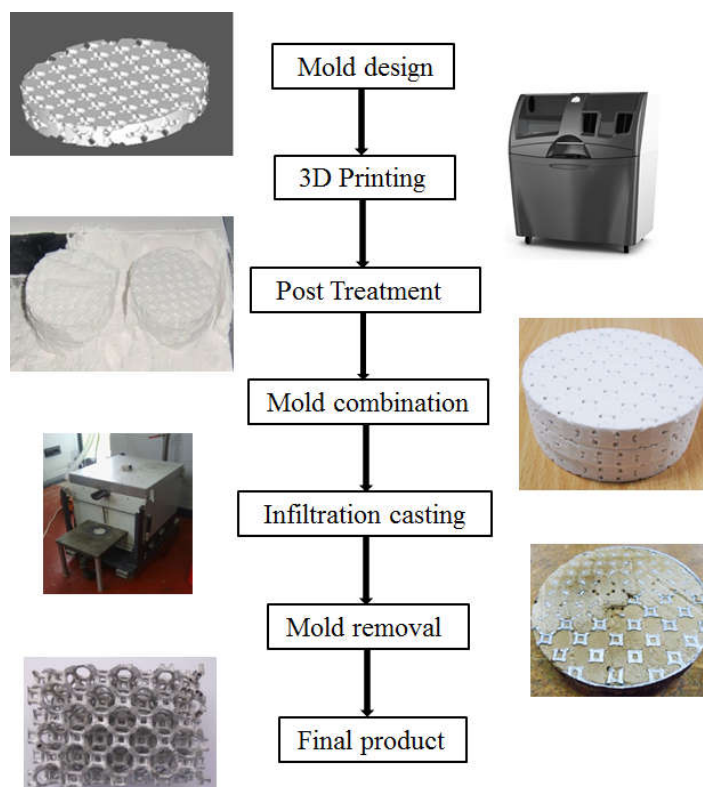


Fig. 6.22. Principe de l'impression 3D

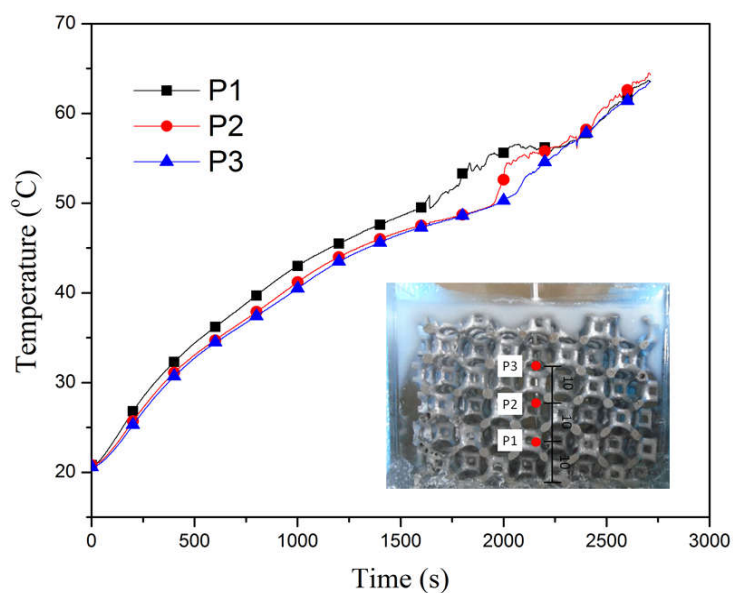


Fig. 6.23. Variation de température de trois points détectés dans le composite à structure Kelvin

6. Conclusion

Pour la mousse d'aluminium élaborée par infiltration à pression négative, les

bulles d'air et le retrait lors du refroidissement sont les causes principales des défauts de fabrication. Pour diminuer des bulles d'air emprisonnées dans l'aluminium fondu, l'angle de versement doit être modifié. En contrôlant la longueur d'infiltration, on pourrait éviter les défauts liés au retrait de refroidissement.

L'addition de mousse d'aluminium faible porosité (MAFP, <67%) dans la paraffine peut accélérer le transfert de chaleur de la paraffine. La conduction et la convection thermique sont les deux modes principaux de transfert de chaleur dans le composite. Lorsque la porosité augmente, la convection naturelle devient plus forte tandis que la conduction thermique devient faible. Lors de la modélisation numérique du MAFP/MCP composite sur leur comportement thermique, le modèle d'équilibre peut satisfaire la simulation numérique du composite à faible porosité $\varepsilon = 67\%$. Avec la haute porosité $\varepsilon = 84\%$, le modèle de non-équilibre peut refléter mieux l'effet de la convection naturelle.

En modélisant la performance thermique avec la combinaison des modèles MAFP/MCP et MAHP/MCP, la porosité optimisée du composite est déterminée dans la plage de 85% à 90%. Pour un composite à porosité optimisée, la modification de la structure de la mousse d'aluminium peut améliorer la performance de stockage d'énergie du composite. Trois méthodes d'optimisation sont étudiées et comparées dans la même condition. En analysant les avantages de différentes méthodes, une méthode d'optimisation est également proposée dans cette étude, qui possède la meilleure performance thermique et améliore l'efficacité thermique jusqu'à 10% par rapport à la paraffine pure.

Si la température de la source de chaleur reste constante, la structure de mousse métallique peut être modifiée afin d'améliorer la performance de stockage d'énergie. La structure optimisée est obtenue lorsque l'épaisseur de l'ailette

métallique est de 5 mm et le gradient de porosité est de 3%. La puissance de stockage d'énergie P de la structure optimisée est de 25% supérieure à celle de la mousse uniforme. La convection thermique dans la nouvelle mousse d'aluminium, qui est préparée par combinaison de l'impression 3D et la méthode par moulage, est améliorée par rapport au composite précédent.

References

- [1] B. Sosnick, Process for making foamlike mass of metal, U.S. Patent 2434775, (1948).
- [2] G.J. Davies, S. Zhen, Metallic foams: their production, properties and applications, *Journal of Materials Science*, 18 (1983) 1899-1911.
- [3] S. Mahjoob, K. Vafai, A synthesis of fluid and thermal transport models for metal foam heat exchangers, *International Journal of Heat and Mass Transfer*, 51 (2008) 3701-3711.
- [4] X. Wang, T.J. Lu, Optimized acoustic properties of cellular solids, *The Journal of the Acoustical Society of America*, 106 (1999) 756-765.
- [5] M.A. Benvenuto, *Industrial Chemistry*, De Gruyter, 2014.
- [6] H.N. Wadley, Cellular metals manufacturing, *Advanced Engineering Materials*, 4 (2002) 726-733.
- [7] N. Garsot, Y. Liu, A. Cherouat, X. Gong, Compressive behavior of porous metal/polymer composite: experiment and numerical modeling, in, 2008.
- [8] K. Berchem, U. Mohr, W. Bleck, Controlling the degree of pore opening of metal sponges, prepared by the infiltration preparation method, *Materials Science and Engineering a-Structural Materials Properties Microstructure and Processing*, 323 (2002) 52-57.
- [9] Y. Su, Analytical and numerical modeling of structure of metal porous polymer composite and its mechanical behaviors, in: *LASMIS, UTT, Troyes, France*, 2011.
- [10] P. Liu, G.F. Chen, *Porous Materials: Processing and Applications*, Elsevier Science, 2014.
- [11] B. Jiang, N.Q. Zhao, C.S. Shi, J.J. Li, Processing of open cell aluminum foams with tailored porous morphology, *Scripta Materialia*, 53 (2005) 781-785.
- [12] I. Kroupova, V. Bednarova, T. Elbel, F. Radkovsky, Proposal of method of removal of mould material from the fine structure of metallic foams used as filters, *Archives of Metallurgy and Materials*, 59 (2014) 727-730.
- [13] S.S. Feng, J.J. Kuang, T. Wen, T.J. Lu, K. Ichimiya, An experimental and numerical study of finned metal foam heat sinks under impinging air jet cooling, *International Journal of Heat and Mass Transfer*, 77 (2014) 1063-1074.
- [14] M.F. Ashby, *Metal Foams: A Design Guide*, Butterworth-Heinemann, 2000.
- [15] X. Yang, W. Wang, C. Yang, L. Jin, T.J. Lu, Solidification of fluid saturated in open-cell metallic foams with graded morphologies, *International Journal of Heat and Mass Transfer*, 98 (2016) 60-69.
- [16] J. Banhart, Manufacture, characterisation and application of cellular metals and metal foams, *Progress in Materials Science*, 46 (2001) 559-632.
- [17] S. Mellouli, H. Dhaou, F. Askri, A. Jemni, S. Ben Nasrallah, Hydrogen storage in metal hydride tanks equipped with metal foam heat exchanger, *International Journal of*

- Hydrogen Energy, 34 (2009) 9393-9401.
- [18] K. Boomsma, D. Poulikakos, F. Zwick, Metal foams as compact high performance heat exchangers, *Mechanics of Materials*, 35 (2003) 1161-1176.
- [19] C.Y. Zhao, Review on thermal transport in high porosity cellular metal foams with open cells, *International Journal of Heat and Mass Transfer*, 55 (2012) 3618-3632.
- [20] M. Wang, N. Pan, Modeling and prediction of the effective thermal conductivity of random open-cell porous foams, *International Journal of Heat and Mass Transfer*, 51 (2008) 1325-1331.
- [21] J. Song, S. He, The heat transfer performance of porous aluminum foam, *Jiangsu Metallurgy*, 36 (2008) 28-30.
- [22] V.V. Calmidi, R.L. Mahajan, Effective thermal conductivity of high porosity fibrous metal foams, *Journal of Heat Transfer*, 121 (1999) 466-471.
- [23] C.Y. Zhao, T.J. Lu, H.P. Hodson, J.D. Jackson, The temperature dependence of effective thermal conductivity of open-celled steel alloy foams, *Materials Science and Engineering: A*, 367 (2004) 123-131.
- [24] A. Bhattacharya, V.V. Calmidi, R.L. Mahajan, Thermophysical properties of high porosity metal foams, *International Journal of Heat and Mass Transfer*, 45 (2002) 1017-1031.
- [25] K. Boomsma, D. Poulikakos, On the effective thermal conductivity of a three-dimensionally structured fluid-saturated metal foam, *International Journal of Heat and Mass Transfer*, 44 (2001) 827-836.
- [26] D.A. Nield, A. Bejan, *Convection in Porous Media*, Springer New York, 2006.
- [27] D.B. Ingham, I. Pop, *Transport Phenomena in Porous Media*, Elsevier Science, 1998.
- [28] P. Nithiarasu, K.N. Seetharamu, T. Sundararajan, Natural convective heat transfer in a fluid saturated variable porosity medium, *International Journal of Heat and Mass Transfer*, 40 (1997) 3955-3967.
- [29] S. Ergun, Fluid flow through packed columns, *Chemical engineering progress*, 48 (1952) 89-94.
- [30] J.-F. Despois, A. Mortensen, Permeability of open-pore microcellular materials, *Acta Materialia*, 53 (2005) 1381-1388.
- [31] V.V. Calmidi, R.L. Mahajan, Forced convection in high porosity metal foams, *Journal of Heat Transfer-Transactions of the Asme*, 122 (2000) 557-565.
- [32] A.J. Otaru, A.R. Kennedy, The permeability of virtual macroporous structures generated by sphere packing models: Comparison with analytical models, *Scripta Materialia*, 124 (2016) 30-33.
- [33] S. Gomez, M.D. Vlad, J. Lopez, E. Fernandez, Design and properties of 3D scaffolds for bone tissue engineering, *Acta Biomaterialia*, 42 (2016) 341-350.
- [34] S. Krishnan, J.Y. Murthy, S.V. Garimella, A two-temperature model for solid-liquid phase change in metal foams, *Journal of Heat Transfer-Transactions of the Asme*, 127 (2005) 995-1004.

- [35] S.W. Churchill, H.H.S. Chu, Correlating equations for laminar and turbulent free convection from a horizontal cylinder, *International Journal of Heat and Mass Transfer*, 18 (1975) 1049-1053.
- [36] K. Saxby, T.D. Hadley, J. Orellana, Y. Pan, K.-S. Lim, Comparative analysis of heat transfer in a counter-current moving bed, *Chemeca 2013: Challenging Tomorrow*, (2013) 182-191.
- [37] X. Zhu, S. Ai, X. Lu, X. Ling, L. Zhu, B. Liu, Thermal conductivity of closed-cell aluminum foam based on the 3D geometrical reconstruction, *International Journal of Heat and Mass Transfer*, 72 (2014) 242-249.
- [38] C. Alkan, A. Sari, Fatty acid/poly(methyl methacrylate) (PMMA) blends as form-stable phase change materials for latent heat thermal energy storage, *Solar Energy*, 82 (2008) 118-124.
- [39] M.M. Farid, A.M. Khudhair, S.A.K. Razack, S. Al-Hallaj, A review on phase change energy storage: Materials and applications, *Energy Conversion and Management*, 45 (2004) 1597-1615.
- [40] M. Kenisarin, K. Mahkamov, Solar energy storage using phase change materials, *Renewable and Sustainable Energy Reviews*, 11 (2007) 1913-1965.
- [41] P. Verma, Varun, S.K. Singal, Review of mathematical modeling on latent heat thermal energy storage systems using phase-change material, *Renewable and Sustainable Energy Reviews*, 12 (2008) 999-1031.
- [42] X. Wang, Y. Zhang, W. Xiao, R. Zeng, Q. Zhang, H. Di, Review on thermal performance of phase change energy storage building envelope, *Chinese Science Bulletin*, 54 (2009) 920-928.
- [43] R. Kandasamy, X.-Q. Wang, A.S. Mujumdar, Transient cooling of electronics using phase change material (PCM)-based heat sinks, *Applied Thermal Engineering*, 28 (2008) 1047-1057.
- [44] A. Abhat, Low temperature latent heat thermal energy storage: Heat storage materials, *Solar Energy*, 30 (1983) 313-332.
- [45] R. Velraj, R.V. Seeniraj, B. Hafner, C. Faber, K. Schwarzer, Heat transfer enhancement in a latent heat storage system, *Solar Energy*, 65 (1999) 171-180.
- [46] J.T. Williams, *Textiles for Cold Weather Apparel*, Elsevier Science, 2009.
- [47] B. Zalba, J.M. Marin, L.F. Cabeza, H. Mehling, Review on thermal energy storage with phase change: materials, heat transfer analysis and applications, *Applied Thermal Engineering*, 23 (2003) 251-283.
- [48] S. Jegadheeswaran, S.D. Pohekar, Performance enhancement in latent heat thermal storage system: A review, *Renewable and Sustainable Energy Reviews*, 13 (2009) 2225-2244.
- [49] M.N.A. Hawlader, M.S. Uddin, M.M. Khin, Microencapsulated PCM thermal-energy storage system, *Applied Energy*, 74 (2003) 195-202.
- [50] L.F. Cabeza, C. Castellon, M. Nogues, M. Medrano, R. Leppers, O. Zubillaga, Use of microencapsulated PCM in concrete walls for energy savings, *Energy and Buildings*,

- 39 (2007) 113-119.
- [51] A. Castell, I. Martorell, M. Medrano, G. Perez, L.F. Cabeza, Experimental study of using PCM in brick constructive solutions for passive cooling, *Energy and Buildings*, 42 (2010) 534-540.
- [52] V.V. Tyagi, S.C. Kaushik, S.K. Tyagi, T. Akiyama, Development of phase change materials based microencapsulated technology for buildings: A review, *Renewable and Sustainable Energy Reviews*, 15 (2011) 1373-1391.
- [53] H. Inaba, C. Dai, A. Horibe, Numerical simulation of Rayleigh–Benard convection in non-Newtonian phase-change-material slurries, *International Journal of Thermal Sciences*, 42 (2003) 471-480.
- [54] X. Hu, Y. Zhang, Novel insight and numerical analysis of convective heat transfer enhancement with microencapsulated phase change material slurries: laminar flow in a circular tube with constant heat flux, *International Journal of Heat and Mass Transfer*, 45 (2002) 3163-3172.
- [55] P. Charunyakorn, S. Sengupta, S.K. Roy, Forced convection heat transfer in microencapsulated phase change material slurries: flow in circular ducts, *International Journal of Heat and Mass Transfer*, 34 (1991) 819-833.
- [56] A.F. Regin, S.C. Solanki, J.S. Saini, Heat transfer characteristics of thermal energy storage system using PCM capsules: A review, *Renewable and Sustainable Energy Reviews*, 12 (2008) 2438-2458.
- [57] A. Sari, A. Karaipekli, Thermal conductivity and latent heat thermal energy storage characteristics of paraffin/expanded graphite composite as phase change material, *Applied Thermal Engineering*, 27 (2007) 1271-1277.
- [58] C.J. Ho, J.Y. Gao, Preparation and thermophysical properties of nanoparticle-in-paraffin emulsion as phase change material, *International Communications in Heat and Mass Transfer*, 36 (2009) 467-470.
- [59] J. Fukai, Y. Hamada, Y. Morozumi, O. Miyatake, Effect of carbon-fiber brushes on conductive heat transfer in phase change materials, *International Journal of Heat and Mass Transfer*, 45 (2002) 4781-4792.
- [60] A. Elgafy, K. Lafdi, Effect of carbon nanofiber additives on thermal behavior of phase change materials, *Carbon*, 43 (2005) 3067-3074.
- [61] S. WU, D. ZHU, X. ZHANG, J. HUANG, Preparation and Melting/Freezing Characteristics of Cu/Paraffin Nanofluid as Phase-Change Material (PCM), American Chemical Society, Washington, DC, ETATS-UNIS, 2010.
- [62] Y. Cui, C. Liu, S. Hu, X. Yu, The experimental exploration of carbon nanofiber and carbon nanotube additives on thermal behavior of phase change materials, *Solar Energy Materials and Solar Cells*, 95 (2011) 1208-1212.
- [63] J. Fukai, M. Kanou, Y. Kodama, O. Miyatake, Thermal conductivity enhancement of energy storage media using carbon fibers, *Energy Conversion and Management*, 41 (2000) 1543-1556.
- [64] F. Frusteri, V. Leonardi, S. Vasta, G. Restuccia, Thermal conductivity

- measurement of a PCM based storage system containing carbon fibers, *Applied Thermal Engineering*, 25 (2005) 1623-1633.
- [65] W.D. Steinmann, R. Tamme, Latent heat storage for solar steam systems, *Journal of Solar Energy Engineering, Transactions of the ASME*, 130 (2008) 0110041-0110045.
- [66] K. Chintakrinda, R.D. Weinstein, A.S. Fleischer, A direct comparison of three different material enhancement methods on the transient thermal response of paraffin phase change material exposed to high heat fluxes, *International Journal of Thermal Sciences*, 50 (2011) 1639-1647.
- [67] P. Lamberg, K. Siren, Approximate analytical model for solidification in a finite PCM storage with internal fins, *Applied Mathematical Modelling*, 27 (2003) 491-513.
- [68] A. Caron-Soupart, J.-F. Fourmigue, P. Marty, R. Couturier, Performance analysis of thermal energy storage systems using phase change material, *Applied Thermal Engineering*, 98 (2016) 1286-1296.
- [69] M. Lacroix, M. Benmadda, Numerical simulation of natural convection-dominated melting and solidification from a finned vertical wall, *Numerical Heat Transfer; Part A: Applications*, 31 (1997) 71-86.
- [70] M. Gharebaghi, I. Sezai, Enhancement of heat transfer in latent heat storage modules with internal fins, *Numerical Heat Transfer; Part A: Applications*, 53 (2008) 749-765.
- [71] G. Karamanis, M. Hodes, Longitudinal-fin heat sink optimization capturing conjugate effects under fully developed conditions, *Journal of Thermal Science and Engineering Applications*, 8 (2016).
- [72] K.J. Kim, Performance of hybrid fin heat sinks for thermal control of light emitting diode lighting modules, *Journal of Electronic Packaging, Transactions of the ASME*, 136 (2014).
- [73] A. Mustaffar, A. Harvey, D. Reay, Melting of phase change material assisted by expanded metal mesh, *Applied Thermal Engineering*, (2015).
- [74] C. Liu, R.E. Murray, D. Groulx, Asme, Experimental study of cylindrical latent heat energy storage systems using lauric acid as the phase change material, *Proceedings of the Asme Summer Heat Transfer Conference, Vol 2* (2012) 447-456.
- [75] D. Zhou, C.Y. Zhao, Experimental investigations on heat transfer in phase change materials (PCMs) embedded in porous materials, *Applied Thermal Engineering*, 31 (2011) 970-977.
- [76] K. Lafdi, O. Mesalhy, S. Shaikh, Experimental study on the influence of foam porosity and pore size on the melting of phase change materials, *Journal of Applied Physics*, 102 (2007).
- [77] S.S. Sundarram, W. Li, The effect of pore size and porosity on thermal management performance of phase change material infiltrated microcellular metal foams, *Applied Thermal Engineering*, 64 (2014) 147-154.
- [78] C.Y. Zhao, W. Lu, Y. Tian, Heat transfer enhancement for thermal energy storage

- using metal foams embedded within phase change materials (PCMs), *Solar Energy*, 84 (2010) 1402-1412.
- [79] Z. Liu, Y. Yao, H. Wu, Numerical modeling for solid-liquid phase change phenomena in porous media: Shell-and-tube type latent heat thermal energy storage, *Applied Energy*, 112 (2013) 1222-1232.
- [80] Z.Q. Yu, Y.L. Feng, W.J. Zhou, Y. Jin, M.J. Li, Z.Y. Li, W.Q. Tao, Study on flow and heat transfer characteristics of composite porous material and its performance analysis by FSP and EDEP, *Applied Energy*, 112 (2013) 1367-1375.
- [81] Z.G. Xu, C.Y. Zhao, Enhanced boiling heat transfer by gradient porous metals in saturated pure water and surfactant solutions, *Applied Thermal Engineering*, 100 (2016) 68-77.
- [82] S. Feng, Y. Zhang, M. Shi, T. Wen, T.J. Lu, Unidirectional freezing of phase change materials saturated in open-cell metal foams, *Applied Thermal Engineering*, (2014).
- [83] A.H. Brothers, D.C. Dunand, Density-graded cellular aluminum, *Advanced Engineering Materials*, 8 (2006) 805-809.
- [84] J.L. Yang, L.J. Yang, C. Xu, X.Z. Du, Numerical analysis on thermal behavior of solid-liquid phase change within copper foam with varying porosity, *International Journal of Heat and Mass Transfer*, 84 (2015) 1008-1018.
- [85] Y.B. Tao, Y. You, Y.L. He, Lattice Boltzmann simulation on phase change heat transfer in metal foams/paraffin composite phase change material, *Applied Thermal Engineering*, 93 (2016) 476-485.
- [86] Y. Su, X. Gong, Mechanical properties of open-cell metal foams under low-velocity impact loading, *World Journal of Engineering*, 9 (2012) 285-292.
- [87] M. Iasiello, S. Cunsolo, M. Oliviero, W.M. Harris, N. Bianco, W.K. Chiu, V. Naso, Numerical Analysis of Heat Transfer and Pressure Drop in Metal Foams for Different Morphological Models, *Journal of Heat Transfer*, 136 (2014) 112601.
- [88] A. Kopanidis, A. Theodorakakos, E. Gavaises, D. Bouris, 3D numerical simulation of flow and conjugate heat transfer through a pore scale model of high porosity open cell metal foam, *International Journal of Heat and Mass Transfer*, 53 (2010) 2539-2550.
- [89] T.J. Lu, H.A. Stone, M.F. Ashby, Heat transfer in open-cell metal foams, *Acta Materialia*, 46 (1998) 3619-3635.
- [90] P. Kumar, F. Topin, Simultaneous determination of intrinsic solid phase conductivity and effective thermal conductivity of Kelvin like foams, *Applied Thermal Engineering*, 71 (2014) 536-547.
- [91] E. Fleming, S. Wen, L. Shi, A.K. da Silva, Experimental and theoretical analysis of an aluminum foam enhanced phase change thermal storage unit, *International Journal of Heat and Mass Transfer*, 82 (2015) 273-281.
- [92] S. Krishnan, S.V. Garimella, J.Y. Murthy, Simulation of thermal transport in open-cell metal foams: Effect of periodic unit-cell structure, *Journal of Heat Transfer*,

- 130 (2008).
- [93] X. Hu, S.S. Patnaik, Modeling phase change material in micro-foam under constant temperature condition, *International Journal of Heat and Mass Transfer*, 68 (2014) 677-682.
- [94] Y. Tian, C.Y. Zhao, A numerical investigation of heat transfer in phase change materials (PCMs) embedded in porous metals, *Energy*, 36 (2011) 5539-5546.
- [95] W. Lu, C.Y. Zhao, S.A. Tassou, Thermal analysis on metal-foam filled heat exchangers. Part I: Metal-foam filled pipes, *International Journal of Heat and Mass Transfer*, 49 (2006) 2751-2761.
- [96] L.A. Caffarelli, L.C. Evans, Continuity of the temperature in the two-phase Stefan problem, *Archive for Rational Mechanics and Analysis*, 81 (1983) 199-220.
- [97] V. Alexiades, *Mathematical Modeling Of Melting And Freezing Processes*, Taylor & Francis, 1992.
- [98] G.W. Evans, A NOTE ON THE EXISTENCE OF A SOLUTION TO A PROBLEM OF STEFAN, *Quarterly of Applied Mathematics*, 9 (1951) 185-193.
- [99] J. Douglas, A uniqueness theorem for the solution of a stefan problem, *Proceedings of the American Mathematical Society*, 8 (1957) 402-408.
- [100] Y. Dutil, D.R. Rousse, N. Ben Salah, S. Lassue, L. Zalewski, A review on phase-change materials: Mathematical modeling and simulations, *Renewable & Sustainable Energy Reviews*, 15 (2011) 112-130.
- [101] V.R. Voller, C. Prakash, A fixed grid numerical modelling methodology for convection-diffusion mushy region phase-change problems, *International Journal of Heat and Mass Transfer*, 30 (1987) 1709-1719.
- [102] A. Sharma, V.V. Tyagi, C.R. Chen, D. Buddhi, Review on thermal energy storage with phase change materials and applications, *Renewable and Sustainable Energy Reviews*, 13 (2009) 318-345.
- [103] C.R. Swaminathan, V.R. Voller, On the enthalpy method, *International Journal of Numerical Methods for Heat & Fluid Flow*, 3 (1993) 233-244.
- [104] G. Worster, *Mathematical Modeling of Melting and Freezing Processes*. By V. Alexiades and A. D. Solomon. Taylor & Francis, 1993. 323 pp. £35, *Journal of Fluid Mechanics*, 251 (1993) 719-720.
- [105] Z. Jie, Z. Dongqi, W. Pengwei, W. Gang, L. Feng, D. Penglong, Numerical Simulation Research of Investment Casting for TiB₂/A356 Aluminum Base Composite, *Rare Metal Materials and Engineering*, 43 (2014) 47-51.
- [106] Y. Liu, Manufacture and mechanical properties of aluminum foams and metal porous polymeric composites, in: *LASMIS, UTT, France, 2007*.
- [107] E. Lacoste, O. Mantaux, M. Danis, Numerical simulation of metal matrix composites and polymer matrix composites processing by infiltration: a review, *Composites Part A: Applied Science and Manufacturing*, 33 (2002) 1605-1614.
- [108] V.J. Michaud, L.M. Compton, A. Mortensen, Capillarity in isothermal infiltration of alumina fiber preforms with aluminum, *Metallurgical and Materials Transactions A*,

- 25 (1994) 2145-2152.
- [109] A. Mortensen, T. Wong, Infiltration of fibrous preforms by a pure metal: Part III. capillary phenomena, *Metallurgical Transactions A*, 21 (1990) 2257-2263.
- [110] A. Mortensen, L.J. Masur, J.A. Cornie, M.C. Flemings, Infiltration of fibrous preforms by a pure metal: Part I. Theory, *Metallurgical Transactions A*, 20 (1989) 2535-2547.
- [111] L.J. Masur, A. Mortensen, J.A. Cornie, M.C. Flemings, Infiltration of fibrous preforms by a pure metal: Part II. Experiment, *Metallurgical Transactions A*, 20 (1989) 2549-2557.
- [112] C. Garcia-Cordovilla, E. Louis, J. Narciso, Pressure infiltration of packed ceramic particulates by liquid metals, *Acta Materialia*, 47 (1999) 4461-4479.
- [113] J. Goicoechea, C. Garcia-Cordovilla, E. Louis, A. Pamies, Surface tension of binary and ternary aluminium alloys of the systems Al-Si-Mg and Al-Zn-Mg, *Journal of Materials Science*, 27 (1992) 5247-5252.
- [114] K. Berchem, U. Mohr, W. Bleck, Controlling the degree of pore opening of metal sponges, prepared by the infiltration preparation method, *Materials Science and Engineering: A*, 323 (2002) 52-57.
- [115] J.M. Molina, E. Piñero, J. Narciso, C. García-Cordovilla, E. Louis, Liquid metal infiltration into ceramic particle preforms with bimodal size distributions, *Current Opinion in Solid State and Materials Science*, 9 (2005) 202-210.
- [116] T. Dopler, A. Modaressi, V. Michaud, Simulation of metal-matrix composite isothermal infiltration processing, *Metallurgical and Materials Transactions B: Process Metallurgy and Materials Processing Science*, 31 (2000) 225-234.
- [117] S.Y. He, Metalci foam and metal porou polymer composite (MPPC): manufacture and mechanical behavior, in: *LASMIS*, UTT, France, 2004.
- [118] H. Chattopadhyay, Simulation of transport processes in squeeze casting, *Journal of Materials Processing Technology*, 186 (2007) 174-178.
- [119] Z. Sun, H. Hu, X. Chen, Q. Wang, W. Yang, Gating system design for a magnesium alloy casting, *Journal of Materials Science & Technology*, 24 (2008) 93-95.
- [120] S.-T. Hong, D.R. Herling, Open-cell aluminum foams filled with phase change materials as compact heat sinks, *Scripta Materialia*, 55 (2006) 887-890.
- [121] B. He, F. Setterwall, Technical grade paraffin waxes as phase change materials for cool thermal storage and cool storage systems capital cost estimation, *Energy Conversion and Management*, 43 (2002) 1709-1723.
- [122] T. Kousksou, A. Jamil, T.E. Rhafiki, Y. Zeraouli, Paraffin wax mixtures as phase change materials, *Solar Energy Materials and Solar Cells*, 94 (2010) 2158-2165.
- [123] H. Inaba, P. Tu, Evaluation of thermophysical characteristics on shape-stabilized paraffin as a solid-liquid phase change material, *Heat and Mass Transfer*, 32 (1997) 307-312.
- [124] N. Ukrainczyk, S. Kurajica, J. Šipušić, Thermophysical Comparison of Five Commercial Paraffin Waxes as Latent Heat Storage Materials, *Chemical and*

- biochemical engineering quarterly, 24 (2010) 129-137.
- [125] T. Kousksou, M. Mahdaoui, A. Ahmed, A.A. Msaad, Melting over a wavy surface in a rectangular cavity heated from below, *Energy*, 64 (2014) 212-219.
- [126] L.A. Diaz, R. Viskanta, Visualization of the solid-liquid interface morphology formed by natural convection during melting of a solid from below, *International Communications in Heat and Mass Transfer*, 11 (1984) 35-43.
- [127] C. Beckermann, R. Viskanta, Natural convection solid/liquid phase change in porous media, *International Journal of Heat and Mass Transfer*, 31 (1988) 35-46.
- [128] B. Kamkari, H. Shokouhmand, F. Bruno, Experimental investigation of the effect of inclination angle on convection-driven melting of phase change material in a rectangular enclosure, *International Journal of Heat and Mass Transfer*, 72 (2014) 186-200.
- [129] M. Moeini Sedeh, J.M. Khodadadi, Thermal conductivity improvement of phase change materials/graphite foam composites, *Carbon*, 60 (2013) 117-128.
- [130] J.W. Paek, B.H. Kang, S.Y. Kim, J.M. Hyun, Effective thermal conductivity and permeability of aluminum foam materials, *International Journal of Thermophysics*, 21 (2000) 453-464.
- [131] W.Q. Li, Z.G. Qu, B.L. Zhang, K. Zhao, W.Q. Tao, Thermal behavior of porous stainless-steel fiber felt saturated with phase change material, *Energy*, 55 (2013) 846-852.
- [132] J. Yang, L. Yang, C. Xu, X. Du, Experimental study on enhancement of thermal energy storage with phase-change material, *Applied Energy*, 169 (2016) 164-176.
- [133] M. Alipanah, X. Li, Numerical studies of lithium-ion battery thermal management systems using phase change materials and metal foams, *International Journal of Heat and Mass Transfer*, 102 (2016) 1159-1168.
- [134] W.Q. Li, Z.G. Qu, Y.L. He, W.Q. Tao, Experimental and numerical studies on melting phase change heat transfer in open-cell metallic foams filled with paraffin, *Applied Thermal Engineering*, 37 (2012) 1-9.
- [135] J.W. Paek, B.H. Kang, S.Y. Kim, J.M. Hyun, Effective Thermal Conductivity and Permeability of Aluminum Foam Materials1, *International Journal of Thermophysics*, 21 (2000) 453-464.
- [136] E. Solórzano, J. Reglero, M. Rodríguez-Pérez, D. Lehmhus, M. Wichmann, J. De Saja, An experimental study on the thermal conductivity of aluminium foams by using the transient plane source method, *International Journal of Heat and Mass Transfer*, 51 (2008) 6259-6267.
- [137] J.F. Despois, A. Mortensen, Permeability of open-pore microcellular materials, *Acta Materialia*, 53 (2005) 1381-1388.
- [138] F. Kuwahara, M. Shirota, A. Nakayama, A numerical study of interfacial convective heat transfer coefficient in two-energy equation model for convection in porous media, *International Journal of Heat and Mass Transfer*, 44 (2001) 1153-1159.
- [139] P.S. Liu, A new method for calculating the specific surface area of porous metal

- foams, *Philosophical Magazine Letters*, 90 (2010) 447-453.
- [140] X. Xiao, P. Zhang, M. Li, Preparation and thermal characterization of paraffin/metal foam composite phase change material, *Applied Energy*, 112 (2013) 1357-1366.
- [141] A. Atal, Y. Wang, M. Harsha, S. Sengupta, Effect of porosity of conducting matrix on a phase change energy storage device, *International Journal of Heat and Mass Transfer*, 93 (2016) 9-16.
- [142] H. Shmueli, G. Ziskind, R. Letan, Melting in a vertical cylindrical tube: Numerical investigation and comparison with experiments, *International Journal of Heat and Mass Transfer*, 53 (2010) 4082-4091.
- [143] N. Wakao, S. Kaguei, T. Funazkri, Effect of fluid dispersion coefficients on particle-to-fluid heat transfer coefficients in packed beds: Correlation of nusselt numbers, *Chemical Engineering Science*, 34 (1979) 325-336.
- [144] A.A. Zukauskas, *Heat Transfer from Tubes in Cross Flow*, (1972).
- [145] N. Dukhan, P. Patel, Equivalent particle diameter and length scale for pressure drop in porous metals, *Experimental Thermal and Fluid Science*, 32 (2008) 1059-1067.
- [146] S. Wei, C. Ming-Hsiung, Steady-state natural convection with phase change, *International Journal of Heat and Mass Transfer*, 33 (1990) 2545-2563.
- [147] B. Binet, M. Lacroix, Numerical study of natural-convection-dominated melting inside uniformly and discretely heated rectangular cavities, *Numerical Heat Transfer; Part A: Applications*, 33 (1998) 207-224.
- [148] P. Jany, A. Bejan, Scaling theory of melting with natural convection in an enclosure, *International Journal of Heat and Mass Transfer*, 31 (1988) 1221-1235.
- [149] C. Barat, J.P. Garandet, The effect of natural convection in liquid phase mass transport coefficient measurements: the case of thermosolutal convection, *International Journal of Heat and Mass Transfer*, 39 (1996) 2177-2182.
- [150] J. Chan Choi, S. Done Kim, G. Young Han, Heat transfer characteristics in low-temperature latent heat storage systems using salt-hydrates at heat recovery stage, *Solar Energy Materials and Solar Cells*, 40 (1996) 71-87.
- [151] A. Najafian, F. Haghighat, A. Moreau, Integration of PCM in domestic hot water tanks: Optimization for shifting peak demand, *Energy and Buildings*, 106 (2015) 59-64.
- [152] F. Zhu, C. Zhang, X. Gong, Numerical analysis and comparison of the thermal performance enhancement methods for metal foam/phase change material composite, *Applied Thermal Engineering*, 109, Part A (2016) 373-383.
- [153] C. Li, G. Peterson, Experimental study of enhanced nucleate boiling heat transfer on uniform and modulated porous structures, *Frontiers in Heat and Mass Transfer (FHMT)*, 1 (2010).
- [154] C.H. Li, T. Li, P. Hodgins, C.N. Hunter, A.A. Voevodin, J.G. Jones, G. Peterson, Comparison study of liquid replenishing impacts on critical heat flux and heat transfer coefficient of nucleate pool boiling on multiscale modulated porous structures, *International Journal of Heat and Mass Transfer*, 54 (2011) 3146-3155.

- [155] R. Stamp, P. Fox, W. O'Neill, E. Jones, C. Sutcliffe, The development of a scanning strategy for the manufacture of porous biomaterials by selective laser melting, *Journal of Materials Science: Materials in Medicine*, 20 (2009) 1839.
- [156] J. Gardan, Additive manufacturing technologies: state of the art and trends, *International Journal of Production Research*, 54 (2016) 3118-3132.
- [157] C. Hutter, D. Büchi, V. Zuber, P. Rudolf von Rohr, Heat transfer in metal foams and designed porous media, *Chemical Engineering Science*, 66 (2011) 3806-3814.
- [158] A. Inayat, J. Schwerdtfeger, H. Freund, C. Körner, R.F. Singer, W. Schwieger, Periodic open-cell foams: Pressure drop measurements and modeling of an ideal tetrakaidecahedra packing, *Chemical Engineering Science*, 66 (2011) 2758-2763.
- [159] D.A. Hollander, M. von Walter, T. Wirtz, R. Sellei, B. Schmidt-Rohlfing, O. Paar, H.-J. Erli, Structural, mechanical and in vitro characterization of individually structured Ti-6Al-4V produced by direct laser forming, *Biomaterials*, 27 (2006) 955-963.
- [160] K. Maeda, T.H.C. Childs, Laser sintering (SLS) of hard metal powders for abrasion resistant coatings, *Journal of Materials Processing Technology*, 149 (2004) 609-615.
- [161] S. Jegadheeswaran, S.D. Pohekar, Performance enhancement in latent heat thermal storage system: A review, *Renewable & Sustainable Energy Reviews*, 13 (2009) 2225-2244.
- [162] S. Feng, M. Shi, Y. Li, T.J. Lu, Pore-scale and volume-averaged numerical simulations of melting phase change heat transfer in finned metal foam, *International Journal of Heat and Mass Transfer*, 90 (2015) 838-847.
- [163] Z. Chen, D. Gao, J. Shi, Experimental and numerical study on melting of phase change materials in metal foams at pore scale, *International Journal of Heat and Mass Transfer*, 72 (2014) 646-655.

Feng ZHU

Doctorat : Matériaux, Mécanique, Optique et Nanotechnologie

Année 2017

Etude expérimentale et numérique des mousses métalliques composites dans une application d'énergie thermique

L'objectif de cette thèse de doctorat est d'étudier expérimentalement et numériquement le comportement thermique des mousses d'aluminium et des matériaux à changement de phase (MCP), présentés sous la forme d'un composite, afin de connaître le phénomène de stockage d'énergie thermique dans ces matériaux. Le procédé de fabrication de la mousse d'aluminium à cellules ouvertes est d'abord analysé numériquement dans le but de réduire les défauts formés durant la fabrication. Les caractéristiques de transfert de chaleur du MCP dans les mousses d'aluminium comportant différentes porosités sont ensuite étudiées en analysant les processus de fusion et la variation de températures dans ces composites. Deux modèles numériques pour la mousse d'aluminium à faible et à haute porosité sont établis afin d'évaluer la performance de stockage d'énergie des composites. Les résultats montrent que la mousse d'aluminium peut améliorer considérablement la performance de transfert de chaleur du MCP en raison de sa conductivité thermique élevée. La performance de stockage d'énergie dépend fortement de la porosité des mousses d'aluminium. Une porosité optimisée met en évidence cette performance et l'amélioration du comportement thermique. La dernière partie de la thèse porte sur une structure améliorée de la mousse par rapport à la structure uniforme : Association de l'ailette métallique et du gradient de porosité de la mousse. Cette nouvelle structure donne ainsi une performance de stockage d'énergie encore meilleure surtout dans le cas d'une source de chaleur isotherme.

Mots clés : mousses métalliques - chaleur, stockage - composites à matrice métallique - analyse thermique - simulation, méthodes de.

Experimental and Numerical Study of Metal Foam Composites in Innovative Application of Thermal Energy Storage

The objective of this Ph.D. thesis is to study the thermal behavior of the aluminum foam and phase change material (PCM) composite by both experimental and numerical methods in order to know the phenomena of storage of thermal energy in these materials. The manufacturing process of open-cell aluminum foam is firstly analyzed numerically to reduce the manufacturing defects in the samples. The heat transfer characteristics of PCM embedded in aluminum foams with different porosities are then investigated by analyzing the melting processes and the temperature variations in the composites. Two numerical models for low and high porosity aluminum foam are established to evaluate the energy storage performance of the composites. The results show that the aluminum foam can greatly improve the heat transfer performance in PCM due to its high thermal conductivity. The energy storage performance depends strongly on the porosity of the aluminum foam/PCM composite. An optimized porosity highlights this performance and improves the thermal behavior. The last part of this thesis proposes an improved structure of aluminum foam with respect to the uniform structure: Association of the metal fin and the foam with graded porosity. This new structure possesses a better energy storage performance especially in the case of the isothermal heat source.

Keywords: metal foams - heat storage - metallic composites - thermal analysis - simulation methods.

Thèse réalisée en partenariat entre :



Ecole Doctorale "Sciences et Technologies"